INSTRUMENTATION CHANNEL ERROR CORRECTION AND ITS EFFECTS ON PROTECTIVE RELAYS

A Dissertation
Presented to
The Academic Faculty

by

Yuan Kong

In Partial Fulfillment
of the Requirements for the Degree
Doctor of Philosophy in the
School of Electrical and Computer Engineering

Georgia Institute of Technology
December 2019

INSTRUMENTATION CHANNEL ERROR CORRECTION AND ITS EFFECTS ON PROTECTIVE RELAYS

Approved by:

Dr. A.P. Meliopoulos, Advisor
School of Electrical and Computer Engineering
Georgia Institute of Technology

Dr. Valerie Thomas
School of Industrial and Systems Engineering
Georgia Institute of Technology

Dr. Maryam Saeedifard
School of Electrical and Computer Engineering
Georgia Institute of Technology

Dr. Jinfeng Ren
Entergy

Dr. Gee-Kung Chang
School of Electrical and Computer Engineering
Georgia Institute of Technology

Date Approved: [August 22, 2019]

To my beloved parents Pengfei and Shuqiong

ACKNOWLEDGEMENTS

It has been a truly life-changing experience for me to pursue my Ph.D. at Georgia Tech. The successful completion of this remarkable experience would not be achieved without the inspiration, encouragement, and support from so many people. I am very grateful to have them and would like to express my sincere appreciation to all of them.

First and foremost, I would like to give my deepest gratitude to my advisor Dr. A.P. Meliopoulos. It has been a great honor to be his Ph.D. student. I could not have finished my Ph.D. study without his patient guidance, tremendous support and encouragement. Along with my Ph.D. journey, he is not just an adviser but also a great mentor. His careful guidance on how to solve problems with rigorous logic thinking rewards my entire research life and the life afterwards. I could not have imagined having a better advisor than him.

I would also like to extend my appreciation to the rest of my committee members: Dr. Maryam Saeedifard, Dr. Gee-Kung Chang, Dr. Valerie Thomas and Dr. Jinfeng Ren for their valuable time contribution in reviewing my dissertation and their insightful comments.

I would also like to thank Dr. George Cokkinides, who has spent valuable time out of his busy schedule to address questions and issues I had during my research.

I am also grateful to Dr. Eugene Litvinov and Dr. Xiaochuan Luo, who provided me a wonderful opportunity to join their team at ISO New England as an intern. It was a most enjoyable experience in my life working with them and I have obtained a lot of

practical experiences and knowledge on dealing with large-scale power system state estimation.

Special thanks go to all of my fellow lab mates in PSCAL (Power System Control and Automation Laboratory) for their constant support and accompany from the very beginning. In particular, I would like to thank Dr. Liangyi Sun, Dr. Yu Liu, Dr. Bai Cui, Dr. Hussain Fareed Albinali, Orestis Vasios, Boqi Xie, Chiyang Zhong, Jiahao Xie and Kaiyu Liu. I appreciate the friendship and enjoyable time spending with them during my Ph.D. journey.

Most of all, I would like to thank my parents. It is their unwavering love, support and encouragement that gives me the courage and confidence to overcome all the difficulties during those most hard time and eventually reach the final stages of my PH.D. study. Words are powerless to express my gratitude for what they have done for me throughout these years. This thesis is dedicated to them with my ultimate respect and forever love.

TABLE OF CONTENTS

LIST OF TABLES

LIST OF FIGURES

LIST OF SYMBOLS AND ABBREVIATIONS

MU	Merging Unit
CT	Current Transformer
PT	Potential Transformer
RP	Reference Point
ANN	Artificial Neural Network
DSE	Dynamic State Estimation
WLS-DSE	Weighted Least Square Dynamic State Estimation
QDM	Quadratized Dynamic Measurement
AQCF	Algebraic Quadratic Companion Form
$\boldsymbol{C}_x$	Covariance Matrix of State Estimates
$\boldsymbol{C}_{\hat{z}}$	Covariance Matrix of Measurement Estimates
$Tr\{\boldsymbol{C}_x\}$	Trace of $\boldsymbol{C}_x$
$Tr\{\boldsymbol{C}_{\hat{z}}\}$	Trace of $\boldsymbol{C}_{\hat{z}}$

SUMMARY

The objective of this research is to propose an on-line instrumentation channel error correction method within merging unit (MU) and to investigate its effects on the performance of protective relays. To realize this objective, the physically based high fidelity models of entire instrumentation channel are developed, which consist of the instrument transformers, the instrumentation cable and the burden resistor. The quadratized dynamic measurement model is derived for both current instrumentation channel and voltage instrumentation channel. Then the quadratic integration is applied to express the measurement model in a standard syntax referred to as Algebraic Quadratic Companion Form (AQCF). A Dynamic State Estimation (DSE) algorithm is constructed to estimate the primary values on a sample by sample basis. The introduction of MU enables that each instrumentation channel of a MU can be designed to provide corrected primary values. Therefore, the proposed error correction method can be an integral part of MU so that MU reports directly primary values that have been corrected, which is applicable in real-time protective relays. Extensive test cases have demonstrated that the proposed algorithm can accurately reconstruct the current transformer (CT) primary samples in different saturation scenarios and with different CT ratio. The error correction method is also effective to reproduce potential transformer (PT) primary side voltage with high accuracy, demonstrated by test cases on voltage instrumentation channel with different PT ratio. An alternative method to validate the estimated samples is presented via substation level dynamic state estimation using legacy or estimated measurement samples, respectively. The validation procedure is to compare the chi-square value,

$Tr\{\boldsymbol{C}_x\}$ and $Tr\{\boldsymbol{C}_{\hat{z}}\}$. After performing the DSE on the substation system, the comparison results of chi-square value, $Tr\{\boldsymbol{C}_x\}$ and $Tr\{\boldsymbol{C}_{\hat{z}}\}$ show that the estimated samples are able to achieve smaller residuals, more accurate state and measurement estimates. To evaluate the effects of errors on protection relay actions, the performance of three typical protection schemes are presented using estimated measurement samples and legacy measurement samples, respectively. The results show that when large instrumentation channel errors introduced by CT saturation, using the legacy measurement samples may lead to dependability problem for distance relay and security problem for current differential relay and setting-less relay. However, the relay performance (dependability and security) can be greatly improved and the mis-operations can be avoided using the estimated measurement samples.

CHAPTER 1. INTRODUCTION

1.1 Problem Statement

The electric power system represents the most important infrastructure that enables high quality of life and supports the economic life of any nation. In 2017, the global electricity consumption has increased to 22,015 TWh [1]. Therefore, the secure and stable operation of power system is crucial to this increasing electricity demand. As the first defense of the power system, the protective relaying system, as shown in Figure 1-1, plays an important role in selectively and reliably isolating a faulty power system component in the minimum possible time. If a relay has a mis-operation or fails to interrupt a faulty power system component timely, it may cause wide disturbances and blackouts, even cascading failures of power system. The Protection System Misoperations Task Force (PSMTF) was formed to analyze one of NERC's top priority reliability issues– protection system misoperations. According to the NERC's Misoperations Report, as shown in Figure 1-2, the three most common causes of misoperations (Incorrect settings/logic/design errors, Relay failures/malfunctions, and Communication Failures) comprise of approximately 1,500 misoperations, or roughly 65% of the total set of misoperations [3]. A reliable protection system requires two fundamental characteristics: dependability and security [4]. Dependability is defined as the degree of certainty that a relay will operate correctly. Thus, dependability refers to the ability of a relaying system to correctly identify the intolerable abnormalities within its protection zone and to successfully interrupt the abnormalities. Security is defined as the

degree of certainty that a relay will not operate incorrectly. Thus, security means that when the relay does not operate, the non-operation is a correct action.

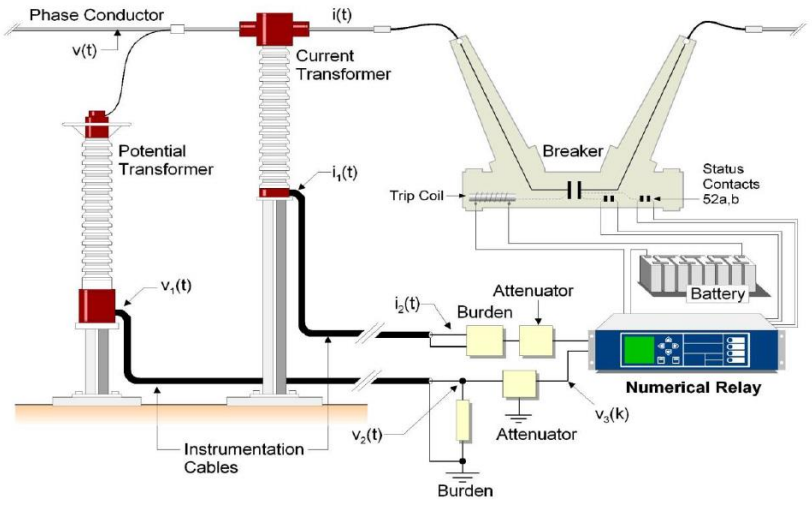

Figure 1-1 A typical protective relay system [2]

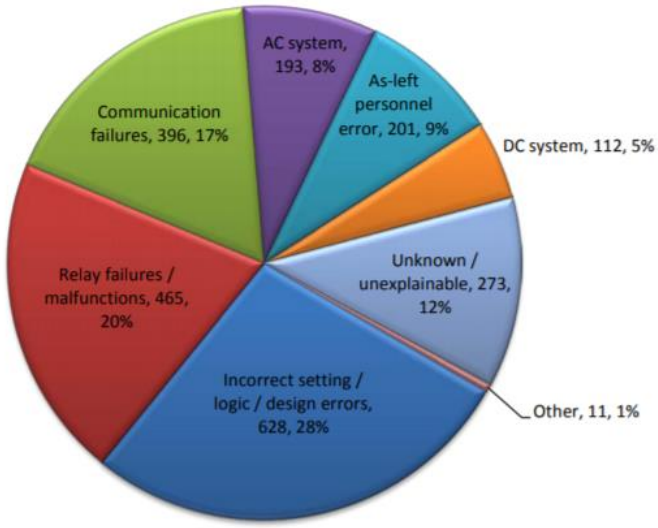

Figure 1-2 NERC wide misoperations by cause code [3]

The performance of any relay system is always dependent upon the quality and validity of the measurements which are the input into the relay. This has been recognized for any protective system for years. The instrumentation subsystem provides the interface between the high current electric power system and the relays that operated at relatively low voltage and current. As shown in Figure 1-3, an instrumentation channel based on Merging Units (MU) consists of instrument transformers (potential transformer and current transformer), copper wires and the MU input circuit. The merging units digitize the input analog data and transmit the digital values to the process bus via fiber optic links. Computing devices (processors) access the data at the process bus and use them for specific applications, one of them is protection. Ideally, the secondary voltage or current values, which are the data input into the MU, should be scaled replicas of the primary values, which are the high voltages and currents of the electric power system. Practically, however, the instrumentation channels will introduce errors which are typically much higher than the errors introduced by the MU analog input and A/D converters. Even as MU are becoming more sophisticated by using higher resolutions, the errors from instrumentation channels remain practically the same. These errors could distort the waveform of primary values and may even cause a mal-operation of the relay. In many cases, the relay's mal-operation could eventually lead to wide power system disturbances and blackouts, as the famous Southwest blackouts in California, 2011[5]. Therefore, to make the protection scheme reliable, it is essential to correct the errors introduced by the instrumentation channels. Furthermore, the effects of the instrumentation channel error correction on protective relays needs to be investigated.

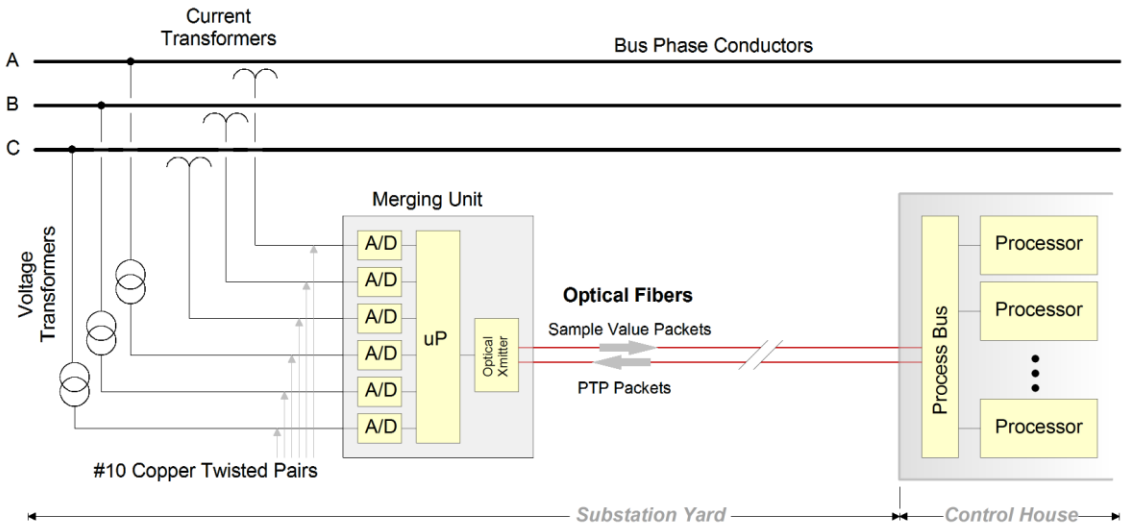

Figure 1-3 Instrumentation subsystem---voltage and current instrumentation channels

1.2 Research Objectives

The objective of this research is to propose an on-line instrumentation channel error correction method within MU and to investigate its effects on protective relays.

To realize this objective, the physically based high fidelity models of entire instrumentation channel are developed, which consist of the instrument transformers (CTs and PTs), the instrumentation cable and the burden resistor. The quadratized dynamic measurement model is derived for both current instrumentation channel and voltage instrumentation channel. Then the quadratic integration is applied to express the measurement model in a standard syntax referred to as **A**lgebraic **Q**uadratic **C**ompanion **F**orm (AQCF). A **D**ynamic **S**tate **E**stimation (**DSE**) algorithm is constructed to estimate the primary values on a sample by sample basis. The introduction of MU enables that each instrumentation channel of a MU can be designed to provide corrected primary values. Therefore, the proposed error correction method can be an integral part of MU so

hat MU reports directly primary values that have been corrected, which is applicable in real-time protective relays. The estimated primary values are validated via performing the substation level dynamic state estimation. Several protection schemes, including distance protection, current differential protection, as well as setting-less protection are investigated in detail to show the effects of the proposed instrumentation channel error correction on protective relays.

1.3 Thesis Outline

The outline of the remaining parts of this dissertation is listed as follows. Specifically, the dissertation consists of 8 Chapters:

Chapter 2 presents background information on the origin of the topic along with presently available technologies that are being used. A thorough literature survey of conventional instrumentation channel error correction methods is provided, and protective relay mis-operations caused by instrumentation channel errors are summarized.

Chapter 3 shows the general and detailed methodology for the derivation of AQCF measurement model. It starts from the quadratized dynamic device model, and then with the measurement definition, the quadratized dynamic measurement model is derived. After applying the quadratic integration, the measurement model is expressed in a standard syntax referred to as **A**lgebraic **Q**uadratic **C**ompanion **F**orm (AQCF), which will be used for dynamic state estimation.

Chapter 4 introduces the detailed mathematical formulation and solution of the developed **D**ynamic **S**tate **E**stimation (**DSE**). Furthermore, the DSE-based protection logic is also discussed in this Chapter.

Chapter 5 illustrates the proposed instrumentation channel error correction in detail. The measurement model of current instrumentation channel and voltage instrumentation channel are developed. Then, the primary samples are estimated via DSE. The results of instrumentation channel error correction are demonstrated through examples.

Chapter 6 presents the validation of the estimated primary samples via substation level dynamic state estimation. The Chi-square value, $Tr\{\boldsymbol{C}_x\}$ and $Tr\{\boldsymbol{C}_z\}$ are utilized to validate the estimated primary samples. The validation results are demonstrated on an example substation system.

Chapter 7 investigates the effects of the error correction on protective relays. The performance of three typical protection schemes is investigated using legacy samples and estimated samples, respectively. Test cases of three typical protection schemes are demonstrated to show the effectiveness of avoiding relay mis-operations with estimated samples.

Chapter 8 summarizes the conclusions and contributions of the proposed research and outlines some directions of future work.

CHAPTER 2. LITERATURE SURVEY

2.1 Overview

This chapter provides the background information of existing technologies related to the proposed research along with a thorough literature review of the research efforts on these topics.

Efforts to account and correct for instrumentation channel errors date back several decades. Section 2.2 introduces background information of instrumentation channel errors. Then, the existing research on instrumentation channel error correction are reviewed and the limitations are identified in Section 2.3. Furthermore, protective relay mis-operations caused by instrumentation channel errors are summarized in Section 2.4, which includes the following protection schemes:

1) Distance Protection

2) Current Differential Protection

3) Setting-Less Protection

2.2 Background

The instrumentation subsystem provides the interface between the high current electric power system and the relays that operate at relatively low voltage and current. Instrumentation channels can be classified into two categories: current instrumentation channel and voltage instrumentation channel. During the past several decades, the current

instrumentation channel has attracted intensive attention because it could introduce enormous errors when current transformer (CT) saturates [6].

A typical secondary current waveform and ideal primary current waveform during CT saturation is shown in Figure 2-1[7]. It shows that the CT saturation could distort the secondary current waveform and lead to inaccurate measurement of primary current, which may even cause mal-operation of protective relays [8]-[10]. Therefore, correcting the errors introduced by the instrumentation channels is essential to improve the reliability of protective relaying system.

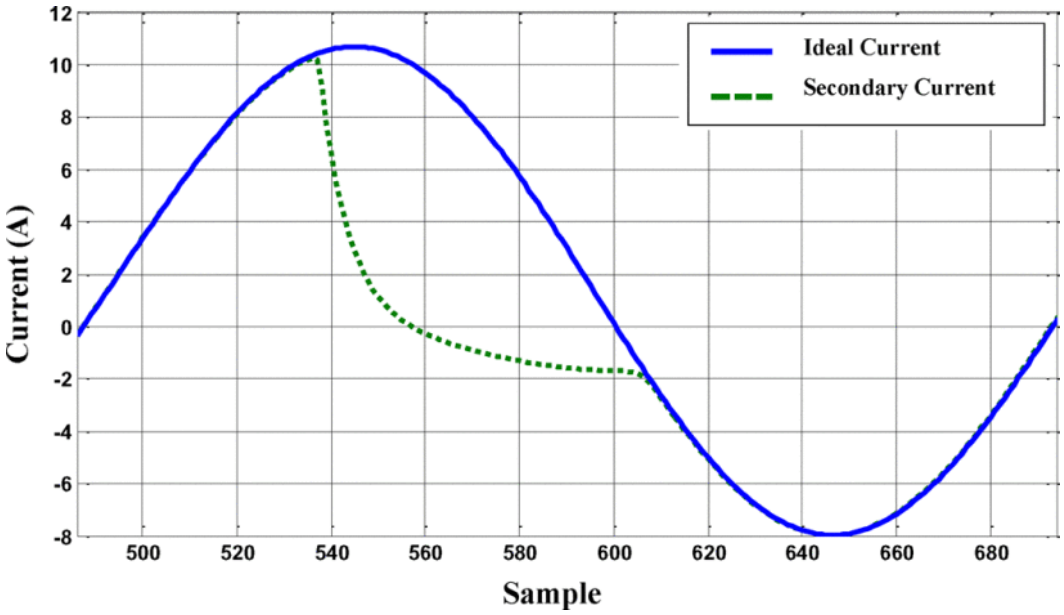

Figure 2-1 Typical CT's distorted secondary current waveform due to saturation and ideal primary current waveform

2.3 Survey of Existing Instrumentation Channel Error Correction Methods

Much work has been devoted to correction of CT distorted secondary current waveform before injecting into the protective relays, which can be classified into four categories:

(1) Approximately estimating the parameter vector of primary current

In 1991, the earliest research on CT primary current estimation was studied by two researchers K.W. Chen and S.T. Glad [11]. This method requires a function be developed which approximates nonlinear core flux characteristics. The researchers tried to represent the primary current as a sinusoid, possibly with harmonics and possibly with some transients, which can be written as:

$$i_1(t) = \boldsymbol{\varphi}(\mathrm{t})^T \boldsymbol{\theta} + e(\mathrm{t})$$

Where:

$\boldsymbol{\theta}$: unknown parameter vector,

$e(\mathrm{t})$: the transients,

$$\boldsymbol{\varphi}(\mathrm{t}) = \begin{bmatrix} 1 & t & \sin\omega t & \cos\omega t & , & \ldots & , & \sin m\omega t & \cos m\omega t \end{bmatrix}^T .$$

Therefore, the primary current could be obtained by estimation of the parameter vector $\boldsymbol{\theta}$. Two different algorithms (Extended Kalman Filter and off-line iterative Gaussian-Newton method) are constructed to obtain the estimation of the parameter vector $\boldsymbol{\theta}$.

This earliest method uses too many simplification and approximation of the modeling. The two main drawbacks are: the model neglects the secondary inductance and it assumes that there is no remnant flux when saturation happens. Therefore, the estimation result is not satisfactory in many cases. Also, in order to apply the Extended Kalman Filter algorithm to estimate the parameter vector, it requires a precise detection

of saturation. However, the saturation detection in [11] is achieved by simply comparing the error between the estimation and the observation. The effectiveness of this saturation detection method needs further investigation. In addition, the off-line iterative Gaussian-Newton method could not be applied in real-time protective relays.

(2) Compensating the secondary current via computation of the magnetizing current

The primary current can be computed by the summation of secondary current and magnetizing current. Therefore, many researchers tried to compensate the secondary current via computation of the magnetizing current [12-14]. Reference [12] computes the magnetizing current by calculating the flux of the current transformer, then adding the magnetizing current to the secondary current to achieve current compensation. However, this method is based on an unrealistic assumption that there is zero remnant flux in the core of current transformer before the occurrence of faults. Therefore, it cannot deal with the situation when remnant flux exists. Also, this method only works well for a specific magnetization curve, which cannot be universally applied in practice.

An improved approach attempts to avoid the remnant flux problem by applying the difference functions or morphological lifting scheme to the detection of the exact first saturation point [13-14]. Once the saturation point is identified, the magnetizing current is approximately proportional to the integration of the secondary current between the time instant of the saturation point and the specified time instant. However, the detection of first saturation point by this approach can be greatly affected by disturbance and noise, which could cause a large deviation from its true values. The authors also mentioned that

when the secondary current is extremely distorted, it is difficult for the approach to distinguish saturation periods from the signal based on shape distortion. In these cases, this approach fails to provide an accurate estimation of primary current.

(3) Estimating the primary current utilizing the unsaturated waveform portions of secondary current

For a partially distorted CT secondary current waveform due to saturation, it can be divided into a saturated waveform portion and an unsaturated waveform portion within each cycle. Based on this characteristic, many researchers tried to estimate the primary current utilizing the unsaturated waveform portions of secondary current [15-17]. The unsaturated waveform portions are separated by identifying a reference point (RP), which is determined by the current data sample exceeds a preset threshold. After setting the RP, the primary current corresponding to the unsaturated portion of secondary current is expressed by the first-order Taylor expansion as [15-16]:

$$i_1(t) = a + bt + c\cos\omega t + d\sin\omega t$$

where a, b, c, d are the unknown parameters to be estimated.

Then, the data samples of the unsaturated portion will be used to estimate these unknown parameters via linear regression. With the estimated parameters, the primary current value could be obtained. However, this method relies too much on the precise RP identification, which is difficult to be guaranteed by simply setting a threshold. Besides, the first-order Taylor approximation of primary current is not accurate enough to account for transients. In addition, this method has a very slow response since it requires more

than one cycle data samples to get enough unsaturated sections to perform the linear regression.

An improved method was proposed in [17], which aims to avoid the slow response problem by utilizing both the data samples of the saturated portion and the unsaturated section. However, the other drawbacks mentioned above still remain.

(4) Reconstructing the secondary current using artificial neural network (ANN)

An alternative approach to reconstruct the CT primary current waveform is applying the artificial neural network (ANN) to learn the nonlinear characteristics of CT magnetization. The first attempt of applying ANN to reconstruct the distorted secondary current due to saturation dates back to 1997[18]. Later on, diverse ANN constructions were applied to reproduce the primary current waveform on the basis of training process [19-26]. Although these ANN-based algorithms are reported to be capable to reconstruct the primary current, there are still many limitations. One limitation of ANN-based method lies in the difficulty in choosing appropriate ANN parameters to universally fit different CT types in practice. Also, the large variation of CT saturation characteristics makes these ANN-based algorithms prone to underfitting. More importantly, the ANN-based method requires a vast amount of off-line training data, which is against to the real-time demand of protective relays.

Besides the aforementioned existing efforts focused on current transformer, reference [27] has introduced an on-line error correction method applied to the potential transformer. This method is formulated as an output tracking problem utilizing repetitive learning control algorithm. The secondary waveform is treated as the output to track the

primary waveform as the input. However, the repetitive learning controller requires a proper chosen gain to guarantee its effectiveness, which is difficult to set. Although the authors in [26] infer that this error correction method can be extended to current transformer, there lacks investigations and results to validate the performance of applying this method on CTs.

2.4 Protective Relay Mis-Operations Caused by Instrumentation Channel Errors

The performance of any relay system is always dependent upon the quality and validity of the measurements, which are the input into the relay. When CT saturation happens, the secondary waveform can be distorted. Thus, the input into the relay is not accurate anymore, which may lead to mis-operation of protective relay. Three typical protection schemes are introduced as follows to discuss the relay mis-operation due to CT saturation.

(1) Distance Protection

Distance protection method uses measured three phase currents and voltages to calculate the impedance between the relay location and the fault point. This means that a distance relay can track the apparent impedance looking into a transmission line. As shown in Figure 2-2, suppose a fault occurs on transmission line MN, the calculated impedance is proportional to the line length l between the fault and the relay location, with the assumption that the line has uniform impedance. Thus, this calculated line length l can be used to identify whether a fault is within the desired zone of protection, and consequently whether or not the relay should trip the line.

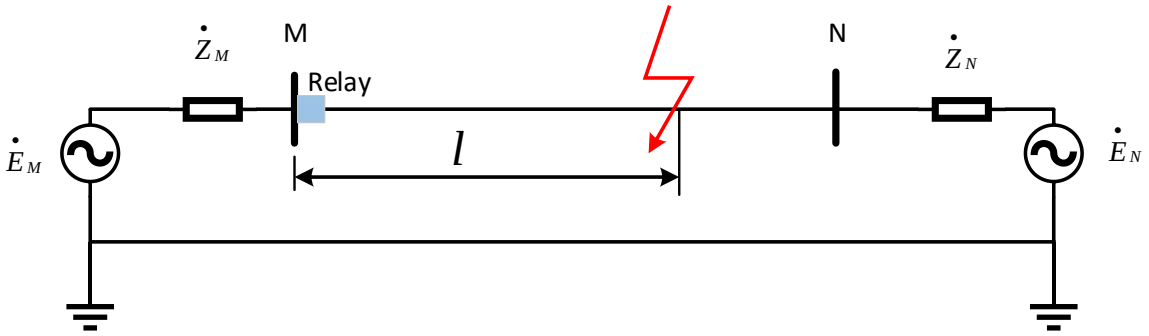

Figure 2-2 Illustration of distance protection principals

The most common characteristic of distance protection is the mho characteristic, a circular type reach characteristic, as shown in Figure 2-3. When the calculated impedance falls into the circular of zone 1, 2 or 3, the corresponding distance relay will issue the trip signal. Ideally, distance protection is an effective and reliable protection scheme for transmission lines. However, CT saturation could increase the measured impedance because it could result in a reduction of the current magnitude and a phase shift in the current. Therefore, CT saturation may cause a dependability problem for distance relay such as underreach in the distance element or slower operating time [28-29].

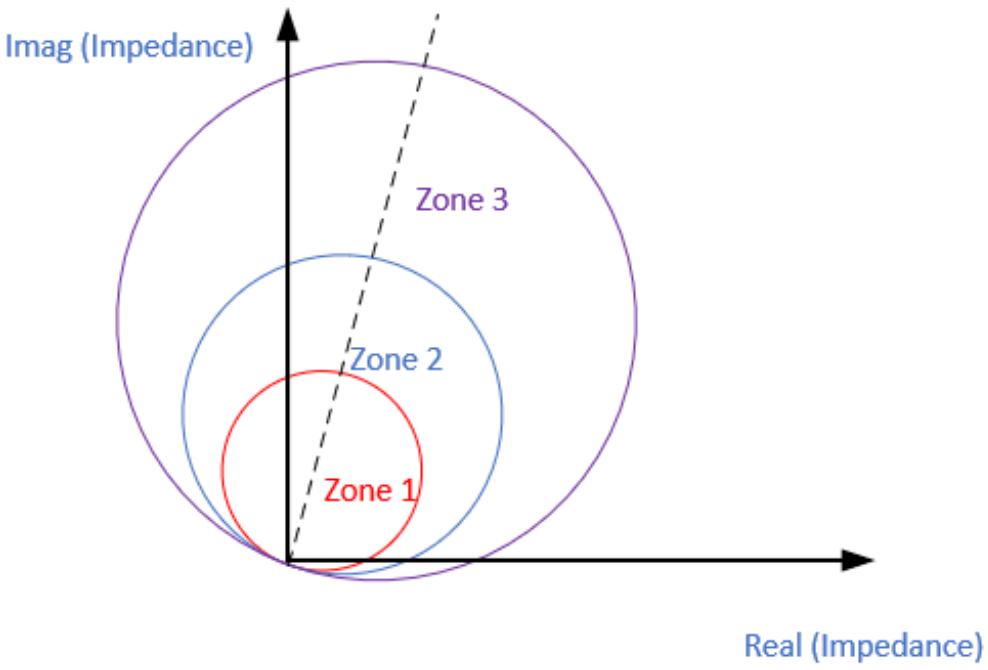

Figure 2-3 Characteristics of distance protection

(2) Current Differential Protection

Differential relay is a common protection scheme used to detect internal faults in protection zones, such as transmission lines, transformers, generators, capacitors and etc. The principal for differential relay is the sum of measured currents from all terminals of the device should be identical to zero under normal operating conditions or external faults. In case of an internal fault, the sum will be a substantial current and the relay will trip the device.

The principal of current differential protection is illustrated using an example of transmission line as protection zone, shown in Figure 2-4. The differential relay calculates the following currents for the protection logic.

1) Operating current: $\dot{I}_{op} = \left| \dot{I}_{s1} + \dot{I}_{s2} \right|$. It should be near zero under normal operating conditions or external faults.

2) Restraining current: $\dot{I}_{res} = \frac{1}{2} \left| \dot{I}_{s1} - \dot{I}_{s2} \right|$. It is the unbalanced current under normal operating conditions or external faults.

if $\left| \dot{I}_{op} \right| > I_{\min}$ and $\left| \dot{I}_{op} \right| / \left| \dot{I}_{res} \right| > K$, the relay will issue the trip signal, as shown in Figure 2-5. Here, the $I_{\min}$ is the minimum pick up current and the typical ratio K is set between 0 and 1.

The differential relay has high sensitivity to detect the internal fault of the protection zone. However, the instrumentation channel errors can bring about security problems to current differential relay. It is obvious that when CT saturation happens, the distorted secondary wave will lead to inaccurate primary current, which can result in substantial operating current under external fault scenarios. In this case, the relay may issue unnecessary trip decision, which is an incorrect operation [30-33].

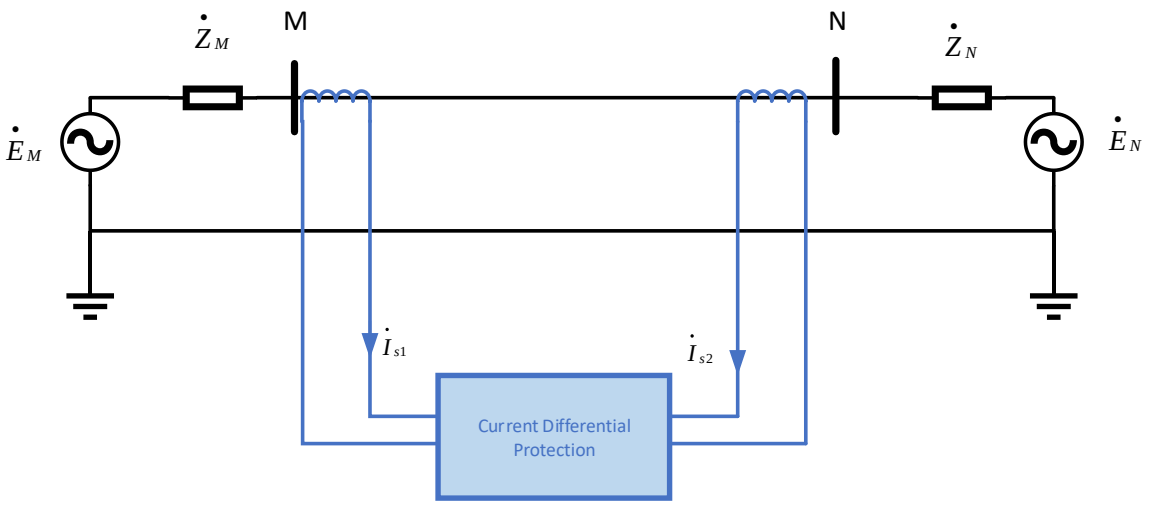

Figure 2-4 Differential protection principal

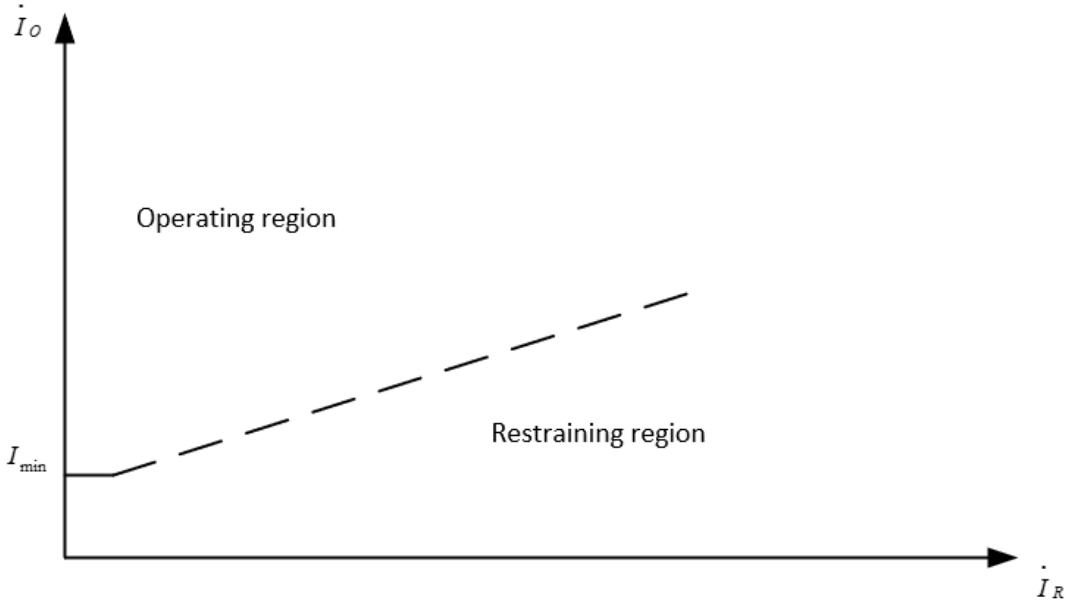

Figure 2-5 Protection logic of differential relay

(3) Setting-Less Protection

A new approach based on component dynamic state estimation has been proposed as a reliable protection scheme, known as DSE-based protection or setting-less protection [34-36], as shown in Figure 2-6. It utilizes DSE to determine whether measurements fit the dynamic model of the protection zone. The dynamic model accurately represents the physical laws that the protection zone must obey. When measurement fit the dynamic model within the accuracy of measurements, it indicates that the protection zone is healthy.

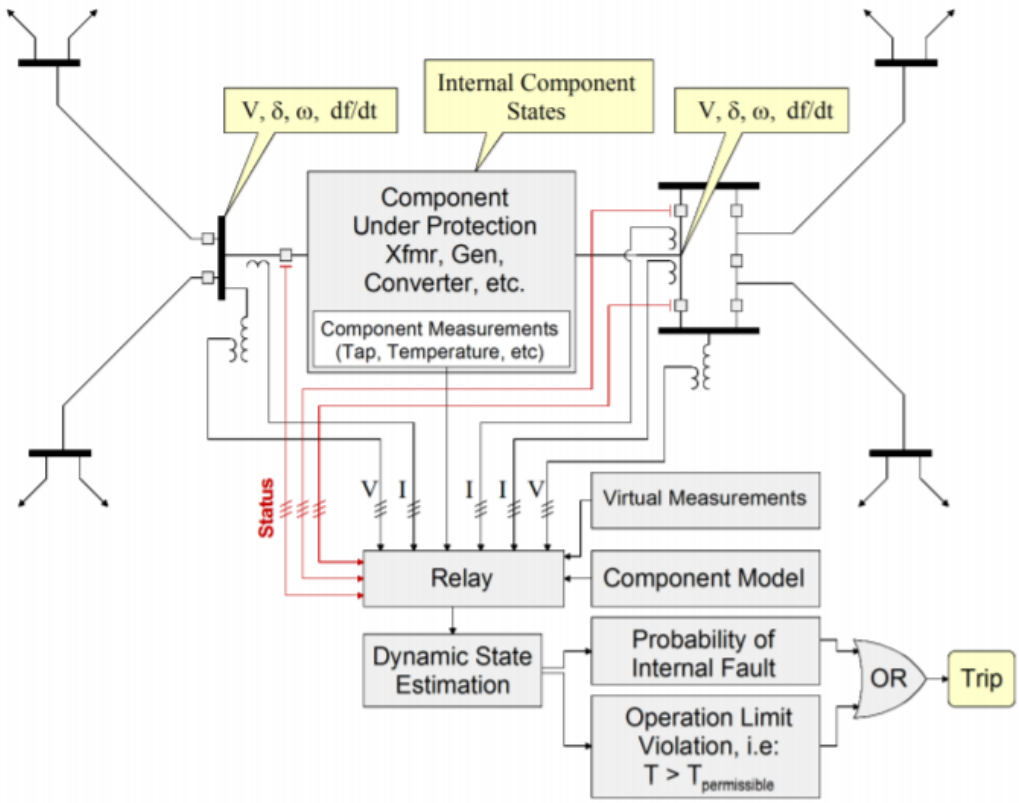

Figure 2-6 Setting-less protection concept [34]

The protection logic of setting-less protection is briefly illustrated in Figure 2-7. The well-known chi-square test calculates the probability that the measurement data are consistent with the protection zone model. The high probability indicates a good fit between the measurements and the model, which indicates that the operating condition of the component is normal. However, if the component has internal faults, the confidence level would be almost zero, which implies the very poor fit between the measurement and the protection zone model. Details of the setting-less protection logic will be introduced later in Chapter 4.

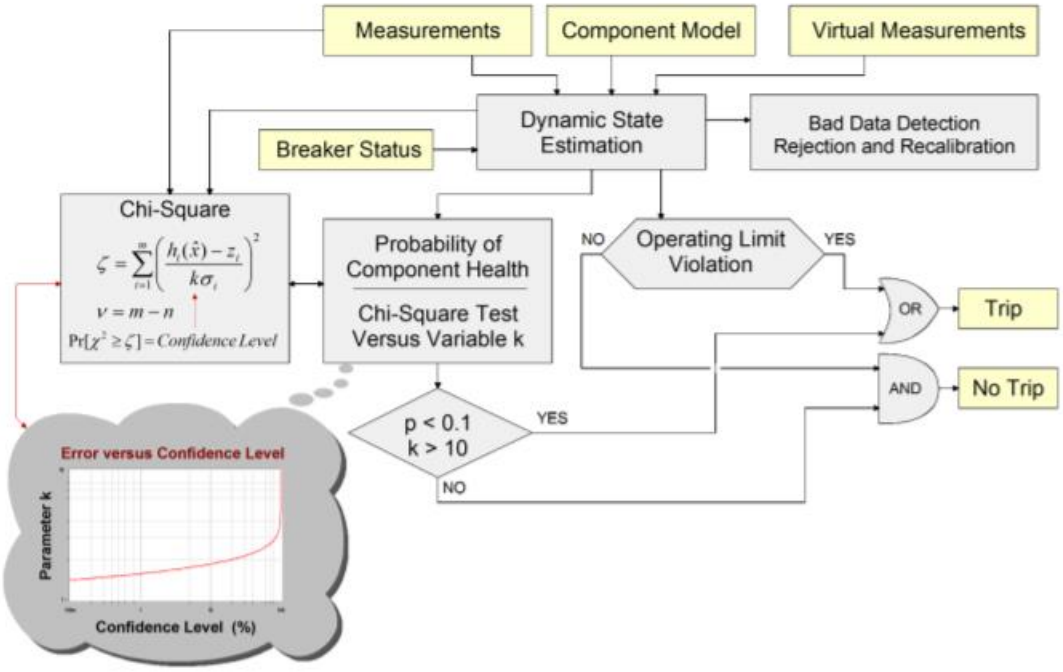

Figure 2-7 Protection logic of setting-less protection [34]

It is important to note that the setting-less protection will perform best when:

(a) The measurements are as accurate as possible;

(b)The accuracy of the dynamic model of the component under protection.

That is to say, large errors introduced by instrumentation channels due to CT saturation may result in a security problem and mis-operation for setting-less protection.

CHAPTER 3. AQCF MEASUREMENT MODEL DERIVATION

3.1 Overview

The dynamic state estimation algorithm is formulated on a standard form referred to as the **A**lgebraic **Q**uadratic **C**ompanion **F**orm (**AQCF**) measurement model. The AQCF measurement model is the result of applying the quadratic integration method to the quadratized dynamic measurement model. This chapter provides a general derivation of the AQCF measurement model step by step.

It starts with the introduction of quadratized dynamic device model in Section 3.2. Then, in Section 3.3, with the measurement definition, the quadratized dynamic measurement model can be derived from the device model. In Section 3.4, quadratic integration is introduced and applied to convert the dynamic measurement model to the algebraic equations, which is referred to as the AQCF measurement model.

3.2 Quadratized Dynamic Device Model Derivation

As the preliminary step to obtain the AQCF measurement model, the quadratized dynamic device model is developed to represent the device physical model. In general, the quadratized dynamic device model is expressed by a set of algebraic and differential equations directly describing the physical circuit in terms of device state variables. Subsequently, these equations will be quadratized by introducing additional state variables to decrease the order of each equation to at most second order, which is referred to as the quaternization procedure. This quadratized dynamic device model can be written in a standard syntax in Equation (3-1) with the following requirements:

1) List all the linear equations for terminal current in Equation Set 1;
2) List all the remaining linear equations in Equation Set 2;
3) All differential terms only appear in the linear equations;
4) List all the remaining quadratic equations in Equation Set 3;
5) The interface states must be listed at the beginning of the states and the interface states' order should be the same as terminal order.

$$
\begin{aligned}
i(t) &= Y_{eqx1}\mathbf{x}(t) + D_{eqxd1}\frac{d\mathbf{x}(t)}{dt} + C_{eqc1} \\
0 &= Y_{eqx2}\mathbf{x}(t) + D_{eqxd2}\frac{d\mathbf{x}(t)}{dt} + C_{eqc2} \\
0 &= Y_{eqx3}\mathbf{x}(t) + \left\{ \begin{array}{c} \vdots \\ \mathbf{x}(t)^T \left\langle F^i_{eqxx3} \right\rangle \mathbf{x}(t) \\ \vdots \end{array} \right\} + C_{eqc3}
\end{aligned}
\tag{3-1}
$$

$$
\mathbf{h}(\mathbf{x}) = Y_{feqx}\mathbf{x} + \left\{ \begin{array}{c} \vdots \\ \mathbf{x}^T \left\langle F^i_{feqxx} \right\rangle \mathbf{x} \\ \vdots \end{array} \right\} + C_{feqc}
$$

Connectivity: TerminalNodeName

Normalization Factors: StateNormFactor, ThroughNormFactor

$$
\textit{subject to}: \qquad \mathbf{h}_{\min} \le \mathbf{h}(\mathbf{x}) \le \mathbf{h}_{\max}
$$

Where:

$i(t)$: the through variables of the device model,

$\mathbf{x}(t)$: external and internal state variables of the device model,

Y_{eqx1}: matrix defining the linear part for states in linear through variable equations,

D_{eqxd1} : matrices defining the differential part for states in linear through variable equations,

C_{eqc1}: constant vector of the device model in linear through variable equations,

Y_{eqx2}: matrix defining the linear part for states in linear virtual equations,

D_{eqxd2} : matrices defining the differential part for state variables in linear virtual equations,

C_{eqc2}: constant vector of the device model in linear virtual equations,

Y_{eqx3}: matrix defining the linear part for states in the remaining quadratic equations,

C_{eqc3}: constant vector of the device model in the remaining quadratic equations,

F_{eqxx3}: matrices defining the quadratic part for states in the remaining quadratic equations,

TerminalNodeName: terminal names defining the connectivity of the device model,

StateNormFactor: Normalization Factors for the states

ThroughNormFactor: Normalization Factors for the through and zero variables

$\mathbf{h}_{\min} \le \mathbf{h}(\mathbf{x}) \le \mathbf{h}_{\max}$: functional constraints

3.3 Quadratized Dynamic Measurement Model Derivation

3.3.1 Measurement Definition

Any measurement can be expressed as a function of state variables and these measurements can be divided into four groups:

1) Actual measurements:

An actual measurement is a measurement obtained by actual meters and its error is determined by the meter's accuracy class.

2) Derived measurements:

A derived measurement is a quantity which can be derived from an actual measurement. It contains the same error as the actual one. An example of derived measurements is illustrated in Figure 3-1, where the measurement z_2 can be derived from actual measurement z_1 by applying the KCL law at node 1.

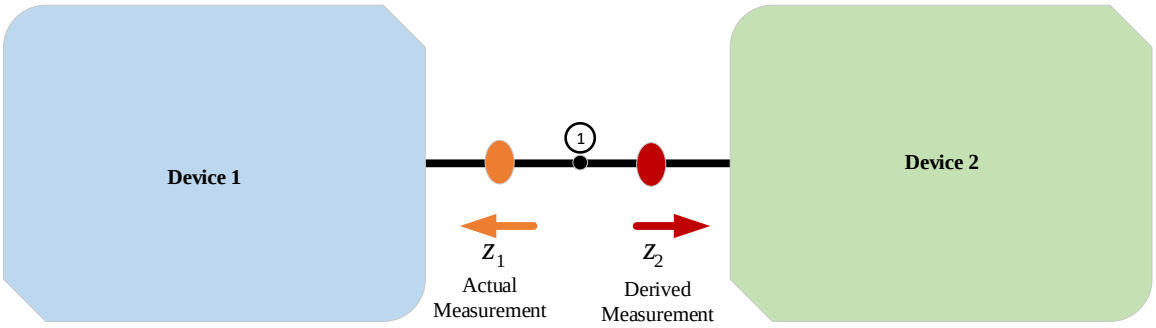

Figure 3-1 Illustration of derived measurement

3) Virtual measurements:

A virtual measurement represents a physical law that must be satisfied, such as KCL or KVL law. All internal equations and KCL equations at interface node are treated as virtual measurements. The virtual measurement contains no error.

4) Pseudo measurements:

A pseudo measurement is a hypothetical measurement for which we may have an idea of its expected value. For example, the ground point voltage is unknown (and difficult to measure). Since the voltage at the ground point is expected to be near zero, it can be treated as a pseudo measurement. Pseudo measurement contains large errors.

3.3.2 Quadratized Dynamic Measurement Model

With the above measurement definition, the quadratized dynamic measurement model can be obtained with a mathematical expression of state variables.

The actual current and voltage measurement can be expressed by Equation (3-2) and Equation (3-3), respectively.

$$z(t) = Y_{zx}\mathbf{x}(t) + D_z \frac{d\mathbf{x}(t)}{dt} + C_z + \eta \tag{3-2}$$

$$z(t) = A\mathbf{x}(t) + \eta \tag{3-3}$$

The derived current and voltage measurement has the same expression as actual one. The pseudo voltage measurement has the same expression as actual one.

For virtual measurements, the linear one and non-linear one can be expressed by Equation (3-4) and Equation (3-5), respectively.

$$0 = Y_{zx}\mathbf{x}(t) + D_z \frac{d\mathbf{x}(t)}{dt} + C_z + \eta \tag{3-4}$$

$$0 = Y_{zx}\mathbf{x}(t) + \mathbf{x}(t)^T F_{zx}\mathbf{x}(t) + C_z + \eta \tag{3-5}$$

In summary, any measurement in the above four groups can be described as an equation that consist of the measurement value and a corresponding function that express this measurement in terms of state variables. All of these expressions can be stacked into a matrix form, referred to as the **Q**uadratized **D**ynamic **M**easurement (QDM) model:

$$z_1(t) = Y_{zx1}\mathbf{x}(t) + D_{z1} \frac{d\mathbf{x}(t)}{dt} + C_{z1} + \eta_1$$

$$z_2(t) = Y_{zx2}\mathbf{x}(t) + D_{z2} \frac{d\mathbf{x}(t)}{dt} + C_{z2} + \eta_2$$

$$z_3(t) = Y_{zx3}\mathbf{x}(t) + \begin{Bmatrix} \vdots \\ \mathbf{x}(t)^T \left\langle F_{zx3}^i \right\rangle \mathbf{x}(t) \\ \vdots \end{Bmatrix} + C_{z3} + \eta_3$$

Where:

$z_1(t)$: through measurement variables

$z_2(t)$: linear virtual measurement variables with zero quantity

$z_3(t)$: nonlinear virtual measurement variables with zero quantity and voltage measurement variables

$\mathbf{x}(t)$: external and internal state variables of the measurement model

Y_{zx1} : matrix defining the linear part for state variables in through measurement equations

D_{z1} : matrices defining the differential part for state variables in through measurement equations

C_{z1} : constant vector in through measurement equations

η_1 : noise vector in through measurement equations

Y_{zx2} : matrix defining the linear part for state variables in linear virtual measurement equations

D_{z2} : matrices defining the differential part for state variables in linear virtual measurement equations

C_{z2} : constant vector in linear virtual measurement equations

η_2 : noise vector in linear virtual measurement equations

Y_{zx3} : matrix defining the linear part for state variables in the remaining measurement equations.

F_{zx3}: matrix defining the quadratic part for state variables in the remaining measurement equations

C_{z3}: constant vector in the remaining measurement equations

η_3: noise vector in the remaining measurement equations

3.4 Algebraic Quadratic Companion Form (AQCF)

The quadratized dynamic measurement model has been derived in previous section. When solving these algebraic and differential equations, we need to eliminate these differential terms and convert the equation to an algebraic one. Here, the quadratic integration is performed to generate the algebraic quadratic companion form (AQCF) measurement model.

The quadratic integration is a member of the family of implicit Runge-Kutta methods. It assumes that time domain function varies quadratically within an integration time step h, as shown in Figure 3-2 [37]. The quadratic curve can be expressed as:

$$x(\tau) = a + b\tau + c\tau^2, \tau \in [0, \mathrm{h}]$$

Where the coefficients a, b and c can be fully determined by the three points $x(t)$, $x(t_m)$ and $x(t-h)$ as:

$$a = x(t-h)\,;\; b = \frac{1}{h}(-3x(t-h) + 4x(t_m) - x(\mathrm{t}))\,;\; c = \frac{2}{h^2}(x(t-h) - 2x(t_m) + x(\mathrm{t}))$$

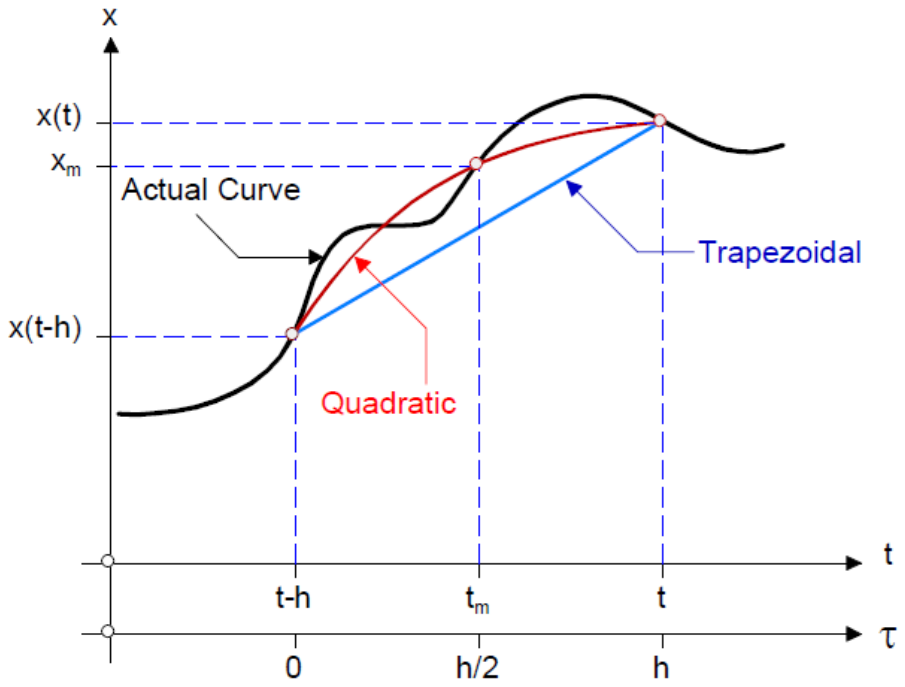

Figure 3-2 Quadratic integration illustration

Then, the general integration results of $x(\mathrm{t})$ over time interval $[t-h,t]$ and $[t-h,t_m]$ is:

$$\int_{t-h}^{t} x(\mathrm{t})\,\mathrm{dt} = \frac{h}{6}x(\mathrm{t}) + \frac{2h}{3}x(\mathrm{t}_m) + \frac{h}{6}x(\mathrm{t}-\mathrm{h})$$

$$\int_{t-h}^{t_m} x(\mathrm{t})\,\mathrm{dt} = -\frac{h}{24}x(\mathrm{t}) + \frac{h}{3}x(\mathrm{t}_m) + \frac{5h}{24}x(\mathrm{t}-\mathrm{h})$$

After applying this quadratic integration to the quadratized dynamic measurement model, the AQCF measurement model is obtained as follows:

$$z\left(t,t_m\right)=\mathbf{h}(\mathbf{x}(t,t_m))=\mathbf{Y}_{mz}\mathbf{x}(t,t_m)+\left\{\begin{array}{c}\vdots\\ \mathbf{x}(t,t_m)^T\mathbf{F}_{mz}^i\mathbf{x}(t,t_m)\\ \vdots\end{array}\right\}+\mathbf{B}_{eq}+\boldsymbol{\eta}_z$$

$$\mathbf{B}_{eq}=\mathbf{N}_{mz}\mathbf{x}(t-h)+\mathbf{M}_{mz}\mathbf{i}(t-h)+\mathbf{K}_{mz}$$

where $\boldsymbol{z}(t,t_m)=[\boldsymbol{z}(\mathrm{t}),\boldsymbol{z}(t_m)]^T$, $\boldsymbol{x}(t,t_m)=[\boldsymbol{x}(\mathrm{t}),\boldsymbol{x}(t_m)]^T$. $\boldsymbol{\eta}_z$ is the error vector in AQCF measurement model Matrices $\boldsymbol{Y}_{mz}$, $\boldsymbol{F}_{mz}$, $\boldsymbol{N}_{mz}$, $\boldsymbol{M}_{mz}$, $\boldsymbol{K}_{mz}$ are coefficient matrices, which can be calculated as:

$$\mathbf{Y}_{mz}=\begin{bmatrix}\frac{4}{h}D_{z1}+Y_{zx1} & -\frac{8}{h}D_{z1}\\ \frac{4}{h}D_{z2}+Y_{zx2} & -\frac{8}{h}D_{z2}\\ Y_{zx3} & 0\\ \frac{1}{2h}D_{z1} & \frac{2}{h}D_{z1}+Y_{zx1}\\ \frac{1}{2h}D_{z2} & \frac{2}{h}D_{z1}+Y_{zx2}\\ 0 & Y_{zx3}\end{bmatrix}$$

$$\mathbf{N}_{mz}=\begin{bmatrix}-Y_{zx1}+\frac{4}{h}D_{z1}\\ -Y_{zx2}+\frac{4}{h}D_{z2}\\ 0\\ \frac{1}{2}Y_{zx1}-\frac{5}{2h}D_{z1}\\ \frac{1}{2}Y_{zx2}-\frac{5}{2h}D_{z2}\\ 0\end{bmatrix}$$

$$\mathbf{M}_{mz} = \begin{bmatrix} I_{size(z_1(t))} \\ 0 \\ 0 \\ -\frac{1}{2} I_{size(z_1(t))} \\ 0 \\ 0 \end{bmatrix}$$

$$\mathbf{F}_{mz} = \begin{bmatrix} 0 & 0 \\ 0 & 0 \\ F_{zx3} & 0 \\ 0 & 0 \\ 0 & 0 \\ 0 & F_{zx3} \end{bmatrix}$$

$$\mathbf{K}_{mz} = \begin{bmatrix} 0 \\ 0 \\ C_{z3} \\ \frac{3}{2} C_{z1} \\ \frac{3}{2} C_{z2} \\ C_{z3} \end{bmatrix}$$

3.5 Summary

The AQCF measurement model derivation is presented in this chapter. It starts from the quadratized dynamic device model by introducing additional state variables to decrease the equation order to 2. Then, with the measurement definition, the quadratized dynamic measurement (QDM) model can be obtained. In order to eliminate the differential terms in the QDM model, the quadratic integration is applied and therefore the AQCF measurement model is derived. The dynamic state estimation algorithm (which will be introduced in Chapter 4) will be performed on the AQCF measurement model.

CHAPTER 4. DYNAMIC STATE ESTIMATION

4.1 Overview

The WLS-DSE has demonstrated satisfactory performance on providing accurate estimation of state variables. In this chapter, the detailed algorithm of WLS-DSE will be introduced. It is performed on the AQCF measurement model to estimate state variables. The DSE-based protection logic is also described in this chapter.

4.2 WLS-DSE Algorithm

The weighted least-square method is used to formulate the dynamic state estimation. This formulation is started by expressing the measurement in terms of the state variables and some unknown measurement errors $\boldsymbol{\eta}_z$ as follows:

$$\mathbf{z}(t,t_m) = \mathbf{h}(\mathbf{x}(t,t_m)) + \eta = \mathbf{Y}_{mz}\mathbf{x}(t,t_m) + \left\{ \begin{array}{c} \vdots \\ \mathbf{x}(t,t_m)^T \mathbf{F}_{mz}^i \mathbf{x}(t,t_m) \\ \vdots \end{array} \right\} + \mathbf{B}_{eq} + \boldsymbol{\eta}_z$$

$$\mathbf{B}_{eq} = \mathbf{N}_{mz}\mathbf{x}(t-h) + \mathbf{M}_z\mathbf{i}(t-h) + \mathbf{K}_{mz}$$

The WLS-DSE algorithm has demonstrated satisfactory performance on providing accurate estimation of state variables. This method is defined as:

$$Min\ J = \left(\mathbf{z}\left(t,t_m\right) - \mathbf{h}\left(\mathbf{x}\left(t,t_m\right)\right)\right)^T \mathbf{W}\left(\mathbf{z}\left(t,t_m\right) - \mathbf{h}\left(\mathbf{x}\left(t,t_m\right)\right)\right)$$

where the weight matrix $\mathbf{W} = diag(1/\sigma_1^2, 1/\sigma_2^2, \cdots, 1/\sigma_i^2, ...)$ and σ_i is the measurement error standard deviation corresponds to the meter error specification. The measurement error η_i has the following statistics:

$$E(\eta_i) = 0$$

$$\text{var}(\eta_i) = \sigma_i^2,$$

$$E(\eta_i \eta_j) = 0, i \neq j$$

The best estimate of the state is obtained from the Gauss-Newton iterative algorithm:

$$\hat{\mathbf{x}}(t,t_m)^{\nu+1} = \hat{\mathbf{x}}(t,t_m)^{\nu} + (\mathbf{H}^{\mathbf{T}}\mathbf{W}\mathbf{H})^{-1}\mathbf{H}^{\mathbf{T}}\mathbf{W}(\mathbf{z}(t,t_m) - \mathbf{h}(\hat{x}(t,t_m)^{\nu}))$$

where $\hat{\mathbf{x}}(t,t_m)$ refers to the best estimate of the state vector $\mathbf{x}(t,t_m)$, and $\mathbf{H} = \frac{\partial \mathbf{h}(\mathbf{x}(t,t_m))}{\partial \mathbf{x}(t,t_m)}$ is the Jacobean matrix of the measurement equations.

The flow chart of the WLS-DSE algorithm is described in Figure 4-1.

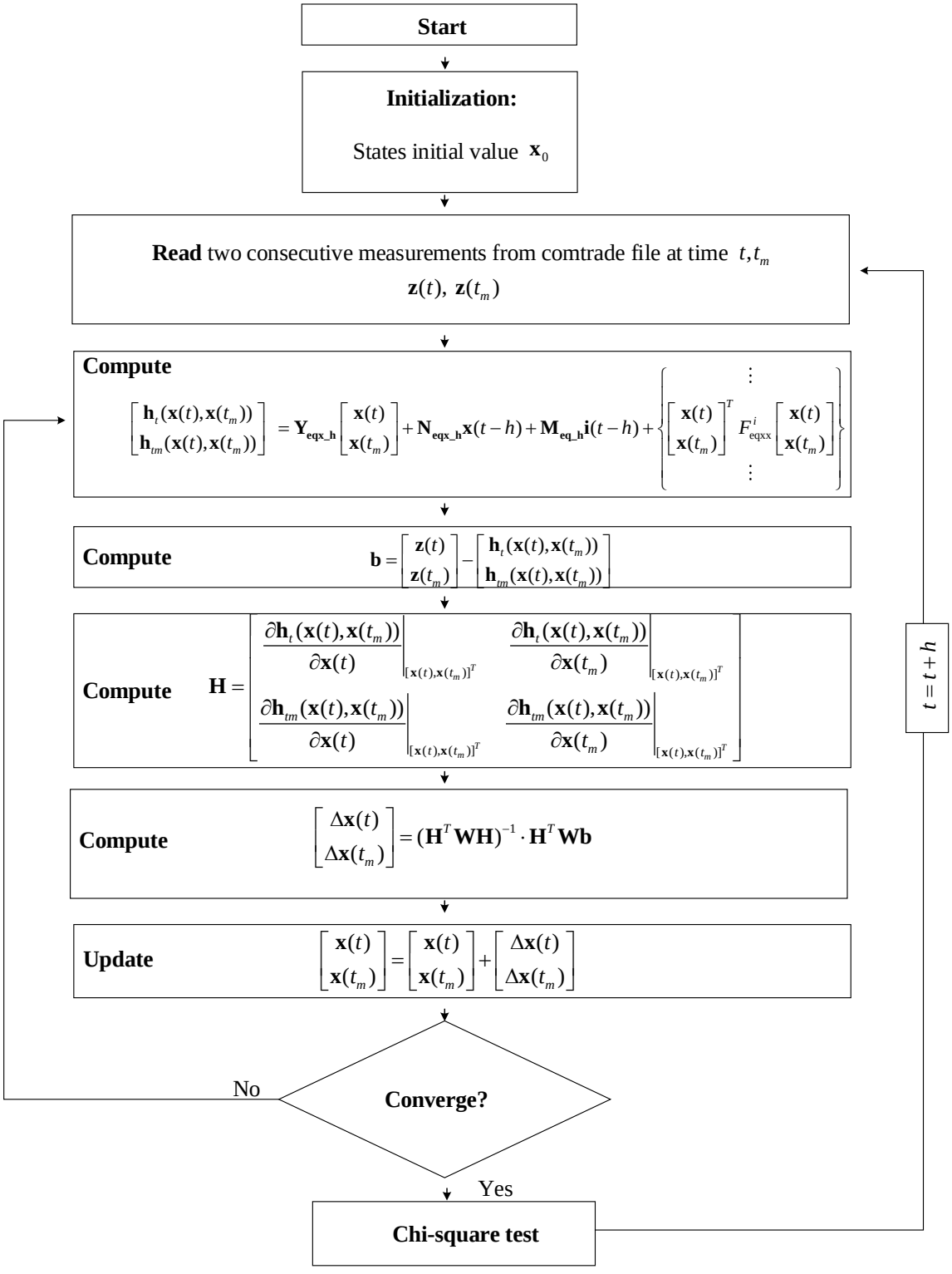

Figure 4-1 The flow chart of WLS-DSE algorithm

4.3 DSE-Based Protection Logic

Dynamic state estimation can be applied to monitor the consistency between the protection zone measurement model and the real-time measurement quantities. This concept can be illustrated by Figure 4-2. All the available physical laws that must be satisfied are expressed by the protection zone measurement model. If any physical law is violated, the dynamic state estimation is able to capture this abnormality.

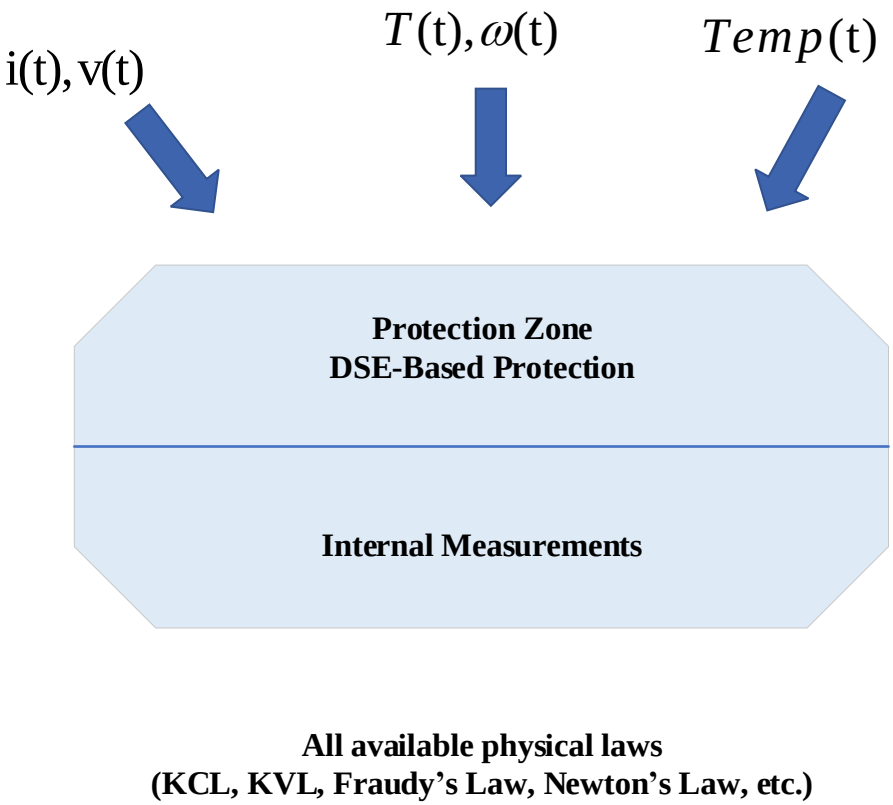

Figure 4-2 Concept of DSE-based protection

The goodness of fit is defined as the probability that the distribution of the measurement errors is within the expected bounds. This probability is called confidence level and is calculated via the well-known Chi-square test as:

$$P_{conf}(t) = \Pr\left[\chi^2 \geq \zeta(t)\right] = 1 - \mathrm{P}(\zeta(t), v) \tag{4-1}$$

$$\zeta(t) = \sum_{i=1}^{m} \left(\frac{z_i(t,t_m) - h_i(\hat{\mathbf{x}}(t,t_m))}{\sigma_i} \right)^2 \tag{4-2}$$

where $\mathrm{P}(\zeta(t), v)$ is the probability of χ^2 distribution given $\chi^2 \leq \zeta(t)$ with degrees of freedom $v = m - n$, which is shown in Figure 4-3.

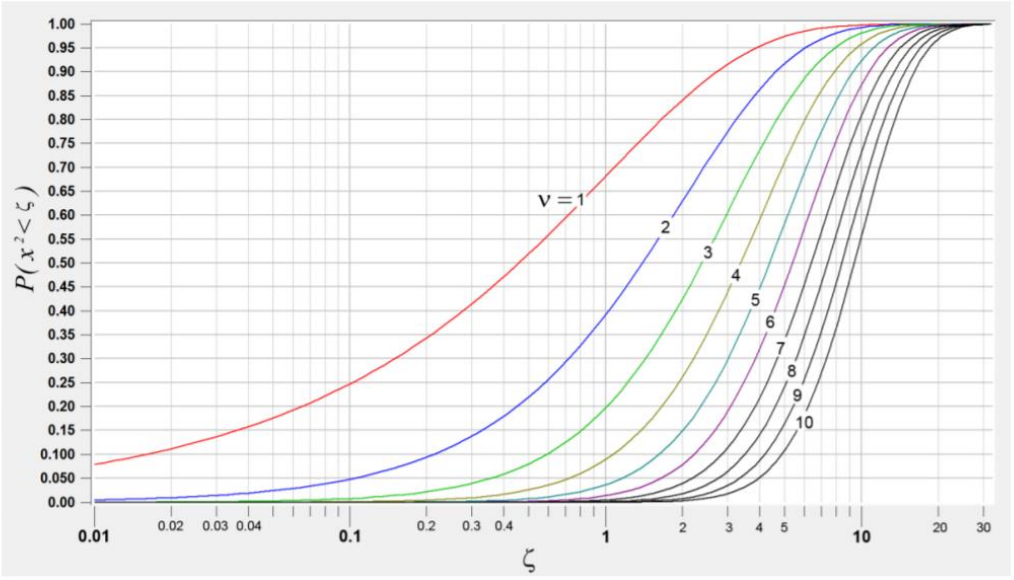

Figure 4-3 Chi-square probability distribution function [37]

A high confidence level means the actual residuals are comparable to the expected errors of the measurements. While a low confidence level implies inconsistency between measurements and model.

The results of the chi-square test can be used for different applications. For the DSE-based protection, the confidence level is used for trip decision. When the confidence level is very low, it means that there is inconsistency between measurements and model, which implies a fault occurring within the protection zone. As for external fault happens, since the measurement can still fit the model, the confidence level can keep at a high value. The protection logic is stated as follows:

$$Trip\_Signal(\mathrm{t}) = \begin{cases} 1, & if \;\; Trip\_Value(\mathrm{t}) \geq \tau_{delay} \\ 0, & if \;\; Trip\_Value(\mathrm{t}) < \tau_{delay} \end{cases} \tag{4-3}$$

$$Trip\_Value(\mathrm{t}) = \int_{t-\tau_{reset}}^{t} (1 - P_{conf}(t))dt$$

Where τ_{reset} and τ_{delay} are the user-defined settings of DSE-based protection.

4.4 Summary

The dynamic state estimation method is presented in this Chapter. The WLS-DSE algorithm has demonstrated satisfactory performance to provide best estimate of state variables. The dynamic state estimation and Chi-square test results can be applied for protection scheme, as known as DSE-based protection or setting-less protection, which can identify internal faults within a protection zone and ignore the external faults.

CHAPTER 5. INSTRUMENTATION CHANNEL ERROR CORRECTION

5.1 Overview

This chapter presents in detail the proposed instrumentation channel error correction method.

In Section 5.2 and Section 5.3, the dynamic device model of current transformer (CT), potential transformer (PT), instrumentation cable and burden resistor are developed. Then, the measurement model for current and voltage instrumentation channel are constructed and are expressed in the syntax of QDM. After applying the quadratic integration, the AQCF measurement model is obtained. The primary samples are estimated through performing DSE on the AQCF measurement model.

In Section 5.4 and 5.5, the error correction results for current instrumentation channel and voltage instrumentation channel are demonstrated through example cases. In Section 5.4, for current instrumentation channel, the error correction results regarding different CT saturation scenarios and different CT ratio cases are presented. In Section 5.5, for voltage instrumentation channel, there are two standard secondary voltage, which is 115 V and 69 V. The error correction results for each of them is also demonstrated.

5.2 Current Instrumentation Channel Measurement Model

5.2.1 Basic Question

A typical current instrumentation channel configuration is depicted in Figure 5-1 [38]. It has three components: the current transformer (CT), the instrumentation cable and the burden resistor. The current instrumentation subsystem is used to convert the high current of the power system into instrumentation level currents that can be fed into the Merging Unit. Standard currents for Merging Unit are 5A and 1A.

Ideally, the currents fed into the merging unit should be scaled replicas of the high currents of electric power system. Practically, however, the current instrumentation channels introduce errors that can distort the secondary waveforms when CT saturates. In other words, the errors introduced by current instrumentation channel will lead to inaccurate primary samples as input to protective relays, which can result in protection mis-operations.

The error correction problem is stated as follows: a measurement is taken of the voltage across the burden to estimate the electric current in the primary of CT. As shown in Figure 5-1, the actual measurement we have is the voltage across the burden resistor, which is "v_{out} ". The current to be estimated is the CT's primary current, i.e. i_p . For this purpose, the dynamic state estimation method will be utilized to estimate i_p.

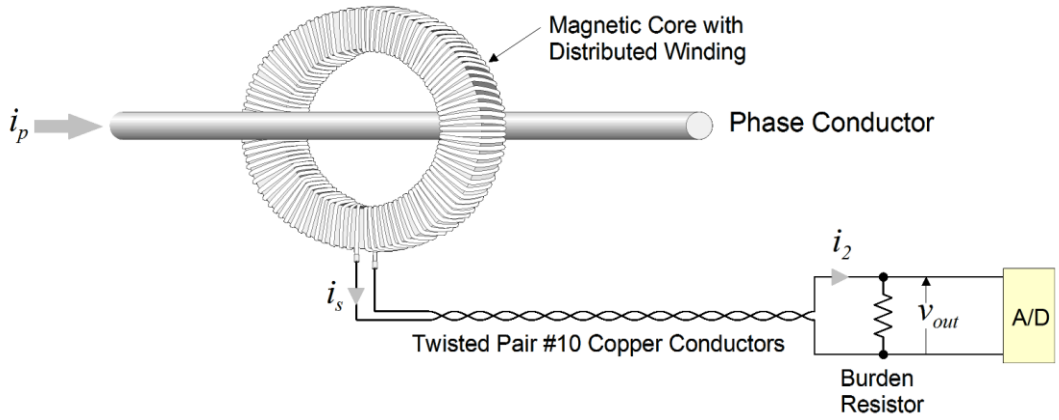

Figure 5-1 Typical current instrumentation channel configuration

5.2.2 Current Transformer Model

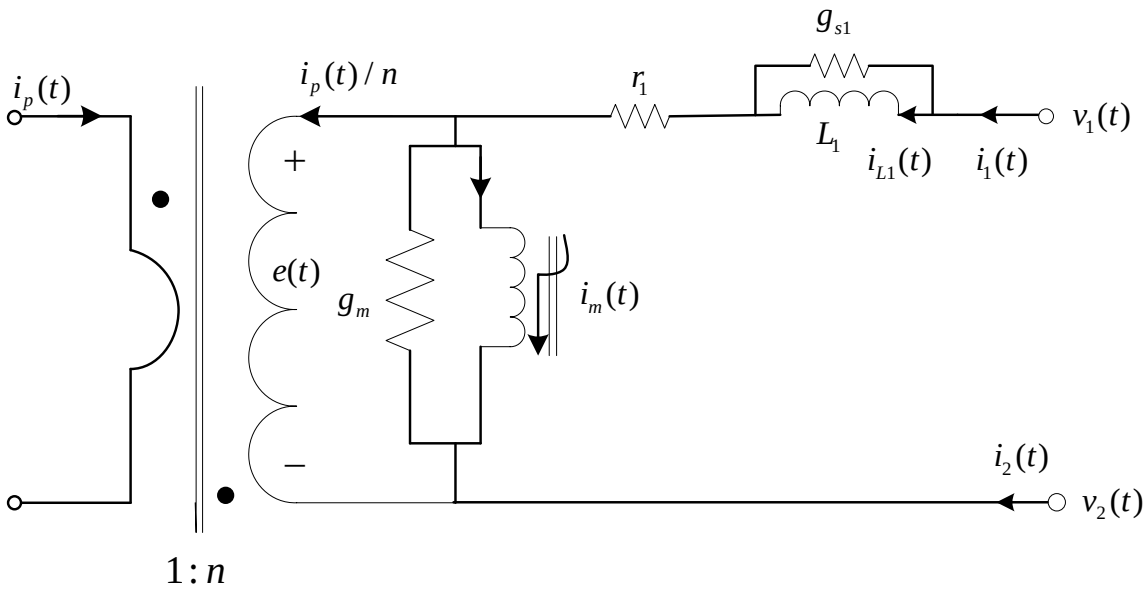

Figure 5-2 Equivalent circuit of CT with saturable core

The CT equivalent circuit is illustrated in Figure 5-2. The nonlinear magnetic characteristics is the key factor of CT saturation. The proposed error correction method is

based on a CT model with saturable core, which is an experimental model [40]. The dynamic model of current transformer is developed as follows:

$$i_1(t) = \frac{1}{n} i_p(t) + g_m e(t) + i_m(t) \tag{5-1}$$

$$i_2(t) = -\frac{1}{n} i_p(t) - g_m e(t) - i_m(t) \tag{5-2}$$

$$0 = -v_1(t) + v_2(t) + \frac{r_1}{n} i_p(t) + (1 + r_1 g_m) e(t) + r_1 i_m(t) + L_1 \frac{di_{L1}(t)}{dt} \tag{5-3}$$

$$0 = -\frac{1}{n} i_p(t) + i_{L1}(t) - g_m e(t) - i_m(t) \tag{5-4}$$

$$0 = e(t) - \frac{d\lambda(t)}{dt} \tag{5-5}$$

$$0 = i_m(t) - i_0 \left(\frac{\lambda(t)}{\lambda_0} \right)^{11} - \frac{1}{L_0} \lambda(t) \tag{5-6}$$

Observe that the Equation (5-6) is nonlinear (exponent of 11). This equation is quadratized by introducing additional state variables to decrease the equation order to 2. Therefore, equation (5-6) will be replaced by the following equations:

$$0 = i_m(t) - \frac{1}{L_0} \lambda(t) - \frac{i_0}{\lambda_0} \lambda(t) y_4(t)$$

$$0 = y_1(t) - \frac{1}{\lambda_0^2} \lambda^2(t)$$

$$0 = y_2(t) - y_1^2(t)$$

$$0 = y_3(t) - y_2^2(t)$$

$$0 = y_4(t) - y_3(t) y_1(t)$$

Hence, the quadratized dynamic model of current transformer is summarized as in Equation (5-7) ~ (5-17):

$$i_1(t) = \frac{1}{n} i_p(t) + g_m e(t) + i_m(t) \tag{5-7}$$

$$i_2(t) = -\frac{1}{n} i_p(t) - g_m e(t) - i_m(t) \tag{5-8}$$

$$0 = -v_1(t) + v_2(t) + \frac{r_1}{n} i_p(t) + (1 + r_1 g_m) e(t) + r_1 i_m(t) + L_1 \frac{di_{L1}(t)}{dt} \tag{5-9}$$

$$0 = -\frac{1}{n} i_p(t) + i_{L1}(t) - g_m e(t) - i_m(t) \tag{5-10}$$

$$0 = -v_1(t) + v_2(t) + \frac{r_1}{n} i_p(t) + (1 + r_1 g_m) e(t) + r_1 i_m(t) + L_1 \frac{di_{L1}(t)}{dt} \tag{5-11}$$

$$0 = e(t) - \frac{d\lambda(t)}{dt} \tag{5-12}$$

$$0 = i_m(t) - \frac{1}{L_0} \lambda(t) - \frac{i_0}{\lambda_0} \lambda(t) y_4(t) \tag{5-13}$$

$$0 = y_1(t) - \frac{1}{\lambda_0^2} \lambda^2(t) \tag{5-14}$$

$$0 = y_2(t) - y_1^2(t) \tag{5-15}$$

$$0 = y_3(t) - y_2^2(t) \tag{5-16}$$

$$0 = y_4(t) - y_3(t) y_1(t) \tag{5-17}$$

5.2.3 Instrumentation Cable Model

Traditional substation instrumentation typically includes long runs of cables connecting the CT secondary outputs to multiple relays. However, the emergence of MU makes it possible to use short cables which directly connect the CT secondary outputs to

MU. Hence, a π-equivalent circuit is developed to represent the instrumentation cable, as depicted in Figure 5-3.

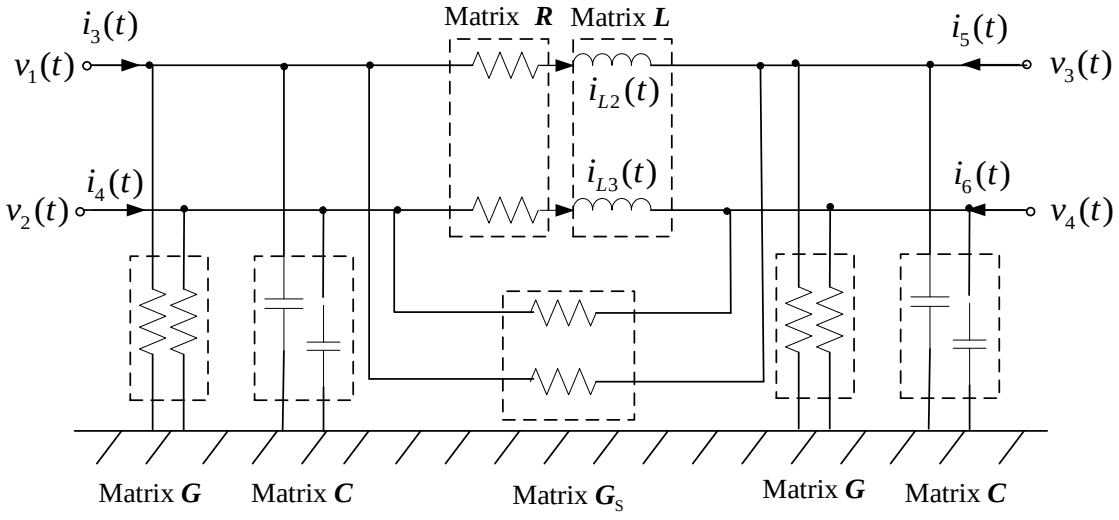

Figure 5-3 π-equivalent circuit of instrumentation cable

The π-equivalent circuit model can be described as:

$$\boldsymbol{i}_k(t) = \left(\boldsymbol{G} + \boldsymbol{G}_S\right) \cdot \boldsymbol{v}_k(t) - \boldsymbol{G}_S \cdot \boldsymbol{v}_{k+1}(t) + \boldsymbol{C} \cdot \frac{d\boldsymbol{v}_k(t)}{dt} + \boldsymbol{i}_{Lk}(t) \tag{5-18}$$

$$\boldsymbol{i}_{k+1}(t) = \left(\boldsymbol{G} + \boldsymbol{G}_S\right) \cdot \boldsymbol{v}_{k+1}(t) - \boldsymbol{G}_S \cdot \boldsymbol{v}_k(t) + \boldsymbol{C} \cdot \frac{d\boldsymbol{v}_{k+1}(t)}{dt} - \boldsymbol{i}_{Lk}(t) \tag{5-19}$$

$$\boldsymbol{0} = -\boldsymbol{v}_k(t) + \boldsymbol{v}_{k+1}(t) + \boldsymbol{R} \cdot \boldsymbol{i}_{Lk}(t) + \boldsymbol{L} \cdot \frac{d\boldsymbol{i}_{Lk}(t)}{dt} \tag{5-20}$$

where:

$$\boldsymbol{v}_k(t) = \begin{bmatrix} v_1(t) \\ v_2(t) \end{bmatrix},\ \boldsymbol{v}_{k+1}(t) = \begin{bmatrix} v_3(t) \\ v_4(t) \end{bmatrix}$$

$$\boldsymbol{i}_k(t) = \begin{bmatrix} i_3(t) \\ i_4(t) \end{bmatrix},\ \boldsymbol{i}_{k+1}(t) = \begin{bmatrix} i_5(t) \\ i_6(t) \end{bmatrix}$$

$$\boldsymbol{i}_{Lk}(t) = \begin{bmatrix} i_{L2}(t) \\ i_{L3}(t) \end{bmatrix}$$

5.2.4 Burden Resistor Model

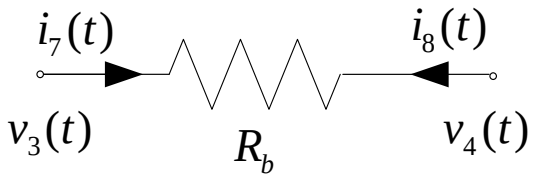

Figure 5-4 Equivalent circuit of burden resistor

The burden of MU is represented by a resistor connected to the instrumentation cable, as shown in Figure 5-4. The burden resistor model is described in Equation (5-21) and Equation (5-22).

$$i_7(t) = (v_3(t) - v_4(t)) / R_b \tag{5-21}$$

$$i_8(t) = (v_4(t) - v_3(t)) / R_b \tag{5-22}$$

5.2.5 Construct Measurement Model of Current Instrumentation Channel

In Section 5.2.2 ~ Section 5.2.4, we have introduced each device model in the current instrumentation channel. Now, the equivalent circuit of the entire current instrumentation channel is described in Figure 5-5. The quadratized dynamic

measurement model of current instrumentation channel is defined in terms of a number of state variables, which is:

$$\mathbf{x} = \begin{bmatrix} 1 & 2 & 3 & 4 & 5 & 6 & 7 & 8 & 9 & 10 & 11 & 12 & 13 & 14 & 15 \\ v_1(t) & v_2(t) & v_3(t) & v_4(t) & i_p(t) & i_{L1}(t) & e(t) & \lambda(t) & i_m(t) & i_{L2}(t) & i_{L3}(t) & y_1(t) & y_2(t) & y_3(t) & y_4(t) \end{bmatrix}$$

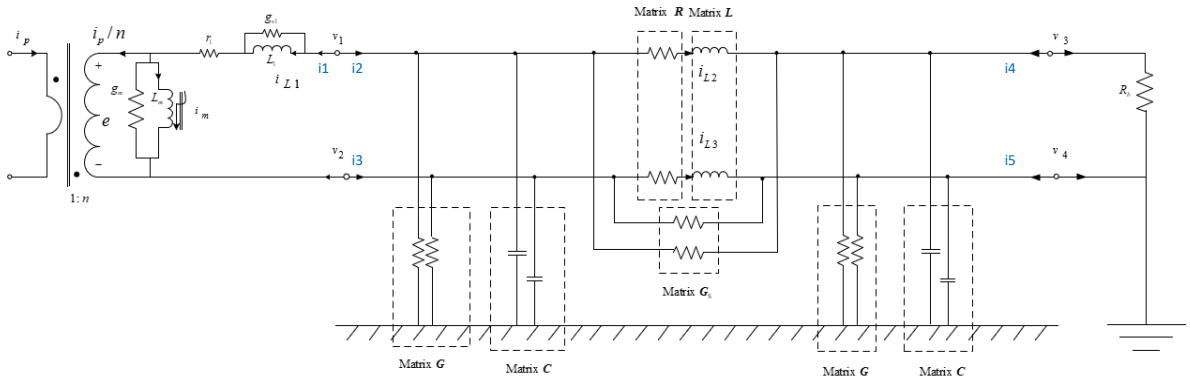

Figure 5-5 Equivalent circuit of current instrumentation channel

Any measurement taken on this circuit can be expressed as a function of the instrumentation channel state variables. In Chapter 3, we have introduced that measurements can be divided into 4 groups. Here, we will specify the actual, virtual, derived and pseudo measurements for current instrumentation channel as follows.

1) Actual measurements: The only actual measurement here is the voltage across the burden resistor:

$$v_{out}(t) = v_3(t) - v_4(t)$$

2) Derived measurements:

$$i_1(t) = i_{L1}(t) + g_{s1}L_1 \frac{di_{L1}(t)}{dt}$$

$$i_2(t) = g_{s11}v_1(t) - g_{s11}v_3(t) + i_{L2}(t) + c_{11}\frac{dv_1(t)}{dt} + c_{12}\frac{dv_2(t)}{dt}$$

$$i_3(t) = g_{s22}v_2(t) - g_{s22}v_4(t) + i_{L3}(t) + c_{21}\frac{dv_1(t)}{dt} + c_{22}\frac{dv_2(t)}{dt}$$

$$i_4(t) = -g_{s11}v_1(t) + g_{s11}v_3(t) - i_{L2}(t) + c_{11}\frac{dv_3(t)}{dt} + c_{12}\frac{dv_4(t)}{dt}$$

$$i_5(t) = -g_{s22}v_2(t) + g_{s22}v_4(t) - i_{L3}(t) + c_{21}\frac{dv_3(t)}{dt} + c_{22}\frac{dv_4(t)}{dt}$$

3) Virtual measurements: All internal equations and KCL equations at interface node are treated as virtual measurements:

$$0 = -v_1(t) + v_2(t) + \frac{r_1}{n}i_p(t) + (1 + r_1 g_m)e(t) + r_1 i_m(t) + L_1\frac{di_{L1}(t)}{dt}$$

$$0 = -\frac{1}{n}i_p(t) + i_{L1}(t) - g_m e(t) - i_m(t) + g_{s1}L_1\frac{di_{L1}(t)}{dt}$$

$$0 = e(t) - \frac{d\lambda(t)}{dt}$$

$$0 = g_{s11}v_1(t) - g_{s11}v_3(t) + \frac{1}{n}i_p(t) + g_m e(t) + i_m(t) + i_{L2}(t) + c_{11}\frac{dv_1(t)}{dt} + c_{12}\frac{dv_2(t)}{dt}$$

$$0 = g_{s22}v_2(t) - g_{s22}v_4(t) - \frac{1}{n}i_p(t) - g_m e(t) - i_m(t) + i_{L3}(t) + c_{21}\frac{dv_1(t)}{dt} + c_{22}\frac{dv_2(t)}{dt}$$

$$0 = -g_{s11}v_1(t) + (g_{s11} + \frac{1}{R_b})v_3(t) - \frac{1}{R_b}v_4(t) - i_{L2}(t) + c_{11}\frac{dv_3(t)}{dt} + c_{12}\frac{dv_4(t)}{dt}$$

$$0 = -g_{s22} v_2(t) - \frac{1}{R_b} v_3(t) + (g_{s22} + \frac{1}{R_b}) v_4(t) - i_{L3}(t) + c_{21} \frac{dv_3(t)}{dt} + c_{22} \frac{dv_4(t)}{dt}$$

$$0 = -v_1(t) + v_3(t) + r_{11} i_{L2}(t) + r_{12} i_{L3}(t) + L_{11} \frac{di_{L2}(t)}{dt} + L_{12} \frac{di_{L3}(t)}{dt}$$

$$0 = -v_2(t) + v_4(t) + r_{21} i_{L2}(t) + r_{22} i_{L3}(t) + L_{21} \frac{di_{L2}(t)}{dt} + L_{22} \frac{di_{L3}(t)}{dt}$$

$$0 = i_m(t) - \frac{1}{L_0} \lambda(t) - \frac{i_0}{\lambda_0} \lambda(t) y_4(t)$$

$$0 = y_1(t) - \frac{1}{\lambda_0^2} \lambda^2(t)$$

$$0 = y_2(t) - y_1^2(t)$$

$$0 = y_3(t) - y_2^2(t)$$

$$0 = y_4(t) - y_3(t) y_1(t)$$

4) Pseudo measurements: Here, the ground point voltage is unknown (and difficult to measure). Since the voltage at the ground point is expected to be near zero, it is treated as a pseudo measurement:

$$0 = v_4(t)$$

In summary, there are 21 measurement equations and the number of state variables is 15. The above QDM of measurements can be written in the QDM syntax as:

$$z_1(t) = Y_{zx1} \mathbf{x}(t) + D_{z1} \frac{d\mathbf{x}(t)}{dt} + C_{z1} + \eta_1$$

$$z_2(t) = Y_{zx2}\mathbf{x}(t) + D_{z2}\frac{d\mathbf{x}(t)}{dt} + C_{z2} + \eta_2$$

$$z_3(t) = Y_{zx3}\mathbf{x}(t) + \left\{ \begin{array}{c} \vdots \\ \mathbf{x}(t)^T \left\langle F_{zx3}^i \right\rangle \mathbf{x}(t) \\ \vdots \end{array} \right\} + C_{z3} + \eta_3$$

Where:

$$z_1(t) = [i_1(t) \quad i_2(t) \quad i_3(t) \quad i_4(t) \quad i_5(t)]^T;$$

$$z_2(t) = [0 \quad 0 \quad ... \quad 0 \quad 0]^T$$

$$z_3(t) = \left[0 \quad 0 \quad 0 \quad 0 \quad 0 \quad Vout(t) \quad 0\right]^T$$

$$Y_{zx1} = \begin{bmatrix} 0 & 0 & 0 & 0 & 0 & 1.0 & 0 & 0 & 0 & 0 & 0 & 0 & 0 & 0 & 0 \\ g_{s11} & 0 & -g_{s11} & 0 & 0 & 0 & 0 & 0 & 0 & 1.0 & 0 & 0 & 0 & 0 & 0 \\ 0 & g_{s22} & 0 & -g_{s22} & 0 & 0 & 0 & 0 & 0 & 0 & 1.0 & 0 & 0 & 0 & 0 \\ -g_{s11} & 0 & g_{s11} & 0 & 0 & 0 & 0 & 0 & 0 & -1.0 & 0 & 0 & 0 & 0 & 0 \\ 0 & -g_{s22} & 0 & g_{s22} & 0 & 0 & 0 & 0 & 0 & 0 & -1.0 & 0 & 0 & 0 & 0 \end{bmatrix}$$

$$D_{z1} = \begin{bmatrix} 0 & 0 & 0 & 0 & 0 & g_{s1}L_1 & 0 & 0 & 0 & 0 & 0 & 0 & 0 & 0 & 0 \\ c_{11} & c_{12} & 0 & 0 & 0 & 0 & 0 & 0 & 0 & 0 & 0 & 0 & 0 & 0 & 0 \\ c_{21} & c_{22} & 0 & 0 & 0 & 0 & 0 & 0 & 0 & 0 & 0 & 0 & 0 & 0 & 0 \\ 0 & 0 & c_{11} & c_{12} & 0 & 0 & 0 & 0 & 0 & 0 & 0 & 0 & 0 & 0 & 0 \\ 0 & 0 & c_{21} & c_{22} & 0 & 0 & 0 & 0 & 0 & 0 & 0 & 0 & 0 & 0 & 0 \end{bmatrix}$$

$$Y_{zx2} = \begin{bmatrix} -1.0 & 1.0 & 0 & 0 & -\frac{r_1}{n} & 0 & 1+r_1 g_m & 0 & r_1 & 0 & 0 & 0 & 0 & 0 & 0 \\ 0 & 0 & 0 & 0 & -\frac{1}{n} & 1.0 & -g_m & 0 & -1.0 & 0 & 0 & 0 & 0 & 0 & 0 \\ 0 & 0 & 0 & 0 & 0 & 0 & 0 & 1.0 & 0 & 0 & 0 & 0 & 0 & 0 & 0 \\ g_{s11} & 0 & -g_{s11} & 0 & \frac{1}{n} & 0 & g_m & 0 & 1.0 & 1.0 & 0 & 0 & 0 & 0 & 0 \\ 0 & g_{s22} & 0 & -g_{s22} & -\frac{1}{n} & 0 & -g_m & 0 & -1.0 & 0 & 1.0 & 0 & 0 & 0 & 0 \\ -g_{s11} & 0 & g_{s11}+g_b & -g_b & 0 & 0 & 0 & 0 & 0 & -1.0 & 0 & 0 & 0 & 0 & 0 \\ 0 & -g_{s22} & -g_b & g_{s22}+g_b & 0 & 0 & 0 & 0 & 0 & 0 & -1.0 & 0 & 0 & 0 & 0 \\ -1.0 & 0 & 1.0 & 0 & 0 & 0 & 0 & 0 & 0 & r_{11} & r_{12} & 0 & 0 & 0 & 0 \\ 0 & -1.0 & 0 & 1.0 & 0 & 0 & 0 & 0 & 0 & r_{21} & r_{22} & 0 & 0 & 0 & 0 \end{bmatrix}$$

$$D_{z2} = \begin{bmatrix} 0 & 0 & 0 & 0 & 0 & L_1 & 0 & 0 & 0 & 0 & 0 & 0 & 0 & 0 & 0 \\ 0 & 0 & 0 & 0 & 0 & g_{s1} L_1 & 0 & 0 & 0 & 0 & 0 & 0 & 0 & 0 & 0 \\ 0 & 0 & 0 & 0 & 0 & 0 & 0 & -1 & 0 & 0 & 0 & 0 & 0 & 0 & 0 \\ c_{11} & c_{12} & 0 & 0 & 0 & 0 & 0 & 0 & 0 & 0 & 0 & 0 & 0 & 0 & 0 \\ c_{21} & c_{22} & 0 & 0 & 0 & 0 & 0 & 0 & 1.0 & 0 & 0 & 0 & 0 & 0 & 0 \\ 0 & 0 & c_{11} & c_{12} & 0 & 0 & 0 & 0 & 0 & 0 & 0 & 0 & 0 & 0 & 0 \\ 0 & 0 & c_{21} & c_{22} & 0 & 0 & 0 & 0 & 0 & 0 & 0 & 0 & 0 & 0 & 0 \\ 0 & 0 & 0 & 0 & 0 & 0 & 0 & 0 & 0 & L_{11} & L_{12} & 0 & 0 & 0 & 0 \\ 0 & 0 & 0 & 0 & 0 & 0 & 0 & 0 & 0 & L_{21} & L_{22} & 0 & 0 & 0 & 0 \end{bmatrix}$$

$$Y_{zx3}=\begin{bmatrix} 0 & 0 & 0 & 0 & 0 & 0 & 0 & -\frac{1}{L_0} & 1.0 & 0 & 0 & 0 & 0 & 0 & 0 \\ 0 & 0 & 0 & 0 & 0 & 0 & 0 & 0 & 0 & 0 & 0 & 1.0 & 0 & 0 & 0 \\ 0 & 0 & 0 & 0 & 0 & 0 & 0 & 0 & 0 & 0 & 0 & 0 & 1.0 & 0 & 0 \\ 0 & 0 & 0 & 0 & 0 & 0 & 0 & 0 & 0 & 0 & 0 & 0 & 0 & 1.0 & 0 \\ 0 & 0 & 0 & 0 & 0 & 0 & 0 & 0 & 0 & 0 & 0 & 0 & 0 & 0 & 1.0 \\ 0 & 0 & 1.0 & -1.0 & 0 & 0 & 0 & 0 & 0 & 0 & 0 & 0 & 0 & 0 & 0 \\ 0 & 0 & 0 & 1.0 & 0 & 0 & 0 & 0 & 0 & 0 & 0 & 0 & 0 & 0 & 0 \end{bmatrix}$$

$$F_{zx3}^{1}[8][15]=-\frac{i_0}{\lambda_0},$$

$$F_{zx3}^{2}[8][8]=-\frac{1}{\lambda_0^{2}},$$

$$F_{zx3}^{3}[12][12]=-1.0,$$

$$F_{zx3}^{4}[13][13]=-1.0$$

$$F_{zx3}^{5}[12][14]=-1.0$$

$$C_{z1}=C_{z2}=C_{z3}=0$$

The definition of the state variables of current instrumentation channel are listed in Table 5-1.

Table 5-1 States of current instrumentation channel

Index	Variable	Description
1	$v_1(t)$	CT secondary bus voltage (V)
2	$v_2(t)$	CT secondary bus voltage, neutral (V)
3	$v_3(t)$	CT burden bus voltage (V)
4	$v_4(t)$	CT burden bus voltage, neutral (V)
5	$i_p(t)$	CT primary current (A)
6	$i_{L1}(t)$	Current through CT secondary inductance (A)
7	$e(t)$	Voltage generated by the flux (V)
8	$\lambda(t)$	Flux linkage (Web)
9	$i_m(t)$	Magnetizing current (A)
10	$i_{L2}(t)$	Current through cable inductance (A)
11	$i_{L3}(t)$	Current through cable inductance, neutral (A)
12	$y_1(t)$	Introduced state for quadratization (p.u.)
13	$y_2(t)$	Introduced state quadratization (p.u.)
14	$y_3(t)$	Introduced state quadratization (p.u.)
15	$y_4(t)$	Introduced state quadratization (p.u.)

As introduced in Chapter 3, the quadratic integration is performed to generate the algebraic quadratic companion form (AQCF) measurement model, which can be expressed in the matrix form as:

$$z\left(t,t_m\right)=\mathbf{h}(\mathbf{x}(t,t_m))=\mathbf{Y}_{mz}\mathbf{x}(t,t_m)+\left\{\begin{array}{c}\vdots\\ \mathbf{x}(t,t_m)^T\mathbf{F}_{mz}^i\mathbf{x}(t,t_m)\\ \vdots\end{array}\right\}+\mathbf{B}_{eq}$$

$$\mathbf{B}_{eq}=\mathbf{N}_{mz}\mathbf{x}(t-h)+\mathbf{M}_{mz}\mathbf{i}(t-h)+\mathbf{K}_{mz}$$

where time stamp t_m is intermediate time stamp of t and $t-h$. $\boldsymbol{z}(t,t_m)=[\boldsymbol{z}(\mathrm{t}),\boldsymbol{z}(t_m)]^T$, $\boldsymbol{x}(t,t_m)=[\boldsymbol{x}(\mathrm{t}),\boldsymbol{x}(t_m)]^T$. Matrices $\boldsymbol{Y}_{mz}$, $\boldsymbol{F}_{mz}$, $\boldsymbol{N}_{mz}$, $\boldsymbol{M}_{mz}$, $\boldsymbol{K}_{mz}$ are coefficient matrices and their calculation can be found in Chapter 3, Section 3.4.

5.3 Voltage Instrumentation Channel Measurement Model

The voltage instrumentation subsystem consists of potential transformer, instrumentation cable and burden resistor. It converts the high voltage of the power system into instrumentation level voltage that can be fed into the Merging Unit. Standard voltages for Merging Units are 69.3 V and 115 V. The equivalent circuit of voltage instrumentation channel is described in Figure 5-6. The error correction problem is stated as follows: a measurement is taken of the voltage across the burden to estimate the electric voltage in the primary of PT.

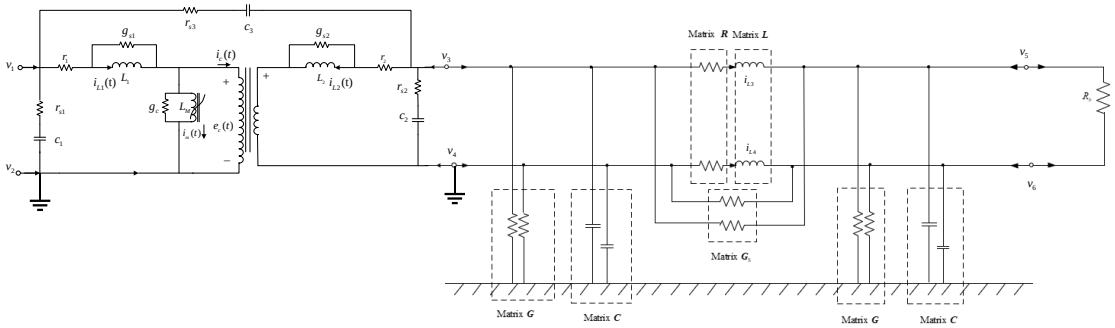

Figure 5-6 Equivalent circuit of voltage instrumentation channel

Following a similar approach for current instrumentation channel, the quadratized dynamic measurement model for the voltage instrumentation channel can be developed. There are 20 equations, which are summarized in Table 5-2and 19 state variables, which is:

$$\mathbf{x}=\begin{bmatrix} 1 & 2 & 3 & 4 & 5 & 6 & 7 & 8 & 9 & 10 & 11 & 12 & 13 & 14 & 15 & 16 & 17 & 18 & 19 \\ v_1(t) & v_2(t) & v_3(t) & v_4(t) & v_5(t) & v_6(t) & i_{L1}(t) & i_{L2}(t) & v_{c1}(t) & v_{c2}(t) & v_{c3}(t) & e(t) & i_c(t) & \lambda(t) & i_m(t) & i_{L3}(t) & i_{L4}(t) & y_1(t) & y_2(t) \end{bmatrix}$$

Table 5-2 Quadratized dynamic measurement model for voltage instrumentation channel

Index	Equation	Measurement Type
1	$0 = g_{s11}v_3(t) - g_{s11}v_5(t) + i_{L2}(t) + i_{L3}(t) + c_{11}\frac{dv_3(t)}{dt} + c_{12}\frac{dv_4(t)}{dt} + g_{s2}L_2\frac{di_{L2}(t)}{dt} + c_2\frac{dv_{c2}(t)}{dt} - c_3\frac{dv_{c3}(t)}{dt}$	Virtual Measurements
2	$0 = g_{s22}v_4(t) - g_{s22}v_6(t) - i_{L2}(t) + i_{L4}(t) + c_{21}\frac{dv_3(t)}{dt} + c_{22}\frac{dv_4(t)}{dt} - g_{s2}L_2\frac{di_{L2}(t)}{dt} - c_2\frac{dv_{c2}(t)}{dt}$	
3	$0 = -g_{s11}v_3(t) + (g_{s11} + \frac{1}{R_b})v_5(t) - \frac{1}{R_b}v_6(t) - i_{L3}(t) + c_{11}\frac{dv_5(t)}{dt} + c_{12}\frac{dv_6(t)}{dt}$	

4	$0 = -g_{s22} v_4(t) - \frac{1}{R_b} v_5(t) + (g_{s22} + \frac{1}{R_b}) v_6(t) - i_{L4}(t) + c_{21} \frac{dv_5(t)}{dt} + c_{22} \frac{dv_6(t)}{dt}$	Virtual Measurements
5	$0 = v_1(t) - v_2(t) - r_1 i_{L1}(t) - e(t) - (L_1 + r_1 \mathrm{g}_{s1} L_1) \frac{di_{L1}(t)}{dt}$	
6	$0 = v_3(t) - v_4(t) - r_2 i_{L2}(t) - \frac{1}{N} e(t) - (L_2 + r_2 \mathrm{g}_{s2} L_2) \frac{di_{L2}(t)}{dt}$	
7	$0 = v_1(t) - v_2(t) - v_{c1}(t) - r_{s1} c_1 \frac{dv_{c1}(t)}{dt}$	
8	$0 = v_1(t) - v_3(t) - v_{c3}(t) - r_{s3} c_3 \frac{dv_{c3}(t)}{dt}$	
9	$0 = v_3(t) - v_4(t) - v_{c2}(t) - r_{s2} c_2 \frac{dv_{c2}(t)}{dt}$	
10	$0 = e(t) - \frac{d\lambda(t)}{dt}$	
11	$0 = i_{L1}(t) - g_m e(t) - i_c(t) - i_m(t) + g_{s1} L_1 \frac{di_{L1}(t)}{dt}$	
12	$0 = i_{L2}(t) + \mathrm{N}\, i_c(t) + g_{s2} L_2 \frac{di_{L2}(t)}{dt}$	
13	$0 = -v_3(t) + v_5(t) + r_{11} i_{L3}(t) + r_{12} i_{L4}(t) + L_{11} \frac{di_{L3}(t)}{dt} + L_{12} \frac{di_{L4}(t)}{dt}$	
14	$0 = -v_4(t) + v_6(t) + r_{21} i_{L3}(t) + r_{22} i_{L4}(t) + L_{21} \frac{di_{L3}(t)}{dt} + L_{22} \frac{di_{L4}(t)}{dt}$	
15	$0 = i_m(t) - \frac{i_0}{\lambda_0} \lambda(t) y_2(t)$	
16	$0 = y_1(t) - \frac{1}{\lambda_0^2} \lambda^2(t)$	

17	$0 = y_2(t) - y_1^2(t)$	
18	$Vout(t) = v_5(t) - v_6(t)$	Actual Measurement
19	$0 = v_2(t)$	Pseudo Measurements
20	$0 = v_4(t)$	

The definition of the state variables of voltage instrumentation channel are listed in Table 5-3. The way to obtain the AQCF measurement model of voltage instrumentation channel is the same to what we do for current instrumentation channel.

Table 5-3 States of voltage instrumentation channel

Index	Variable	Description
1	$v_1(t)$	PT primary bus voltage (V)
2	$v_2(t)$	PT primary bus voltage, neutral (V)
3	$v_3(t)$	PT secondary bus voltage (V)
4	$v_4(t)$	PT secondary bus voltage, neutral (V)
5	$v_5(t)$	PT burden bus voltage (V)
6	$v_6(t)$	PT burden bus voltage, neutral (V)
7	$i_{L1}(t)$	Current through PT primary inductance (A)

8	$i_{L2}(t)$	Current through PT secondary inductance (A)
9	$v_{c1}(t)$	Voltage across parasitic capacitance, primary side (V)
10	$v_{c2}(t)$	Voltage across parasitic capacitance, secondary side (V)
11	$v_{c3}(t)$	Voltage across parasitic capacitance, pri-sec side (V)
12	$e(t)$	Voltage generated by the flux (V)
13	$i_c(t)$	Current through PT primary winding (A)
14	$\lambda(t)$	Flux linkage (Web)
15	$i_m(t)$	Magnetizing current (A)
16	$i_{L3}(t)$	Current through cable inductance (A)
17	$i_{L4}(t)$	Current through cable inductance, neutral (A)
18	$y_1(t)$	Introduced state for quadratization (p.u.)
19	$y_2(t)$	Introduced state for quadratization (p.u.)

5.4 Current Instrumentation Channel Error Correction Results

5.4.1 Simulation System Description

As shown in Figure 5-7, the current transformer is measuring the phase A current of Line 1 from bus G1 to bus MID. The ratio for the current transformer is 800:5A, and the error class for the CT is 10C100, as shown in Figure 5-8. The instrumentation cable is #10 copper cable with the length 96 meters. The burden resistance is 0.1 Ω. The merging unit is measuring the voltage across the burden resistor.

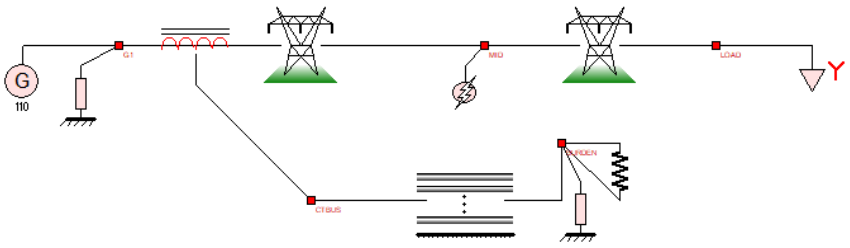

Figure 5-7 Example system for current instrumentation channel error correction

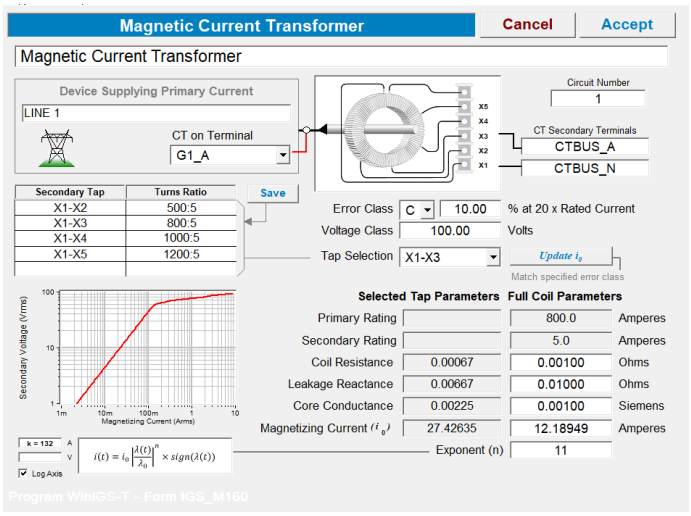

Figure 5-8 Magnetic current transformer parameters

5.4.2 Case 1 --- CT Mild Saturation

To study the performance of the proposed error correction method on a mild level of CT saturation, a phase A to ground fault on the line MN is simulated. This fault yields fault current hat causes mild CT saturation of the instrumentation channel. Figure 5-9 (a) shows the measurement voltage across the burden resistor. If zooming up the secondary waveform during fault, as shown in Figure 5-9 (b), it is obvious that the secondary waveform is distorted due to CT saturation. If without error correction for current instrumentation channel, such a distortion will lead to inaccurate measurement of primary current.

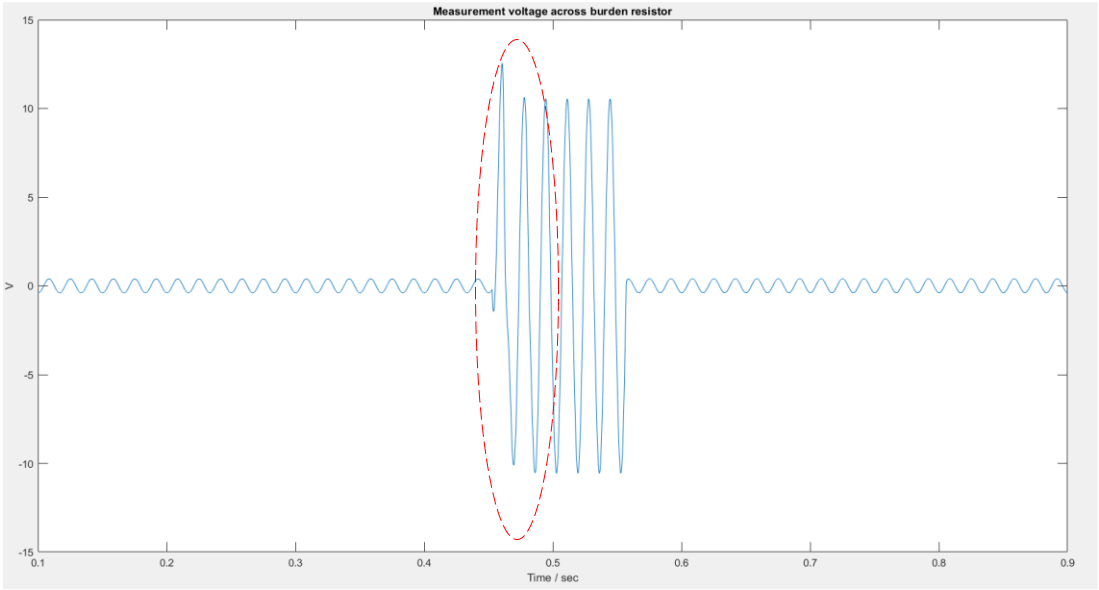

(a)

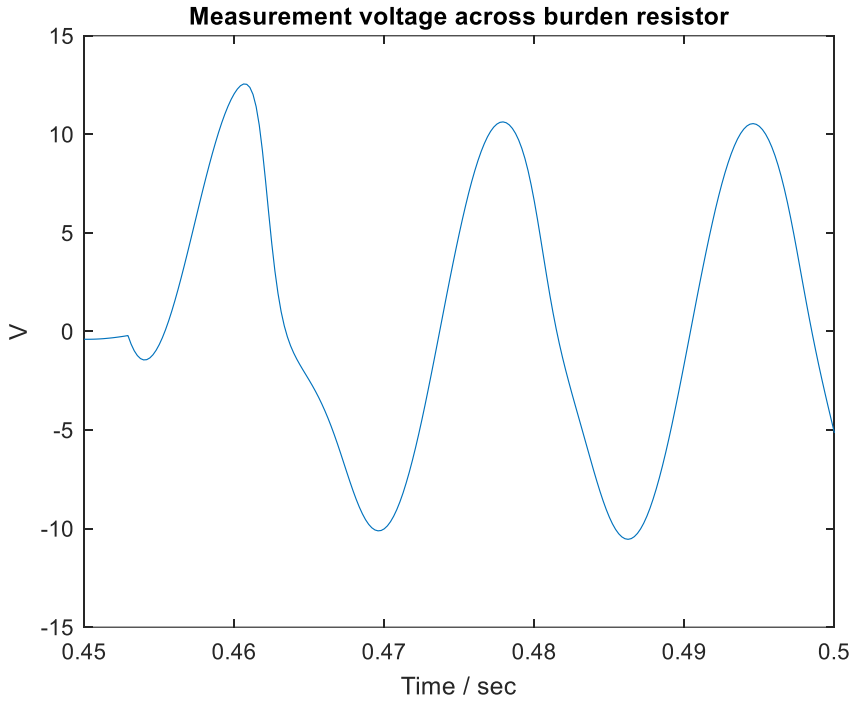

(b)

Figure 5-9 (a) Measurement voltage across burden resistor, CT mild saturation case; (b) Zooming up measurement voltage

The error correction results are shown in Figure 5-10, where top set of traces provide a graph of the estimated primary current, the actual primary current and the primary current computed by simply multiplying the measurement secondary current time the transformation ratio. The last quantity is referred to as "Ratio*CT Secondary Current". The bottom set of traces of Figure 5-10 provides the error between the uncorrected primary current and the actual one as well as the error between the estimated primary current and the actual one. It is obvious that the estimated primary current tracks the actual one very well while the uncorrected one has a sizeable difference from the actual one. Note that without error correction the error exceeds 50%, while with error correction the error is below 3%.

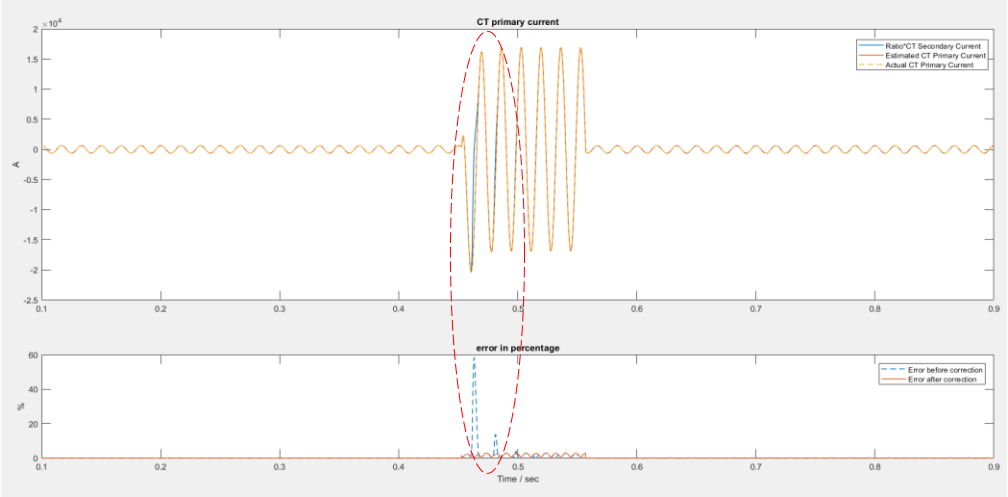

(a)

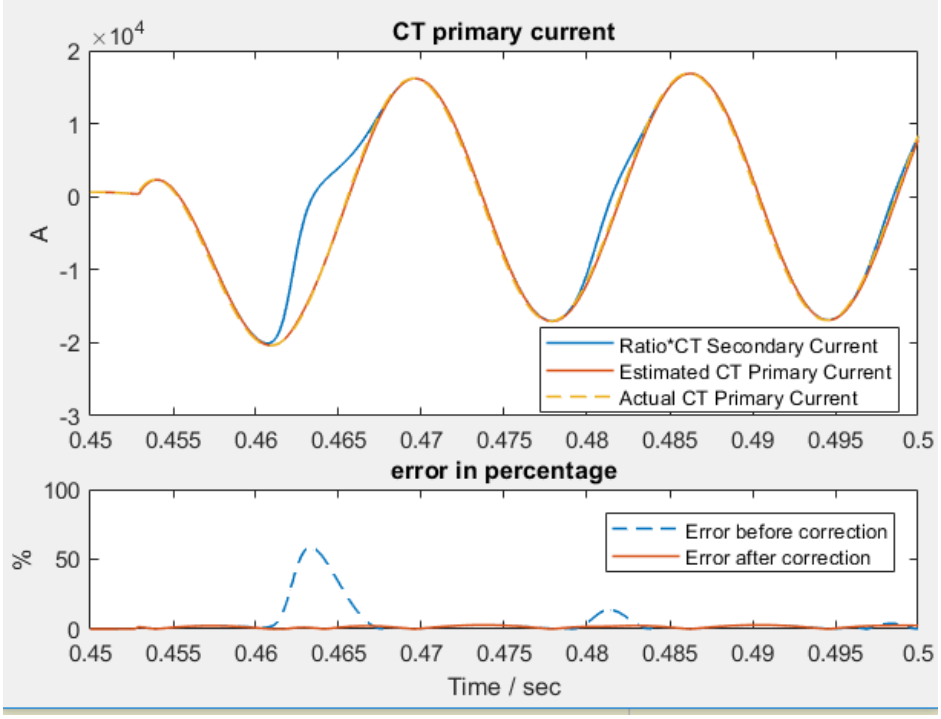

(b)

Figure 5-10 (a) Comparison between the CT primary current before and after correction with the actual one --- CT mild saturation case (b) Zooming up comparison results

5.4.3 Case 2 --- CT Severe Saturation

To validate the proposed method for severe level of CT saturation, an inter-phase fault (AC fault) is simulated on the line MN. As shown in Figure 5-11, the maximum error before correction reaches 128%, while the maximum error after correction is below 4.8%. The error correction result shows that even for severe CT saturations, the proposed method is effective in reproducing the CT primary current.

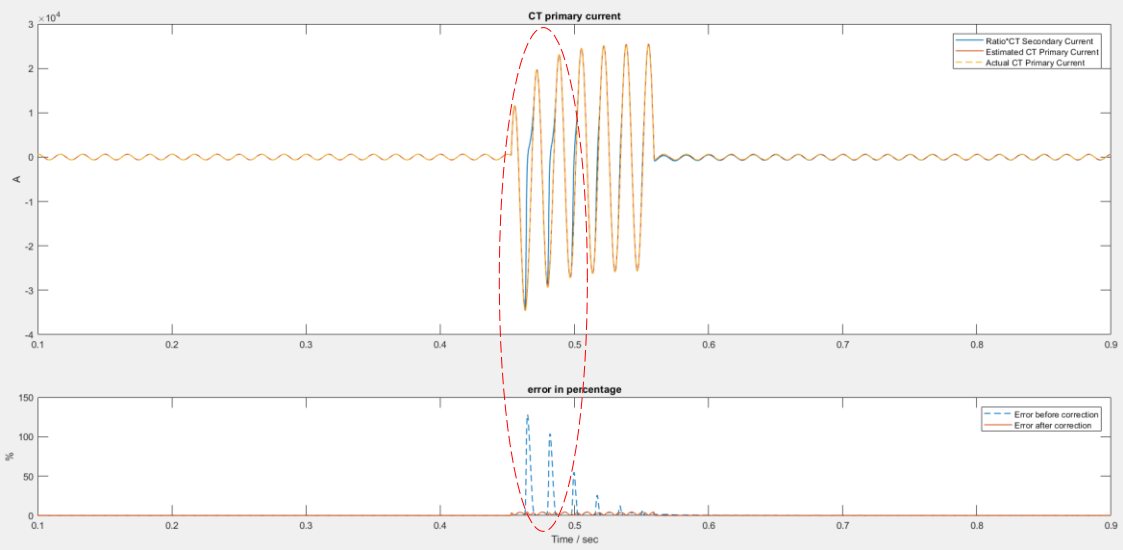

(a)

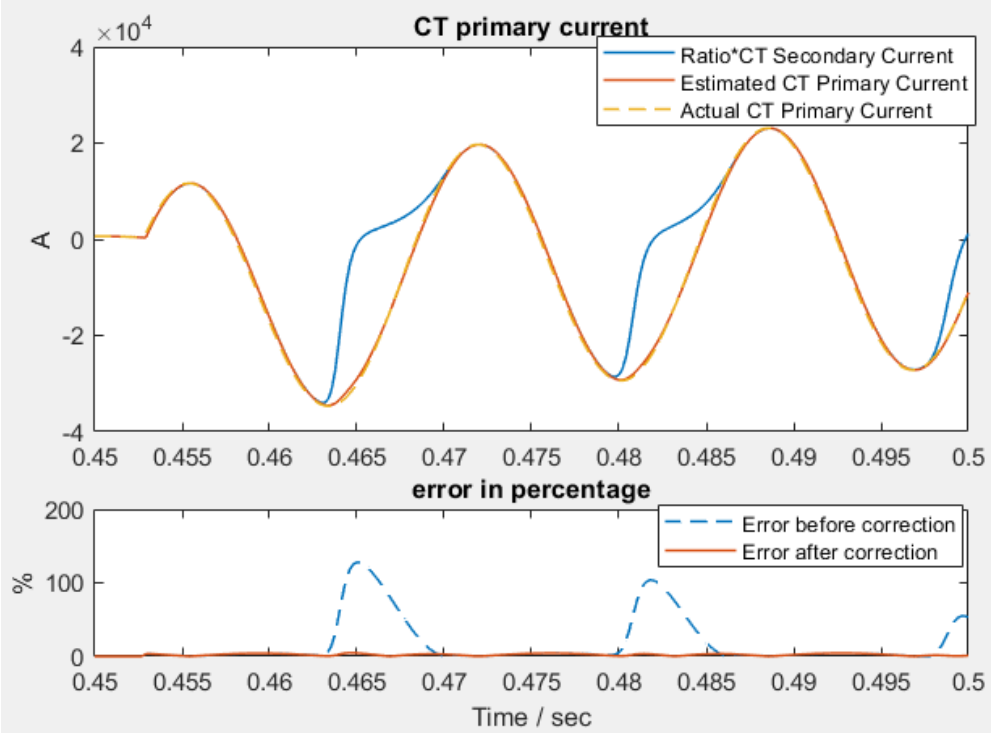

(b)

Figure 5-11 (a) Comparison between the CT primary current before and after correction with the actual one—CT severe saturation case (b) Zooming up comparison results

5.4.4 Case 3 --- CT Ratio 2000: 5

This is a case to show the error correction result for CT with different ratio, and different error class. The ratio of CT in this case is 2000: 5 A and the error class is 10C200. The comparison between the CT primary current before and after error correction with actual one is shown in Figure 5-12. It can be seen that the estimated result matches the actual primary current with less than 4% error, while without error correction, the error can reach 120%.

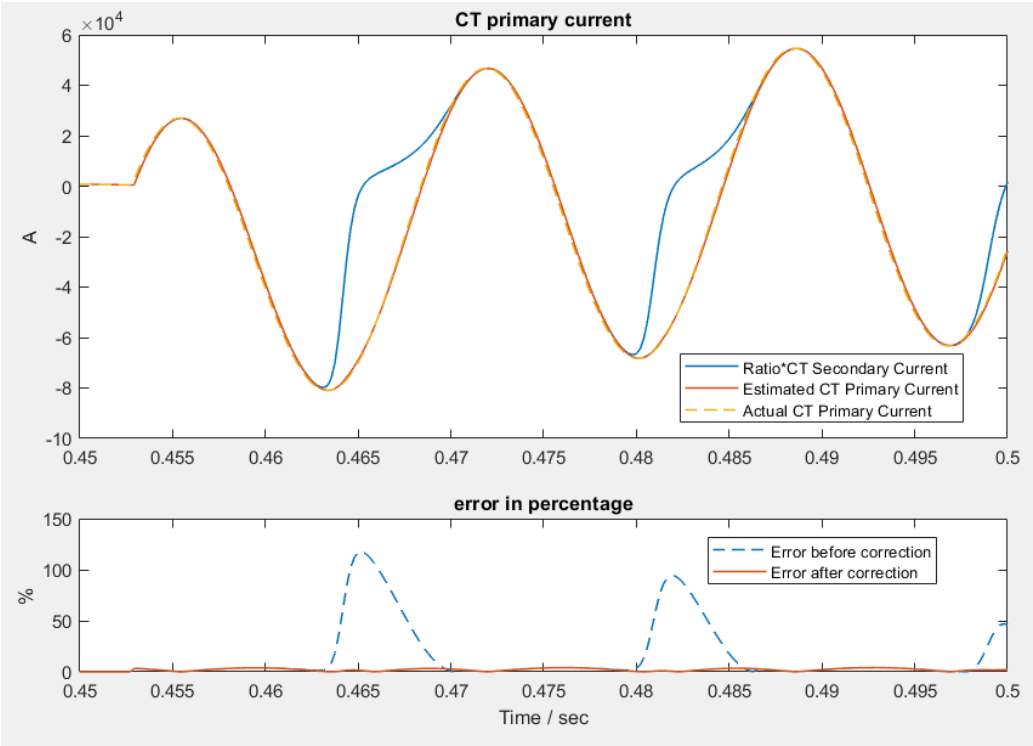

Figure 5-12 Comparison between the CT primary current before and after correction with the actual one—CT ratio 200:5 A

5.5 Voltage Instrumentation Channel Error Correction Results

5.5.1 Simulation System Description

As shown in Figure 5-13, the PT is measuring the phase A to neutral voltage of bus Load. PT with the ratio of 63.395 kV: 115 V and 66.395 kV: 69.3 V are tested in Section 5.5.2 and Section 5.5.3, respectively. The PT parameters are shown in Figure 5-14. The instrumentation cable is #10 copper cable with the length 96 meters. The burden resistance is 100 Ω. The merging unit is measuring the voltage across the burden resistor.

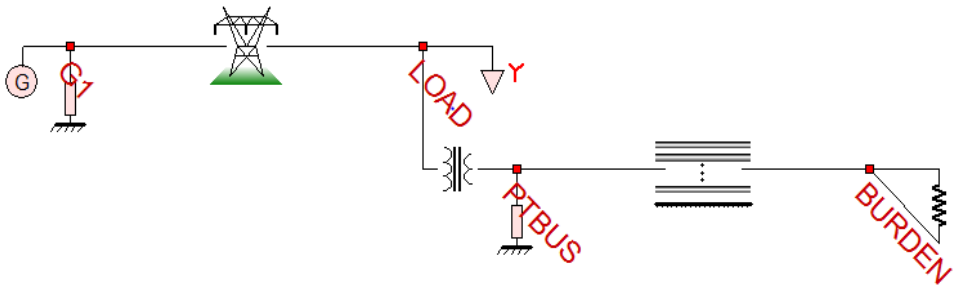

Figure 5-13 Example system for voltage instrumentation channel error correction

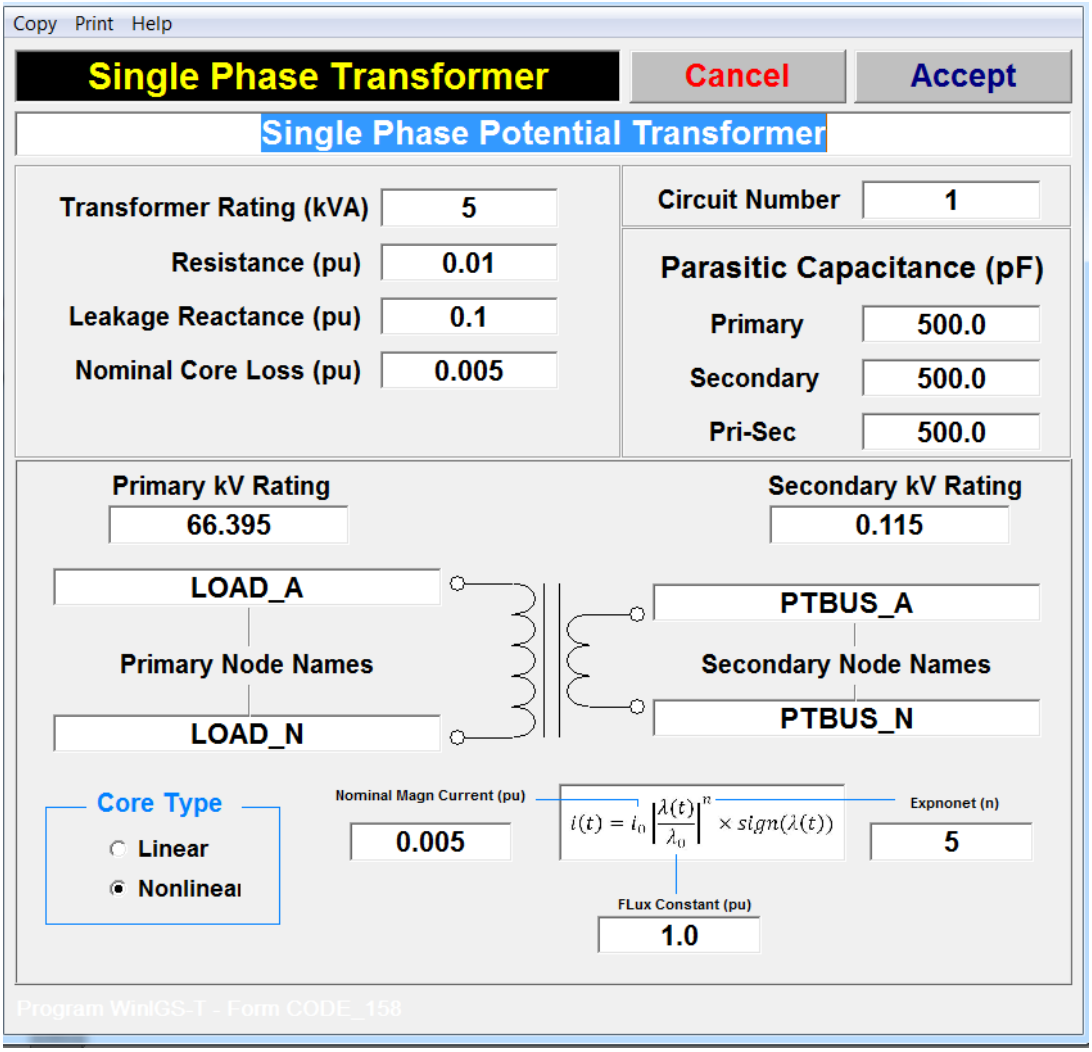

Figure 5-14 Potential transformer parameters

5.5.2 Case 1 --- PT Ratio 66.395 kV :115 V

The error correction performance is investigated on a voltage instrumentation channel with the PT of the ratio 66.395 kV :115V. As shown in Figure 5-15, top set of traces provide a graph of the estimated primary voltage, the actual primary voltage and the primary voltage computed by simply multiplying the measurement secondary voltage

time the transformation ratio. The last quantity is referred to as “Ratio*PT Secondary Voltage”. The bottom set of traces of Figure 5-15 provides the error in percentage (y axis in log plot) between the uncorrected primary voltage and the actual one as well as the error between the estimated primary voltage and the actual one. It shows that the estimated primary voltage tracks the actual one much better than the uncorrected one. Note that without error correction, the error can reach 1%, while after error correction, the error is only 0.004%.

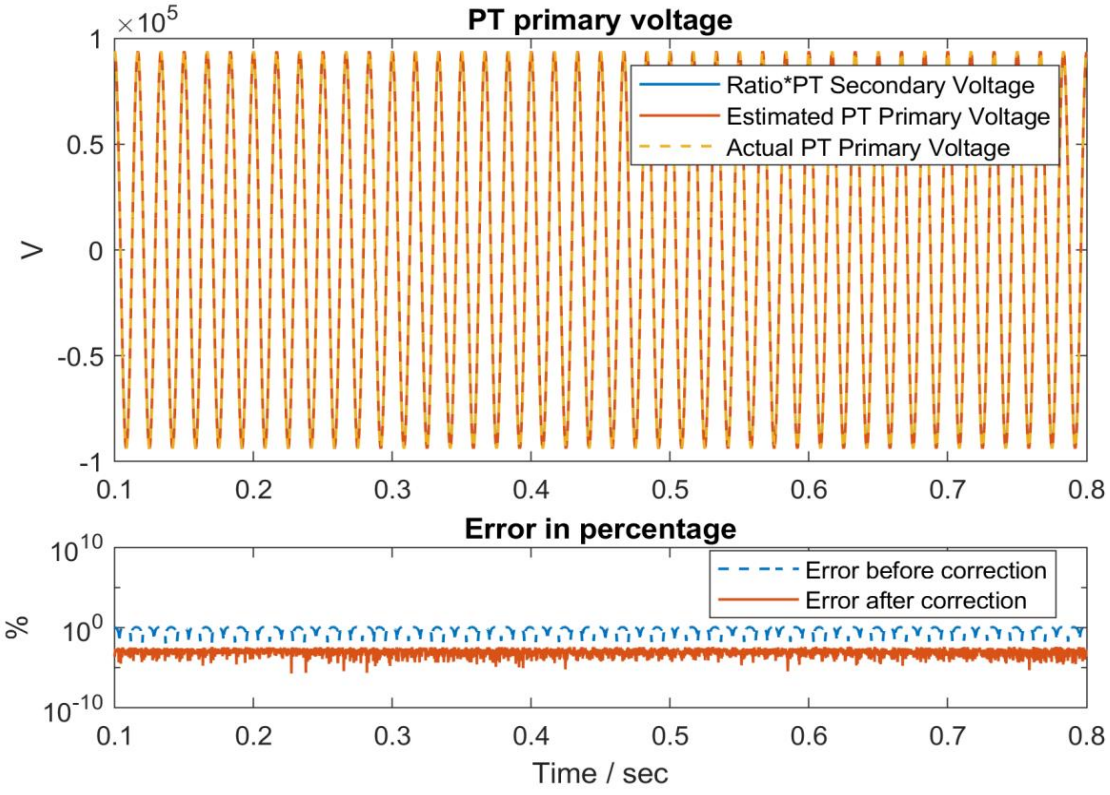

Figure 5-15 Comparison between the PT primary voltage before and after correction with the actual one -- PT ratio 66.395 kV: 115 V case

5.5.3 Case 2 --- PT Ratio 66.395 kV :69.3 V

Another voltage instrumentation channel error correction case with a PT ratio of 66.395 kV: 69.3 V is shown in Figure 5-16. It shows that without error correction, the error can reach 1.2%, while after error correction, the error is only 0.004%.

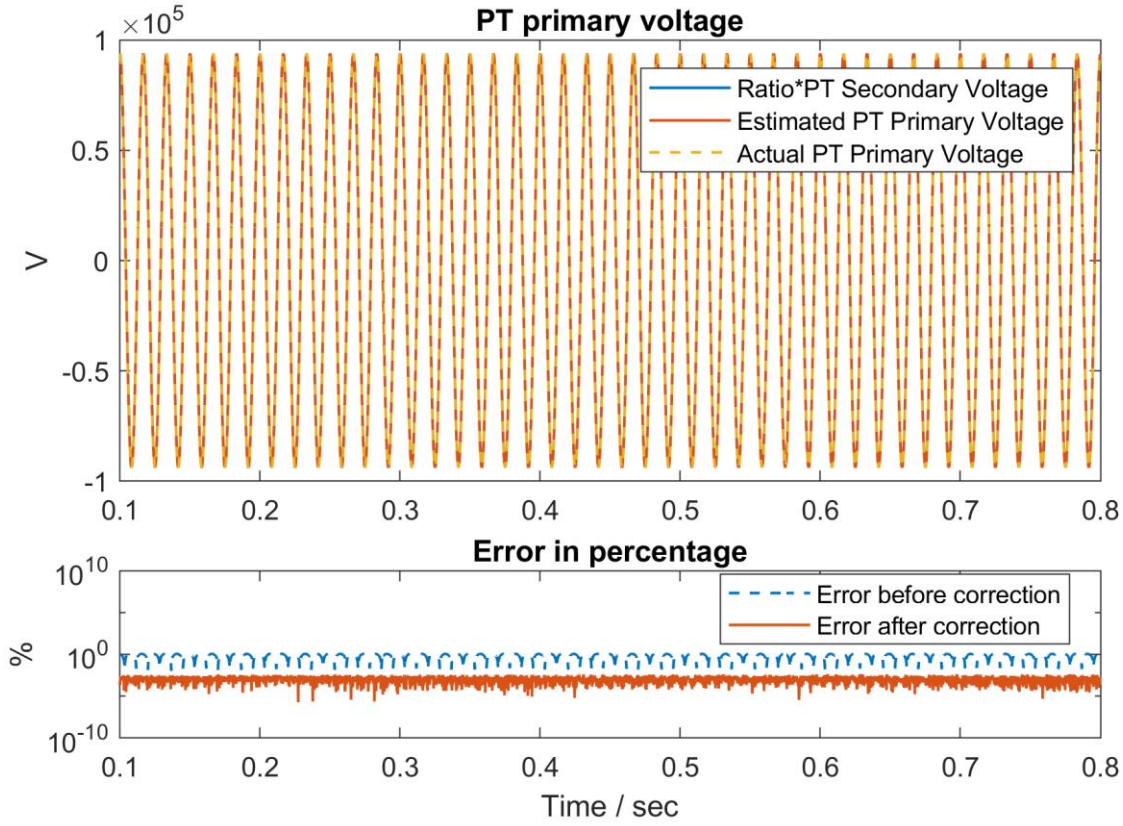

Figure 5-16 Comparison between the PT primary voltage before and after correction with the actual one -- PT ratio 66.395 kV: 69.3 V case

5.6 Summary

This chapter has presented the proposed instrumentation channel error correction. It starts from the development of measurement model of current instrumentation channel and voltage instrumentation channel. In each measurement model, the measurements are divided into 4 groups: actual, derived, virtual and pseudo measurements. The measurement model is first expressed in QDM and then the AQCF measurement model is generated by applying quadratic integration. The DSE is performed on AQCF measurement model to estimate the primary quantities. Extensive test cases have demonstrated that the proposed algorithm can accurately reconstruct the CT primary samples in different saturation scenarios and with different CT ratio. The error correction method is also effective to reproduce PT primary side voltage with high accuracy, demonstrated by test cases on voltage instrumentation channel with different PT ratio.

CHAPTER 6. VALIDATION OF THE ESTIMATED PRIMARY SAMPLES

6.1 Overview

This Chapter discusses and presents a validation procedure of the estimated primary samples. In Chapter 5, we have compared the estimated primary samples with the actual one to show that the estimated samples provide a good reproduction of primary quantities. However, in practice, the actual samples are not available. Therefore, it is necessary to come up with an alternative method to validate the estimated samples.

There are two options of measurement samples in practical power systems, one option is the estimated primary samples by the error correction, the other is the legacy samples without error correction. The validation problem is to decide which measurement option is better. This chapter presents details of the validation of the estimated primary samples, assuming that the primary quantities are known through simulation. In an actual application, the primary values are not known. Section 6.2 presents a validation procedure without knowledge of the primary quantities. Specifically, the validation method is based on comparison of the substation level dynamic state estimation results for two measurement options: (a) legacy measurement samples and (b) estimated measurement samples. After performing the substation DSE using legacy or estimated measurement samples, respectively, the Chi-square value, $Tr\{\boldsymbol{C}_x\}$ and $Tr\{\boldsymbol{C}_{\hat{z}}\}$ are computed for each one of these cases and are compared . If substation DSE using the estimated measurement samples can achieve a smaller Chi-square value, a smaller

$Tr\{\boldsymbol{C}_x\}$ and a smaller $Tr\{\boldsymbol{C}_{\hat{z}}\}$ compared to the results using legacy measurement samples, it indicates that the results using estimated samples are more accurate. An example substation system is used to illustrate the validation procedure.

6.2 Comparison of Two Measurement Options via Substation DSE

6.2.1 Example Substation System

As shown in Figure 6-1 and Figure 6-2, a simplified substation will be taken as an example to illustrate how to validate the estimated primary samples. The substation is fed by a 115-kV system via a 115-kV transmission line. The substation model includes: (a) the 115-kV transmission line, (b) the 115kV bus M, (c) the 115 kV / 34.5 kV 36 MVA transformer, (d) the 34.5 kV bus N, (e) the 34.5 kV distribution line and (f) the breakers connected with bus M or bus N.

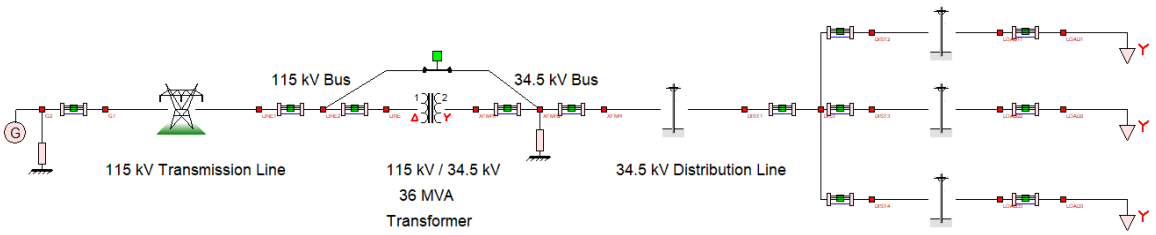

Figure 6-1 One-line diagram of the substation used in the simulation

As shown in Figure 6-2, instrumentation channels are installed in the substation to measure the three-phase current and voltage values of the corresponding protection zones. For current instrumentation channel, the CT ratio is 800:5A with the error class of 10C100. The instrumentation cable is #10 copper cable with the length 96 meters. The burden resistance is 0.1 Ω. For voltage instrumentation channel, the PT ratio is 66. 395kV:115V (115 kV bus) or 19. 919kV:115V (34.5 kV bus). The instrumentation cable is #10 copper cable with the length 96 meters. The burden resistance is 100 Ω. The secondary side measurement of each instrumentation channel is measured by Merging Unit with of 0.1%.

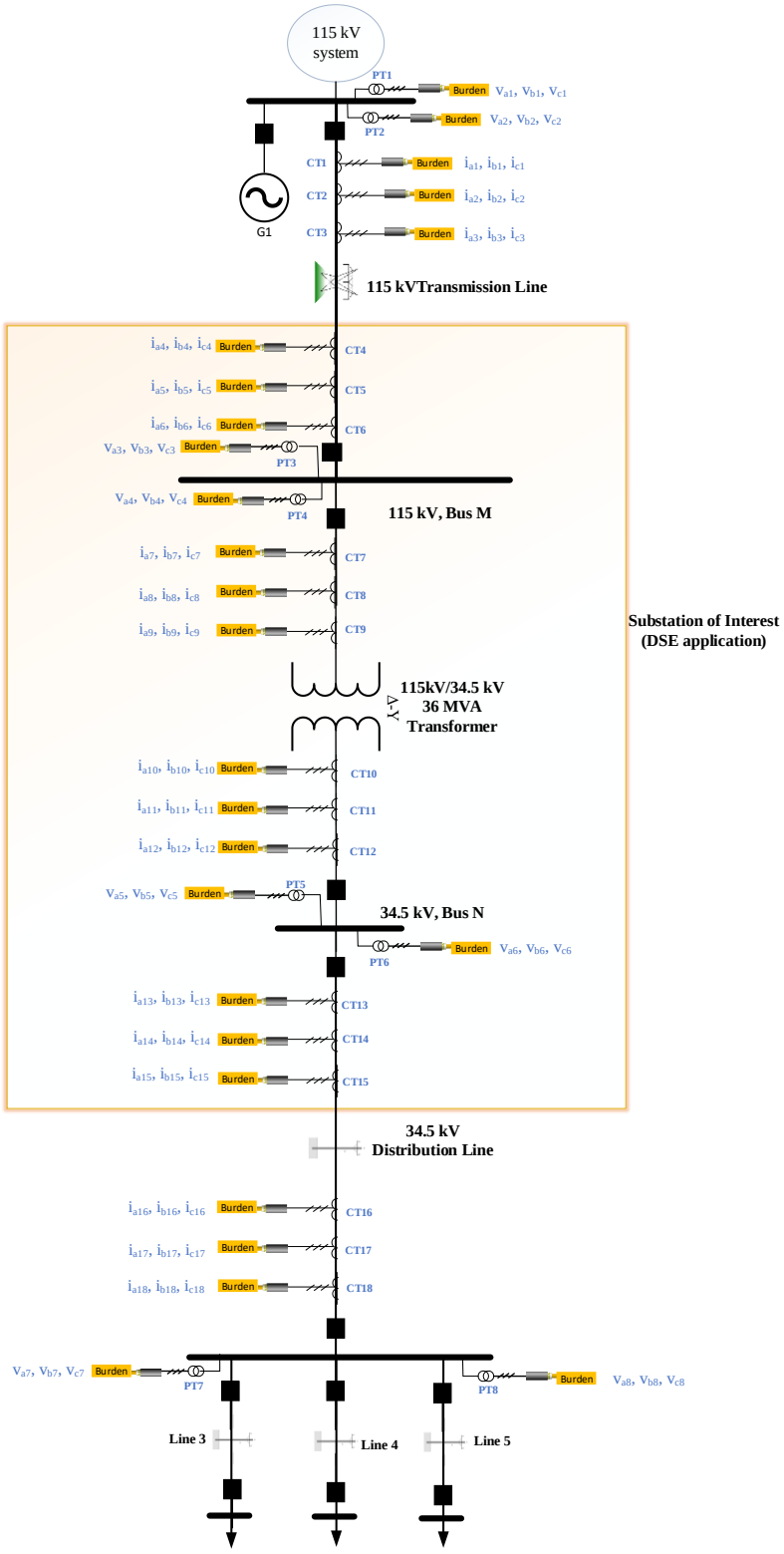

Figure 6-2 One-line diagram substation configuration with instrumentation channels

6.2.2 Measurement Options

As listed in Table 6-1, there are two options of the primary measurement samples: 1) Legacy samples and 2) Estimated samples. The legacy samples are obtained from the secondary value by multiplying the nominal transformation ratio with the secondary value, while the estimated samples are reproduced by the error correction method. The standard deviation of legacy or estimated primary measurement are calculated as follows:

1) Standard deviation of legacy primary measurement

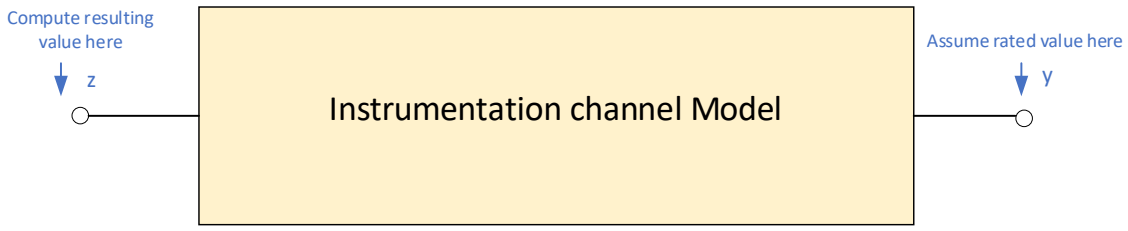

Figure 6-3 Legacy sample standard deviation calculation illustration

As shown in Figure 6-3, let y denote the rated secondary value and z denoted the computed resulting primary value. Then, the error introduced by the instrumentation channel can be computed by a simplified procedure as: $e = \frac{z - y * Ratio_{No\min al}}{y * Ratio_{No\min al}}$, We postulates that the standard deviation introduced by the instrumentation channel is $\sigma_{instr.channel} = e$.

The standard deviation of legacy measurement is determined by the sum of the two independent sources of error: the error introduced by instrumentation channel and the error of secondary measurement. Let σ_m denote the standard deviation of secondary measurement, therefore, the standard deviation of legacy primary measurement is:

$$\sigma_{Lega} = \sqrt{\sigma_{instr.channel}{}^2 + \sigma_m{}^2}$$

For example, assuming rated secondary side current is 5A, the ratio of the CT is 800 A: 5A. The instrumentation cable length used in our model is 96 meters. The secondary side measurement standard deviation $\sigma_m = 0.001$.

The instrumentation channel standard deviation is:

$$\sigma_{instr.channel} = e = \frac{z - y * Ratio_{No\min al}}{y * Ratio_{No\min al}} = \frac{801.334A - 5A*(800A/5A)}{5A*(800A/5A)} = 0.0017$$

$$\sigma_{Lega} = \sqrt{\sigma_{instr.channel}{}^2 + \sigma_m{}^2} = \sqrt{0.0017^2 + 0.001^2} \approx 0.002$$

Following a similar approach, we can calculate the standard deviation of legacy voltage as shown in the example below:

$$\sigma_{instr.channel} = e = \frac{z - y * Ratio}{y * Ratio} = \frac{66.8614kV - 115*66.395kV/115V}{115*66.395kV/115V} = 0.007$$

$$\sigma_{Lega} = \sqrt{\sigma_{instr.channel}{}^2 + \sigma_m{}^2} = \sqrt{0.007^2 + 0.001^2} \approx 0.0071$$

In summary, the standard deviation of each legacy measurement is listed in Table 6-1.

2) Standard deviation of estimated primary measurement

The standard deviation for estimated primary voltage or current measurement is calculated from instrumentation channel covariance matrix. For example, the estimated current measurement standard deviation σ_{pri_est} is calculated as: $\sigma_{pri\_est} = \sqrt{CX_{channel}}_{(i,i)}$

Where $CX_{channel}$ is the covariance matrix of the instrumentation channel measurement model and the index i denotes the state index of the primary current.

The standard deviation of each estimated primary measurements is listed in Table 6-1.

Table 6-1 Measurement options

Instr. Channel	Legacy Samples	$\sigma_{\text{pri\_Lega}}$	Estimated Samples	σ_{pri_Est}
$CT1_{ABC}$~ $CT3_{ABC}$	$Cur\text{-}Lega1_{ABC}$~$Cur\text{-}Lega3_{ABC}$	0.002	$Cur\text{-}Est1_{ABC}$~$Cur\text{-}Est3_{ABC}$	0.00102
$CT4_{ABC}$~ $CT6_{ABC}$	$Cur\text{-}Lega4_{ABC}$~$Cur\text{-}Lega6_{ABC}$	0.002	$Cur\text{-}Est4_{ABC}$~$Cur\text{-}Est6_{ABC}$	0.00102
$CT7_{ABC}$~ $CT9_{ABC}$	$Cur\text{-}Lega7_{ABC}$~$Cur\text{-}Lega9_{ABC}$	0.002	$Cur\text{-}Est7_{ABC}$~$Cur\text{-}Est9_{ABC}$	0.00102
$CT10_{ABC}$~ $CT12_{ABC}$	$Cur\text{-}Lega10_{ABC}$~$Cur\text{-}Lega12_{ABC}$	0.002	$Cur\text{-}Est10_{ABC}$~$Cur\text{-}Est12_{ABC}$	0.00102
$CT13_{ABC}$~ $CT15_{ABC}$	$Cur\text{-}Lega13_{ABC}$~$Cur\text{-}Lega15_{ABC}$	0.002	$Cur\text{-}Est13_{ABC}$~$Cur\text{-}Est15_{ABC}$	0.00102
$CT16_{ABC}$~ $CT18_{ABC}$	$Cur\text{-}Lega16_{ABC}$~$Cur\text{-}Lega18_{ABC}$	0.002	$Cur\text{-}Est16_{ABC}$~$Cur\text{-}Est18_{ABC}$	0.00102
$PT1_{ABC}$~ $PT2_{ABC}$	$Vol\text{-}Lega1_{ABC}$~$Vol\text{-}Lega2_{ABC}$	0.0071	$Vol\text{-}Est1_{ABC}$~Vol- $Est2_{ABC}$	0.0013
$PT3_{ABC}$~ $PT4_{ABC}$	$Vol\text{-}Lega3_{ABC}$~$Vol\text{-}Lega4_{ABC}$	0.0071	$Vol\text{-}Est3_{ABC}$~Vol- $Est4_{ABC}$	0.0013
$PT5_{ABC}$~ $PT6_{ABC}$	$Vol\text{-}Lega5_{ABC}$~$Vol\text{-}Lega6_{ABC}$	0.0071	$Vol\text{-}Est5_{ABC}$~Vol- $Est6_{ABC}$	0.0013
$PT7_{ABC}$~ $PT8_{ABC}$	$Vol\text{-}Lega7_{ABC}$~$Vol\text{-}Lega8_{ABC}$	0.0071	$Vol\text{-}Est7_{ABC}$~Vol- $Est8_{ABC}$	0.0013

6.2.3 Substation Measurement Model

In order to validate the estimated primary samples, the DSE on the substation AQCF model $\mathbf{h}_s(\mathbf{x}(t,t_m))$ is performed using these two measurement options, respectively. There are in total 114 measurements and 42 states, which means that the redundancy is 272%.

The substation AQCF measurement model is constructed from substation device model followed by the approach introduced in Chapter 3. The substation device model is provided in Appendix A and B. The substation AQCF measurement model for each

measurement option is listed in Table 6-2. The standard deviation for actual current measurement and actual voltage measurement has been listed in Table 6-1 and the standard deviation for virtual and pseudo measurement are assigned as 0.0001 p.u. and 0.1 p.u.

Table 6-2 The substation measurement model for two respective measurement option

Measurement option	Substation measurement model
Legacy samples	$\mathbf{z}_{Leaga}(t,t_m)=\mathbf{h}_s(\mathbf{x}(t,t_m))+\boldsymbol{\eta}_L$
Estimated samples	$\mathbf{z}_{\mathrm{Est}}(t,t_m)=\mathbf{h}_s(\mathbf{x}(t,t_m))+\boldsymbol{\eta}_E$

6.2.4 Substation DSE Results Comparison

With the measurements described in Section 6.2.2 and the substation measurement model described in Section 6.2.3, the substation level dynamic state estimation is solved by utilizing the WLS-DSE algorithm, which is illustrated in Section 4.2.

The state estimation results using the two respective measurement options are listed in Table 6-3. These quantities are compared to validate the estimated primary samples as follows.

Table 6-3 Substation DSE results for two respective measurement option

Measurement option	Chi-square	Covariance matrix of state estimates	Covariance matrix of measurement estimates
Legacy samples	$\text{Chi}-\text{Square}^{L}(t)$	$\boldsymbol{C}_{\boldsymbol{x}}^{\ L}$	$\boldsymbol{C}_{\hat{\boldsymbol{z}}}^{\ L}$
Estimated samples	$\text{Chi}-\text{Square}^{E}(t)$	$\boldsymbol{C}_{\boldsymbol{x}}^{\ E}$	$\boldsymbol{C}_{\hat{\boldsymbol{z}}}^{\ E}$

(1) Chi-square value comparison

The Chi-square value quantifies how well the measurement fit the model and is computed as:

$$\text{Chi}-\text{Square}(t) = (\mathbf{z}(t,t_m) - \mathbf{h}(\hat{\mathbf{x}}(t,t_m))^T W (\mathbf{z}(t,t_m) - \mathbf{h}(\hat{\mathbf{x}}(t,t_m))$$

Therefore, if $\text{Chi}-\text{Square}^{E}(t) < \text{Chi}-\text{Square}^{L}(t)$, it indicates the estimated samples can make the residuals smaller; otherwise, the legacy samples can have smaller residuals.

(2) $Tr\{\boldsymbol{C}_x\}$ comparison

Let $\hat{\boldsymbol{x}}$ denotes the state estimates and $\bar{\boldsymbol{x}}$ denotes the true unknow values. A more accurate state estimates means a smaller value of $E\left\{\left\|\hat{\boldsymbol{x}} - \bar{\boldsymbol{x}}\right\|^2\right\}$, which is:

$$
\begin{aligned}
E\left\{\left\|\hat{\boldsymbol{x}}-\bar{\boldsymbol{x}}\right\|^2\right\} &= E\left\{(\hat{\boldsymbol{x}}-\bar{\boldsymbol{x}})^T(\hat{\boldsymbol{x}}-\bar{\boldsymbol{x}})\right\} \\
&= E\left\{Tr\left[(\hat{\boldsymbol{x}}-\bar{\boldsymbol{x}})(\hat{\boldsymbol{x}}-\bar{\boldsymbol{x}})^T\right]\right\} \\
&= Tr\left\{E\left[(\hat{\boldsymbol{x}}-\bar{\boldsymbol{x}})(\hat{\boldsymbol{x}}-\bar{\boldsymbol{x}})^T\right]\right\} \\
&= Tr\left\{\boldsymbol{C}_x\right\}
\end{aligned}
\tag{6-1}
$$

where:

$\boldsymbol{C}_x$ represents the covariance matrix of state estimates and it can be computed by $\boldsymbol{C}_x = (\boldsymbol{H}^T\boldsymbol{W}\boldsymbol{H})^{-1}$.

$Tr\{\boldsymbol{C}_x\}$ represents the trace of $\boldsymbol{C}_x$.

The formula (6-1) shows that the value of $E\left\{\left\|\hat{\boldsymbol{x}}-\bar{\boldsymbol{x}}\right\|^2\right\}$ can be quantified by $Tr\{\boldsymbol{C}_x\}$. Therefore, if $Tr\{\boldsymbol{C}_x{}^E\} < Tr\{\boldsymbol{C}_x{}^L\}$, it indicates that the estimated samples can achieve more accurate state estimates. Otherwise, the legacy samples can achieve more accurate state estimates.

(3) $Tr\{\boldsymbol{C}_{\hat{\boldsymbol{z}}}\}$ comparison

Let $\hat{\boldsymbol{z}} = \boldsymbol{h}(\hat{\boldsymbol{x}})$ denotes the measurement estimates and $\bar{\boldsymbol{z}} = \boldsymbol{h}(\bar{\boldsymbol{x}})$ denotes the true unknown values. A more accurate state estimates means a smaller value of $E\left\{\left\|\hat{\boldsymbol{z}}-\bar{\boldsymbol{z}}\right\|^2\right\}$, which is:

$$
\begin{aligned}
E\left\{\left\|\hat{\boldsymbol{z}}-\overline{\boldsymbol{z}}\right\|^2\right\} &= E\left\{(\hat{\boldsymbol{z}}-\overline{\boldsymbol{z}})^T(\hat{\boldsymbol{z}}-\overline{\boldsymbol{z}})\right\} \\
&= E\left\{Tr\left[(\hat{\boldsymbol{z}}-\overline{\boldsymbol{z}})(\hat{\boldsymbol{z}}-\overline{\boldsymbol{z}})^T\right]\right\} \\
&= Tr\left\{E\left[(\hat{\boldsymbol{z}}-\overline{\boldsymbol{z}})(\hat{\boldsymbol{z}}-\overline{\boldsymbol{z}})^T\right]\right\} \\
&= Tr\left\{\boldsymbol{C}_{\hat{\boldsymbol{z}}}\right\}
\end{aligned}
\tag{6-2}
$$

Where:

$\boldsymbol{C}_{\hat{\boldsymbol{z}}}$ represents the covariance matrix of measurement estimates and it can be computed by $\boldsymbol{C}_{\hat{\boldsymbol{z}}} = \boldsymbol{H}(\boldsymbol{H}^T\boldsymbol{W}\boldsymbol{H})^{-1}\boldsymbol{H}^T$.

$Tr\left\{\boldsymbol{C}_{\hat{\boldsymbol{z}}}\right\}$ represents the trace of $\boldsymbol{C}_{\hat{\boldsymbol{z}}}$.

The formula (6-2) shows that the value of $E\left\{\left\|\hat{\boldsymbol{z}}-\overline{\boldsymbol{z}}\right\|^2\right\}$ can be quantified by $Tr\left\{\boldsymbol{C}_{\hat{\boldsymbol{z}}}\right\}$. Therefore, if $Tr\left\{\boldsymbol{C}_{\hat{\boldsymbol{z}}}^{E}\right\} < Tr\left\{\boldsymbol{C}_{\hat{\boldsymbol{z}}}^{L}\right\}$, it indicates that the estimated samples can achieve more accurate measurement estimates. Otherwise, the legacy samples can achieve more accurate measurement estimates.

6.3 Validation Results of the Estimated Primary Samples

In this Section, the validation results are shown by comparing the substation level DSE results on example substation shown in Figure 6-2 . The system is first under normal operation. Then an AC fault occurs on Line 3 at t=1.161sec and clears at t=1.27sec. In the following analysis, we will first show the legacy measurement samples and the estimated measurement samples. Then, the comparison of substation DSE results using the estimated samples and legacy samples will be demonstrated in this Section as follows.

6.3.1 Measurement Samples Example

6.3.1.1 Legacy Measurement Samples example

Figure 6-4 and Figure 6-5 shows the example legacy samples of 3-phase current and voltage measurements, respectively. It is obvious that there is distortion due to CT saturation in the waveforms of legacy current of *Cur-Lega 10*, *Cur-Lega 13* and *Cur-Lega 16* in Phase A and Phase C.

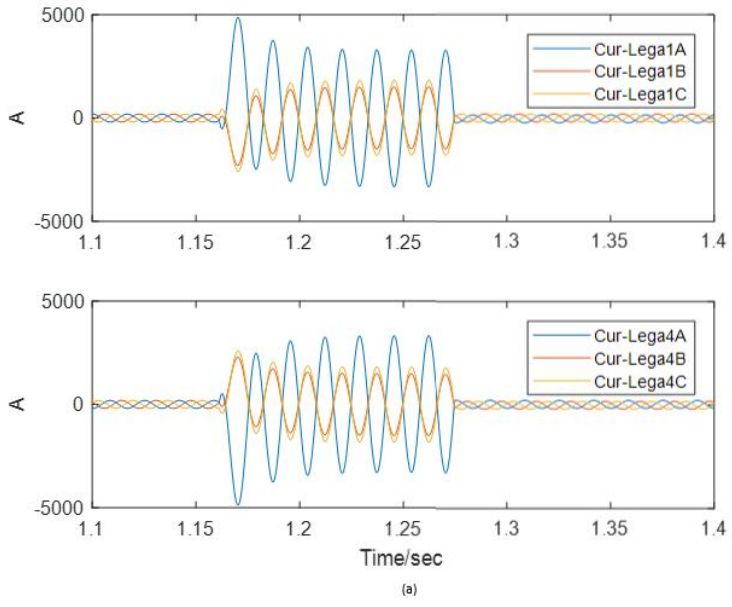

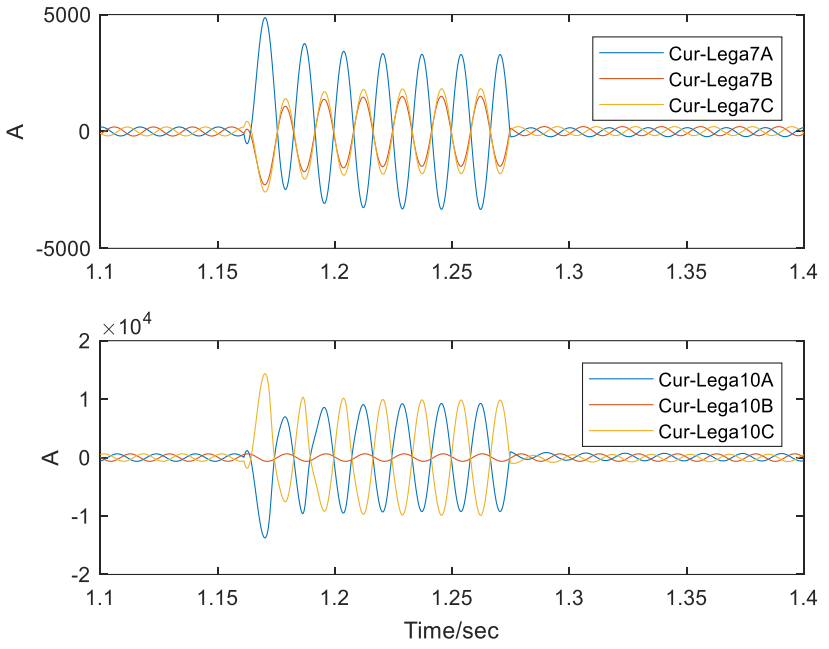

(b)

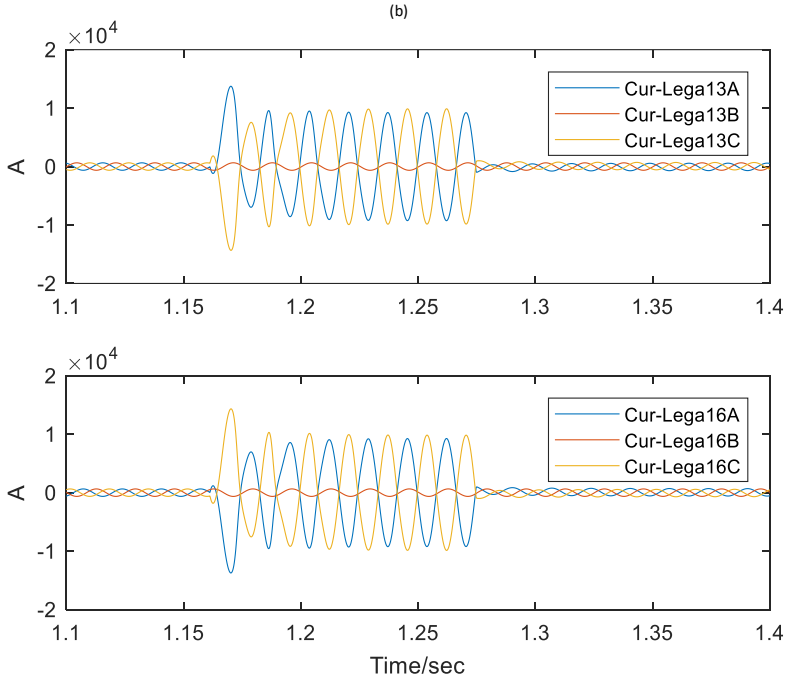

(c)

Figure 6-4 Legacy currents measurement samples example

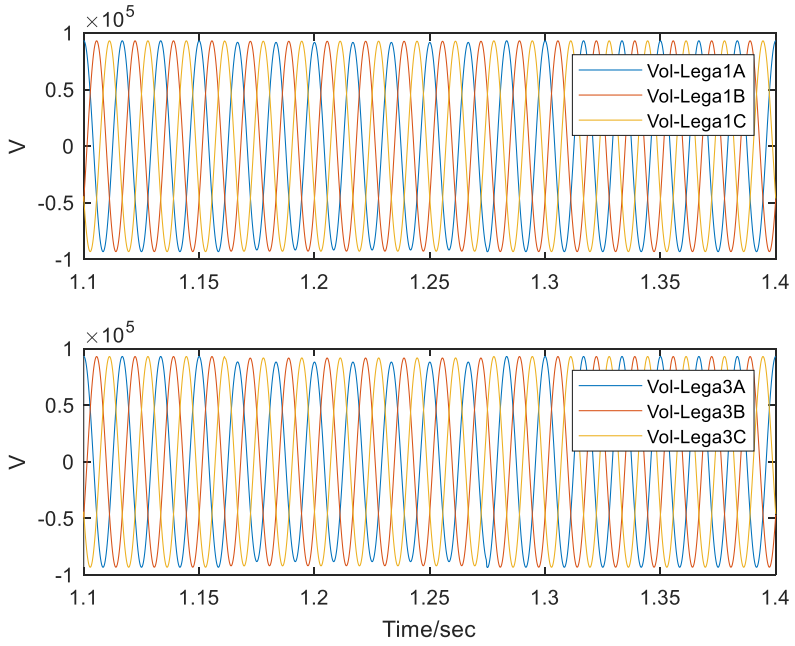

(a)

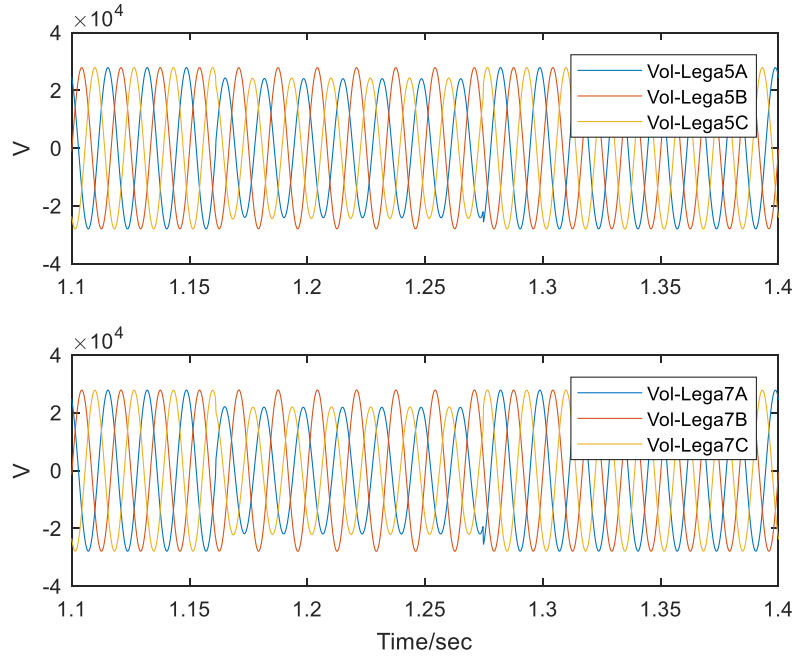

(b)

Figure 6-5 Legacy voltage measurement samples example

6.3.1.2 Estimated Measurement Samples Example

Figure 6-6 and Figure 6-7 show the example estimated samples of 3-phase current and voltage measurements, respectively.

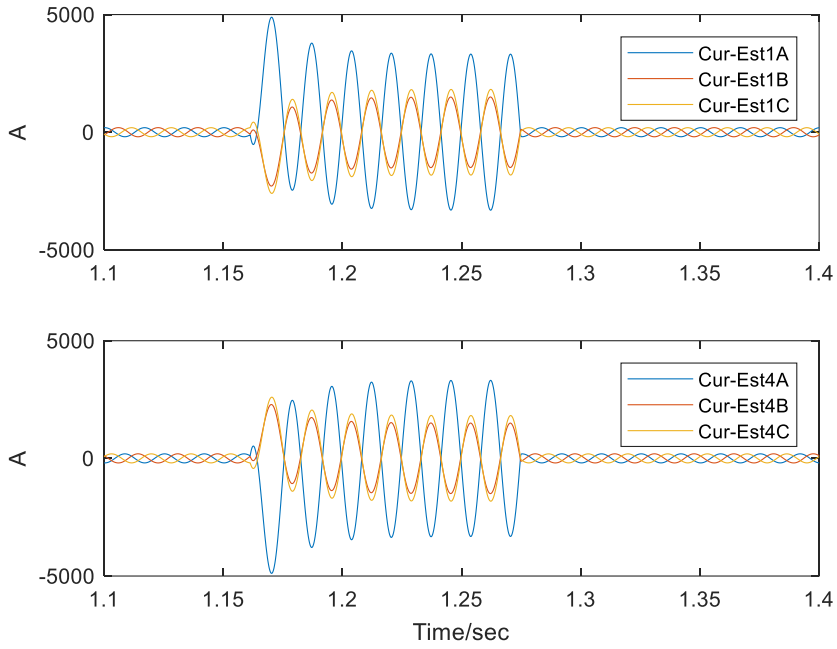

(a)

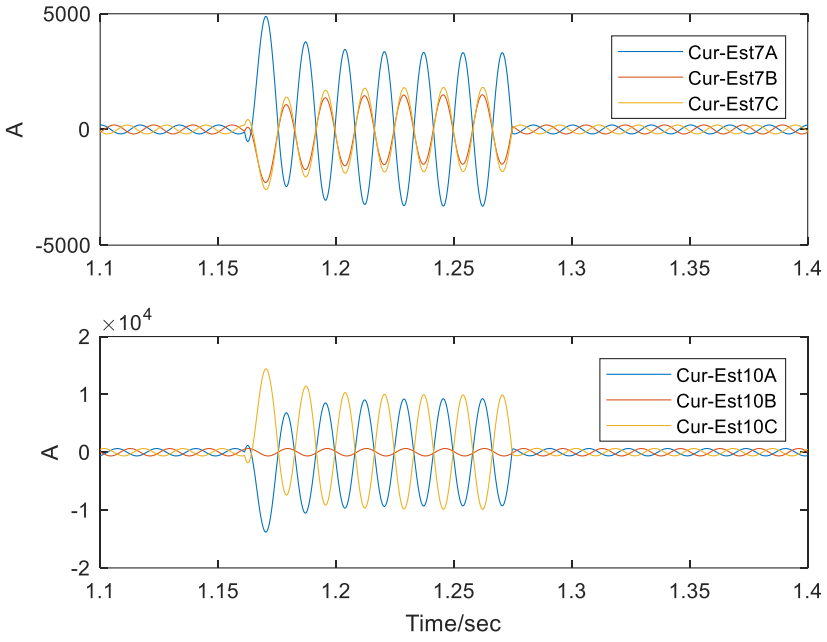

(b)

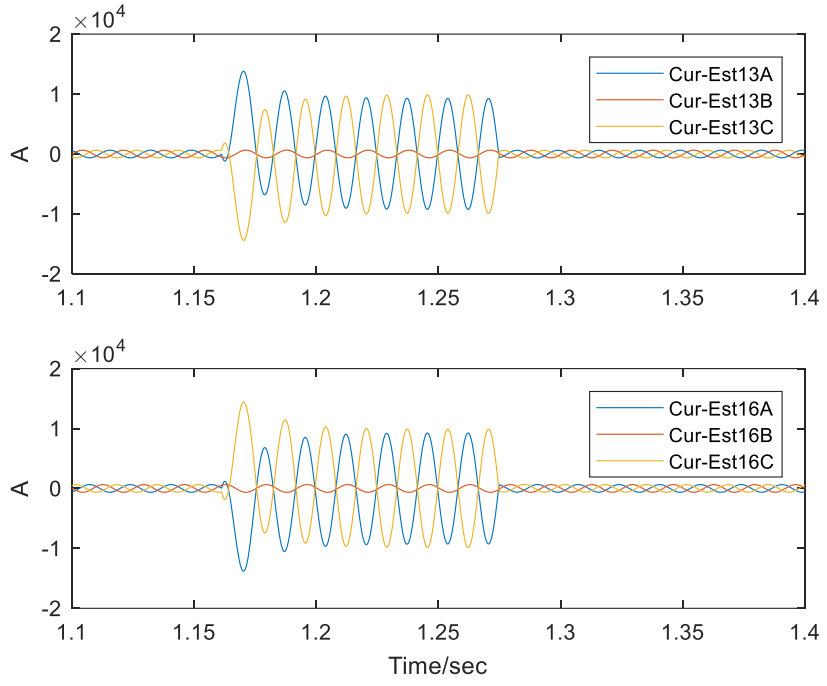

(c)

Figure 6-6 Estimated current measurement samples example

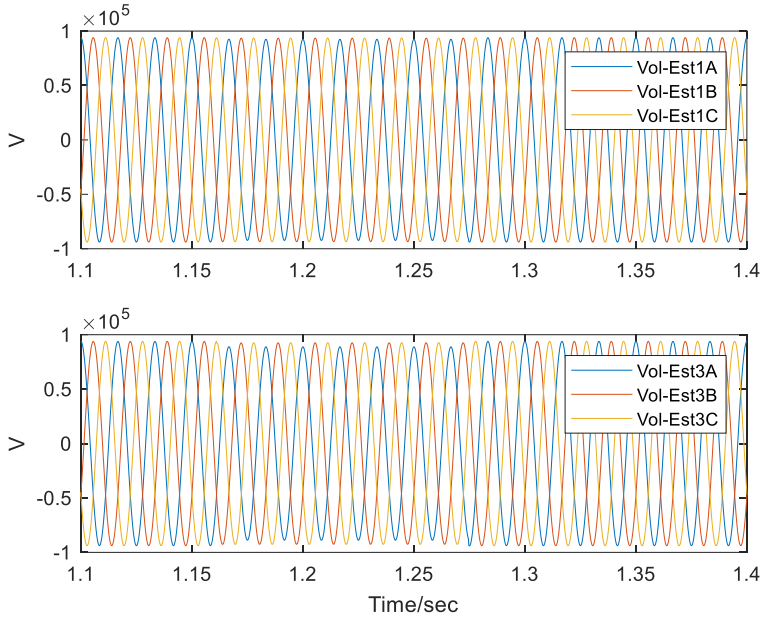

(a)

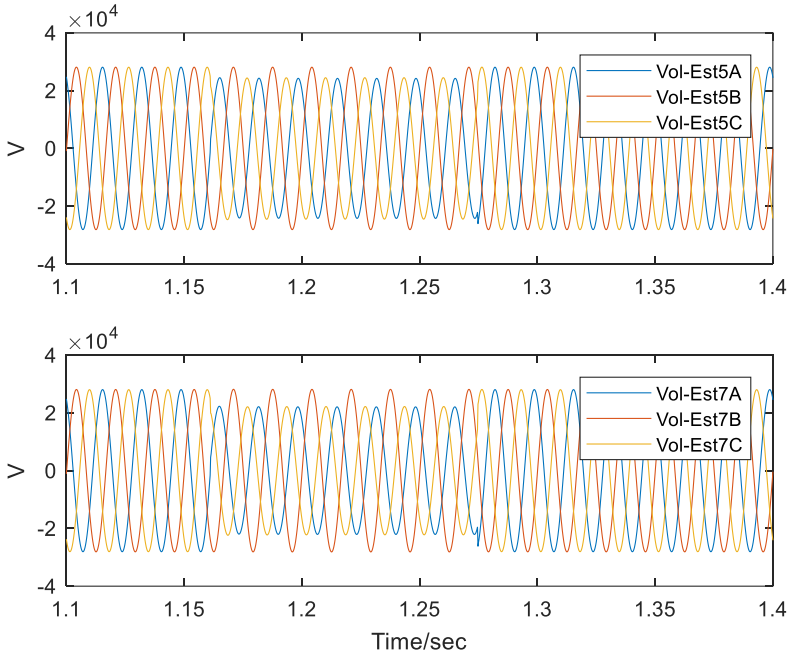

(b)

Figure 6-7 Estimated voltage measurement samples example

6.3.1.3 Comparison of legacy and estimated measurement samples example

From Figure 6-5, we can see that the distortion exists in the current waveform of *Cur-Lega 10, Cur-Lega 13 and Cur-Lega 16.* Phase A of *Cur-Lega 10* and *Cur-Est 10, Cur-Lega 13* and *Cur-Est 13, as well as Cur-Lega 16* and *Cur-Est 16* are demonstrated in Figure 6-8 ~ Figure 6-10 as examples to show the current waveforms difference between legacy and estimated samples during the saturation. The top set of traces in Figure 6-8 ~ Figure 6-10 provide a graph of the legacy current samples and the estimated current samples. The bottom set of traces provides the error between the legacy and the estimated measurement samples. It is obvious that the estimated current samples could compensate the distorted legacy samples.

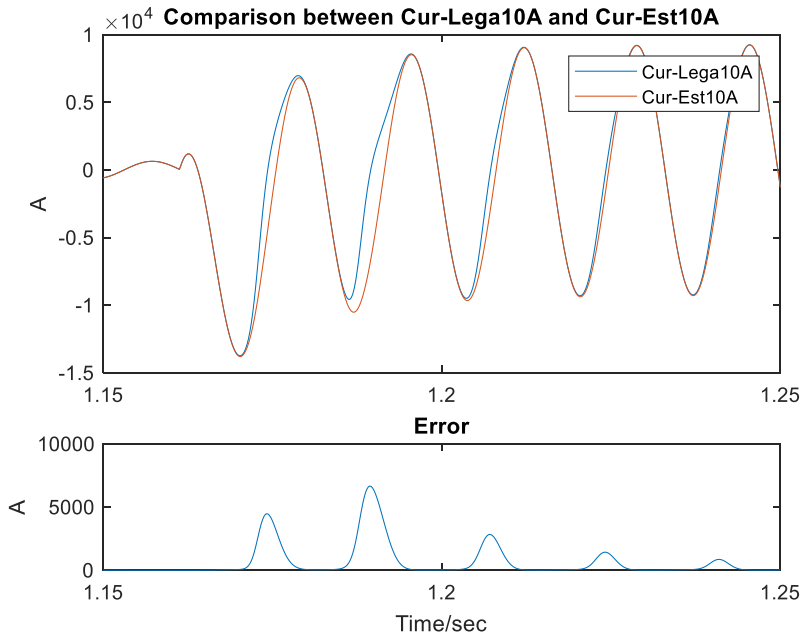

Figure 6-8 Comparison of legacy (Cur-Lega10A) and estimated (Cur-Est 10A) measurement samples

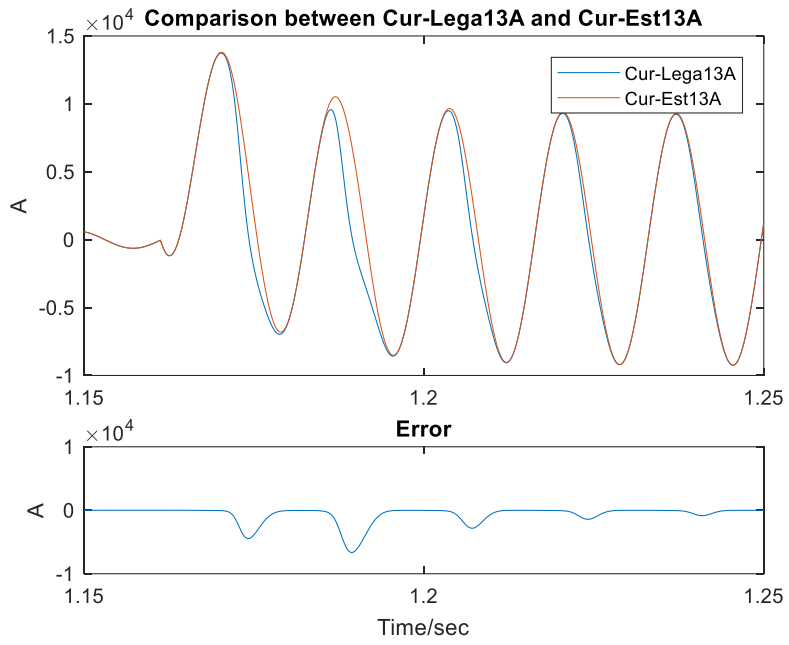

Figure 6-9 Comparison of legacy (Cur-Lega13A) and estimated (Cur-Est 13A) measurement samples

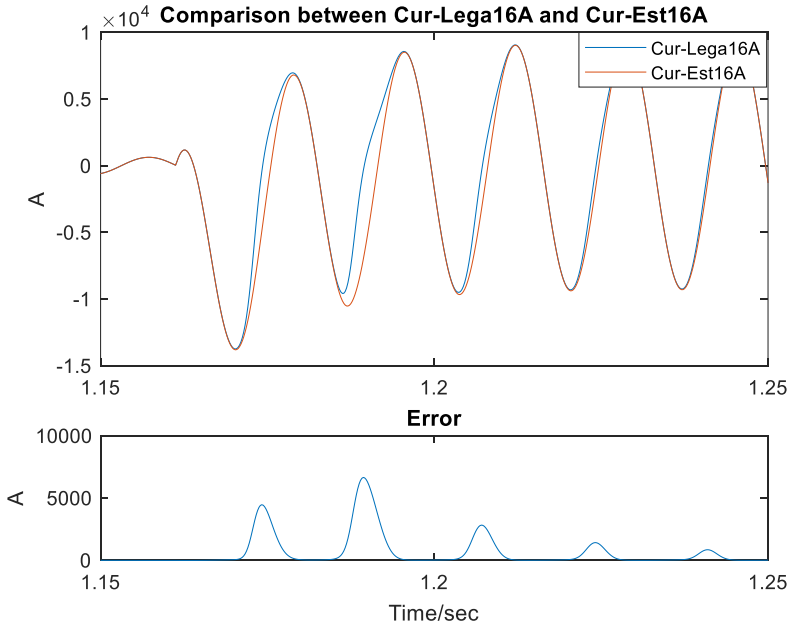

Figure 6-10 Comparison of legacy (Cur-Lega16A) and estimated (Cur-Est16A) measurement samples

6.3.2 Substation DSE Results Example

6.3.2.1 Substation DSE Results Example Using Legacy Measurement Samples

The substation DSE using the legacy measurement samples provides the DSE legacy results. Take the DSE results of Phase A current as an example, the legacy measurement samples and the substation DSE estimated measurements, as well as the residuals and normalized residuals are shown in Figure 6-11.

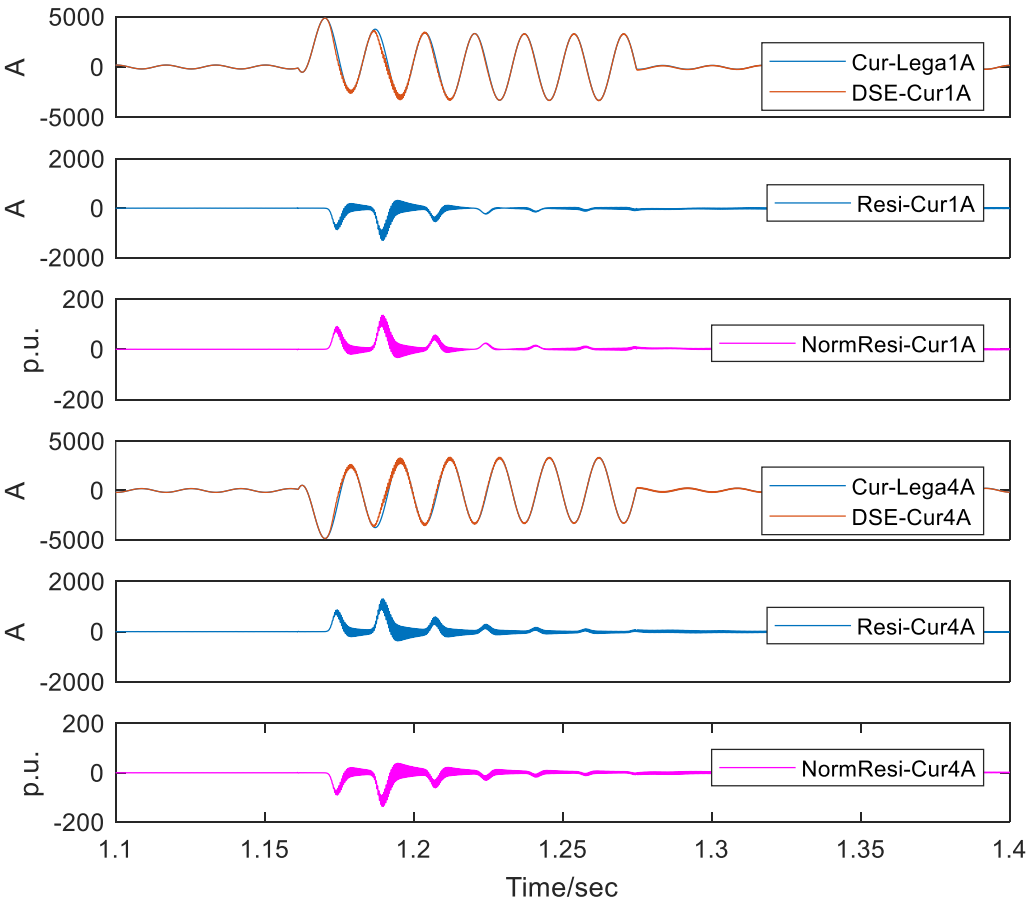

(a)

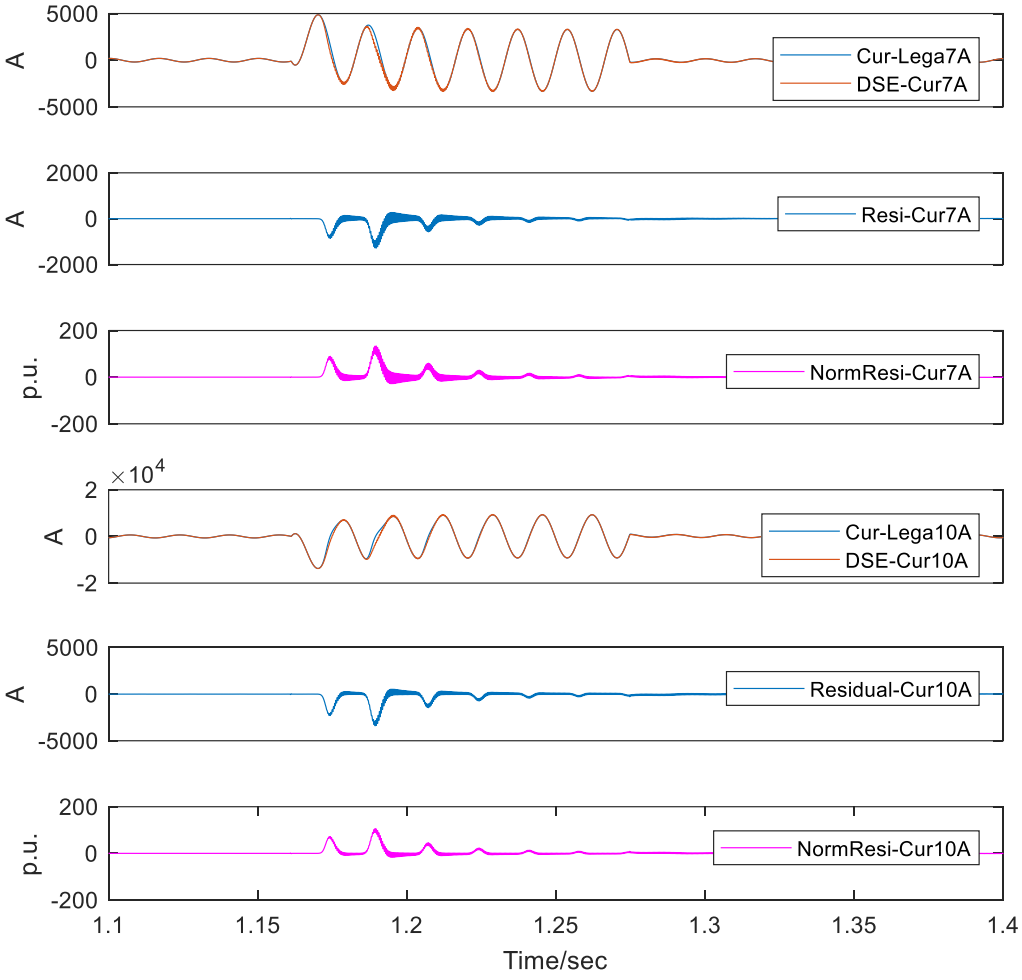
5000
0
-5000
A
Cur-Lega7A
DSE-Cur7A
2000
0
-2000
A
Resi-Cur7A
200
0
-200
p.u.
NormResi-Cur7A
×10^4
2
0
-2
A
Cur-Lega10A
DSE-Cur10A
5000
0
-5000
A
Residual-Cur10A
200
0
-200
p.u.
NormResi-Cur10A
1.1
1.15
1.2
1.25
1.3
1.35
1.4
Time/sec

(b)

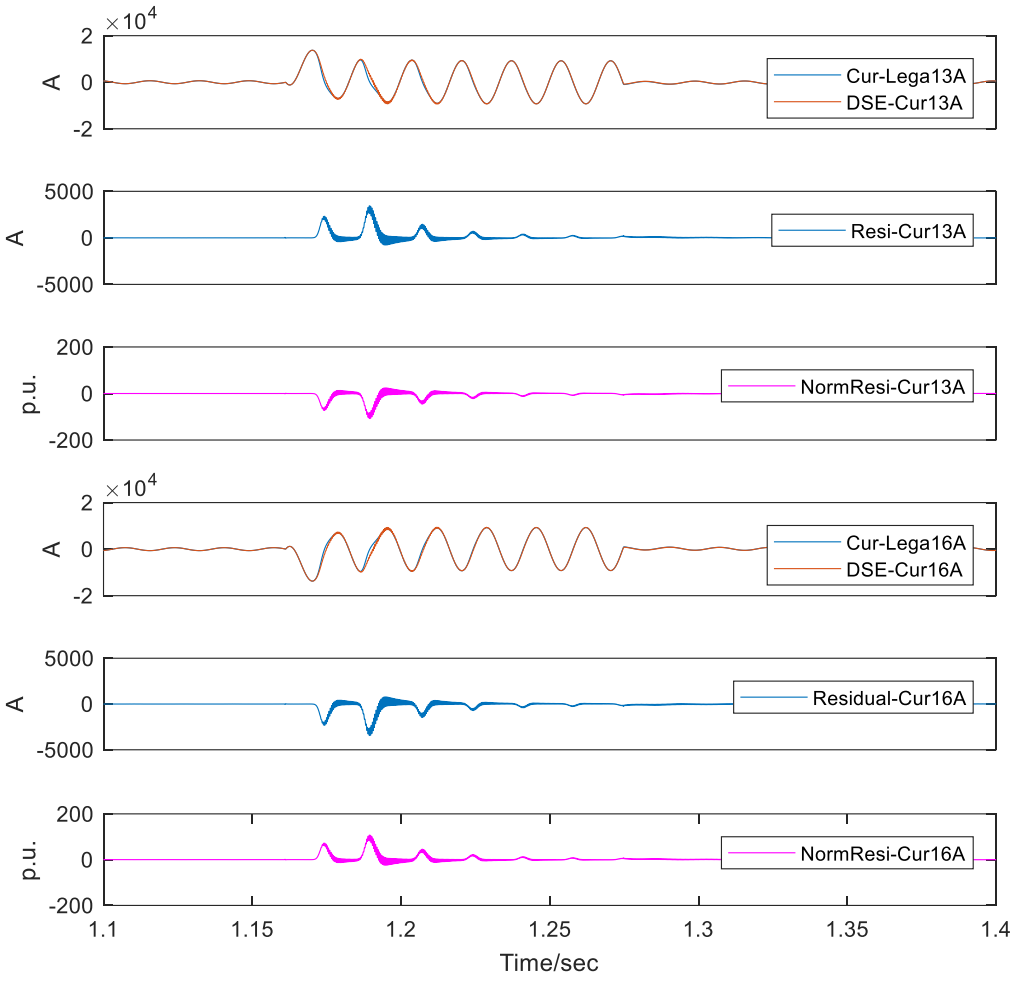

(c)

Figure 6-11 DSE results example using legacy measurements

When using the legacy measurement samples, it can be seen from Figure 6-11 that the current normalized residual can reach about 200 p.u. (200 times greater than meter accuracy).

6.3.2.2 Substation DSE Results Using Estimated Measurement Samples

The substation DSE using the estimated measurement samples provides the DSE results. Considering the DSE results of Phase A current as an example, the estimated measurement samples and the substation DSE estimated measurements, as well as the residuals and the normalized residuals are shown in Figure 6-12.

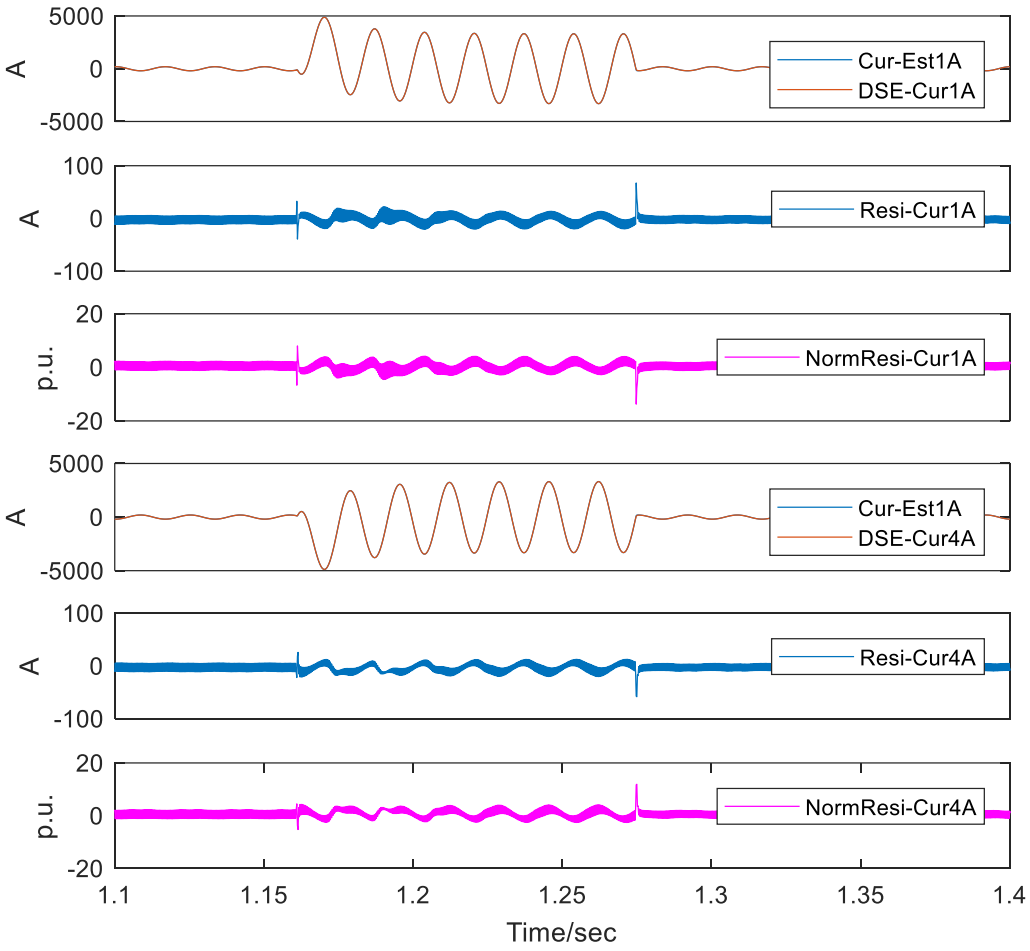

(a)

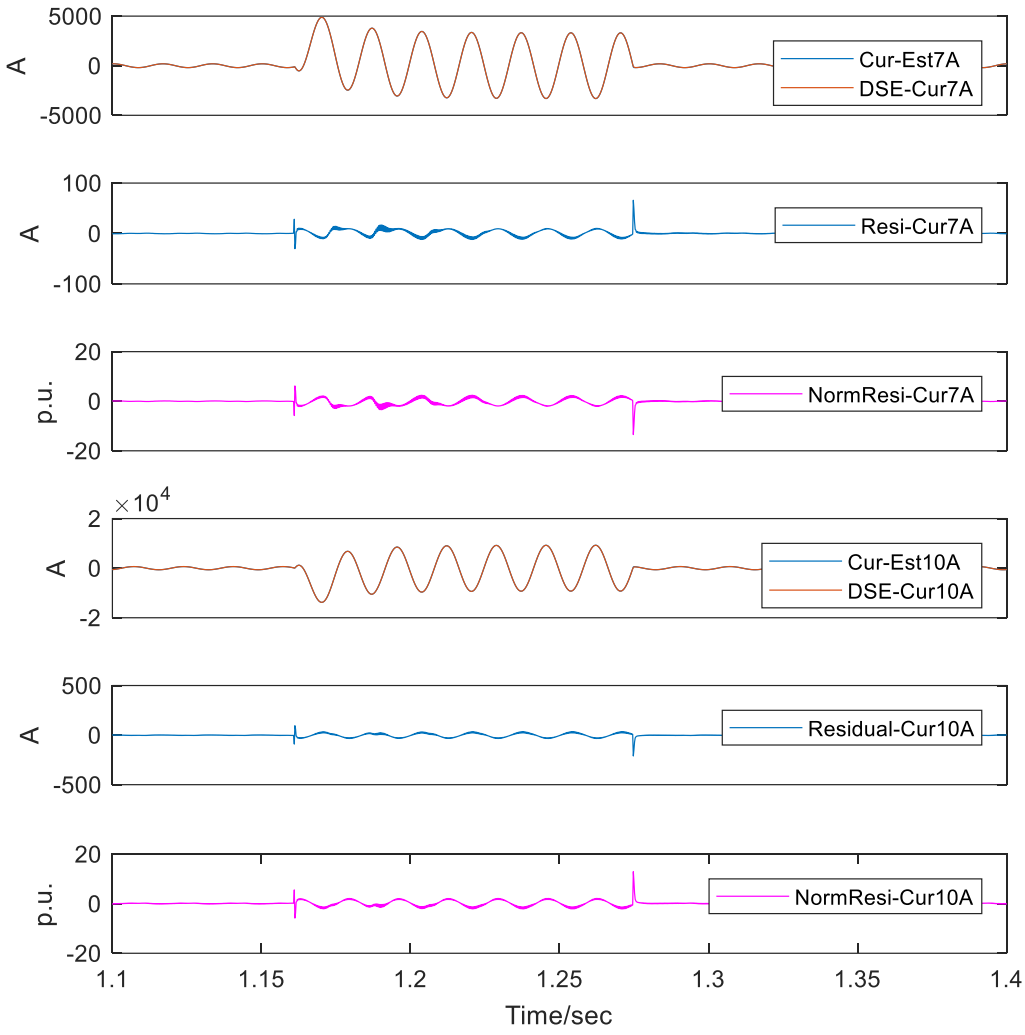
5000
0
-5000
A
Cur-Est7A
DSE-Cur7A
100
0
-100
A
Resi-Cur7A
20
0
-20
p.u.
NormResi-Cur7A
×10^4
2
0
-2
A
Cur-Est10A
DSE-Cur10A
500
0
-500
A
Residual-Cur10A
20
0
-20
p.u.
NormResi-Cur10A
1.1
1.15
1.2
1.25
1.3
1.35
1.4
Time/sec

(b)

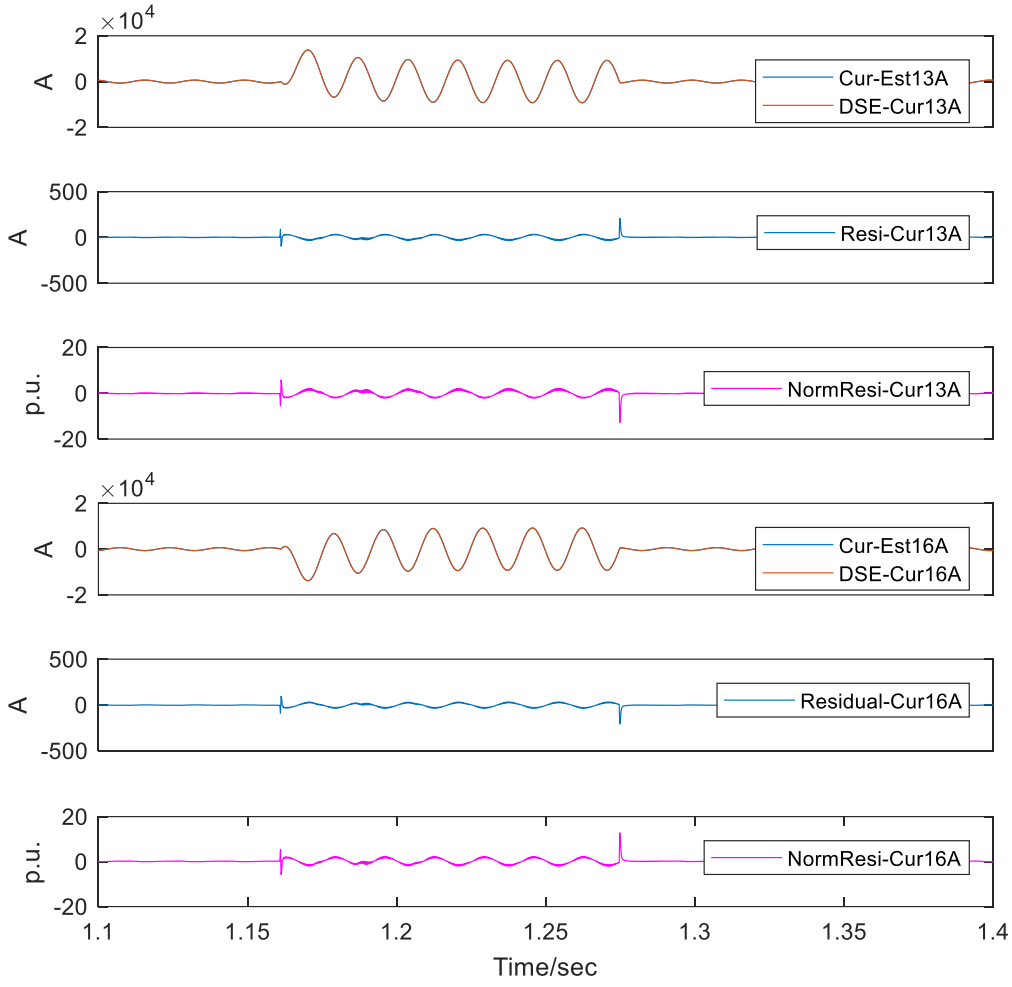

(c)

Figure 6-12 DSE results example using estimated measurements

It can be seen from Figure 6-12 that when using the estimated measurement samples for substation DSE, the current normalized residual can reach about 20 p.u., which is much smaller than the normalized residuals of substation DSE results using legacy measurement samples.

6.3.3 Substation DSE Comparison Results

1) Chi-square comparison

As illustrated in Section 6.2.4, the estimated measurement samples can be validated by comparing the Chi-square value. Let $\mathbf{h}_s(\mathbf{x}(t,t_m)$ denotes the substation power system model. The Chi-square for substation DSE using legacy or estimated samples are computed as:

- Chi-Square for substation DSE using legacy samples:

$$\text{Chi}-\text{Square}^L(t) = (\mathbf{z}_{Lega}(t,t_m) - \mathbf{h}_s(\mathbf{x}(t,t_m)))^T \mathbf{W}_{Lega}(\mathbf{z}_{Lega}(t,t_m) - \mathbf{h}_s(\mathbf{x}(t,t_m)))$$

- Chi-Square for substation DSE using estimated samples:

$$\text{Chi}-\text{Square}^E(t) = (\mathbf{z}_{Est}(t,t_m) - \mathbf{h}_s(\mathbf{x}(t,t_m)))^T \mathbf{W}_{Est}(\mathbf{z}_{Est}(t,t_m) - \mathbf{h}_s(\mathbf{x}(t,t_m)))$$

Figure 6-13shows the chi-square value comparison of substation DSE. The top traces of Figure 6-13 provide a graph of $\text{Chi}-\text{Square}^L(t)$ and $\text{Chi}-\text{Square}^E(t)$. The bottom trace shows $\text{Chi}-\text{Square}^L(t)$ minus $\text{Chi}-\text{Square}^E(t)$. It is obvious that $\text{Chi}-\text{Square}^L(t)$ is greater than $\text{Chi}-\text{Square}^E(t)$, which means using the estimated samples can achieve a smaller residual.

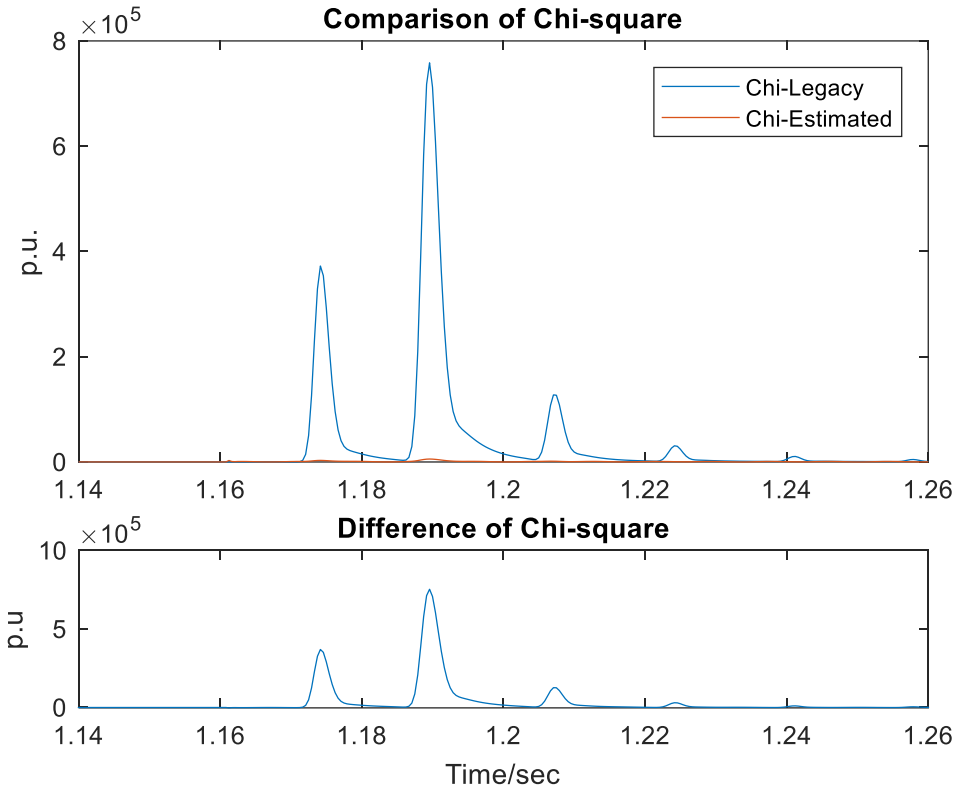

Figure 6-13 Chi-Square comparison results

2) $Tr\{\boldsymbol{C}_x\}$ Comparison

As illustrated in Section 6.2.4, a more accurate state estimates means a smaller value of $E\left\{\left\|\hat{\boldsymbol{x}}-\bar{\boldsymbol{x}}\right\|^2\right\}$, which can be quantified by $Tr\{\boldsymbol{C}_x\}$.

- When using the legacy samples for substation DSE

$$Tr\left\{\boldsymbol{C}_x{}^L\right\}=Tr\left\{(\boldsymbol{H}_s{}^T\boldsymbol{W}_{Lega}\boldsymbol{H}_s)^{-1}\right\}$$

- When using the estimated samples for substation DSE

$$Tr\left\{\boldsymbol{C}_x{}^E\right\}=Tr\left\{(\boldsymbol{H}_s{}^T\boldsymbol{W}_{Est}\boldsymbol{H}_s)^{-1}\right\}$$

Where $\boldsymbol{H}_s$ is the Jacobean matrix of substation DSE model, $\boldsymbol{W}_{Lega}$ =diag{…, $1/\sigma^2_{Lega,i}$,…} and $\boldsymbol{W}_{Est}$ =diag{…, $1/\sigma^2_{Est,i}$,…} denotes the weight matrix for legacy samples or estimated samples, respectively.

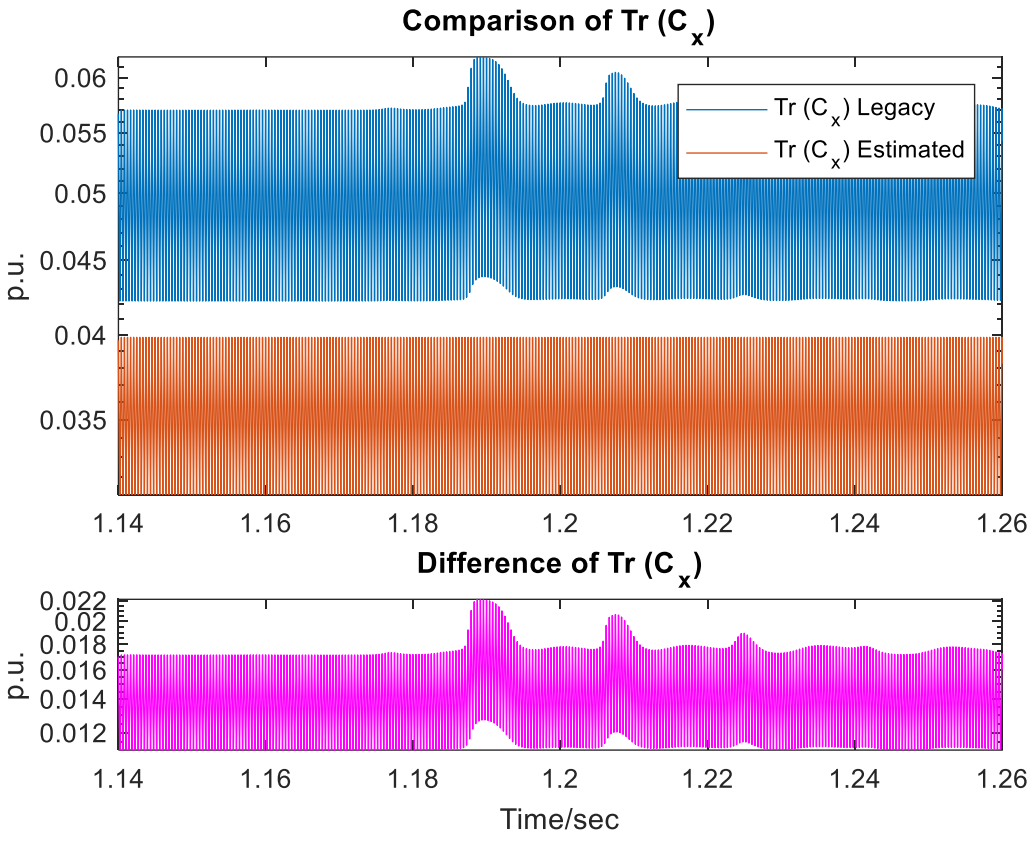

Figure 6-14 Comparison results of $Tr\{\boldsymbol{C}_x\}$

Figure 6-14 demonstrates the comparison of $Tr\{\boldsymbol{C}_x\}$ for the substation DSE. The top traces of Figure 6-14 provide a graph of $Tr\{\boldsymbol{C}_x{}^L\}$ and $Tr\{\boldsymbol{C}_x{}^E\}$. The bottom trace shows the difference between $Tr\{\boldsymbol{C}_x{}^L\}$ and $Tr\{\boldsymbol{C}_x{}^E\}$. It is obvious that $Tr\{\boldsymbol{C}_x{}^E\}$ < $Tr\{\boldsymbol{C}_x{}^L\}$, which indicates that the estimated samples can achieve more accurate state

estimates. Specifically, using the estimated samples can offer an on average improvement of $\frac{0.05-0.035}{0.035}=42\%$ for $Tr\{\boldsymbol{C}_x\}$.

3) $Tr\{\boldsymbol{C}_{\hat{z}}\}$ Comparison

As illustrated in Section 6.2.4, a more accurate state estimates means a smaller value of $E\left\{\left\|\hat{\boldsymbol{z}}-\overline{\boldsymbol{z}}\right\|^2\right\}$, which can be quantified by $Tr\{\boldsymbol{C}_{\hat{z}}\}$.

- When using the legacy samples for substation DSE

$$Tr\{\boldsymbol{C}_{\hat{z}}{}^{L}\}=Tr\{\boldsymbol{H}_s(\boldsymbol{H}_s{}^{\boldsymbol{T}}\boldsymbol{W}_{Lega}\boldsymbol{H}_s)^{-1}\boldsymbol{H}_s{}^{\boldsymbol{T}}\}$$

- When using the estimated samples for substation DSE

$$Tr\{\boldsymbol{C}_{\hat{z}}{}^{E}\}=Tr\{\boldsymbol{H}_s(\boldsymbol{H}_s{}^{\boldsymbol{T}}\boldsymbol{W}_{Est}\boldsymbol{H}_s)^{-1}\boldsymbol{H}_s{}^{\boldsymbol{T}}\}$$

Figure 6-15 depicts the comparison of $Tr\{\boldsymbol{C}_{\hat{z}}\}$ for the substation DSE. The top traces of Figure 6-15 provide graphs of $Tr\{\boldsymbol{C}_{\hat{z}}{}^{L}\}$ and $Tr\{\boldsymbol{C}_{\hat{z}}{}^{E}\}$, respectively. The bottom trace shows the difference between $Tr\{\boldsymbol{C}_x{}^{L}\}$ and $Tr\{\boldsymbol{C}_x{}^{E}\}$.

It can be seen clearly that $Tr\{\boldsymbol{C}_{\hat{z}}{}^{E}\} < Tr\{\boldsymbol{C}_{\hat{z}}{}^{L}\}$, which indicates that the estimated samples can achieve more accurate measurement estimates. Specifically, using the estimated samples can offer an on average improvement of $\frac{(11*10^{-3}-9*10^{-3})}{9*10^{-3}}=22\%$ for $Tr\{\boldsymbol{C}_{\hat{z}}\}$.

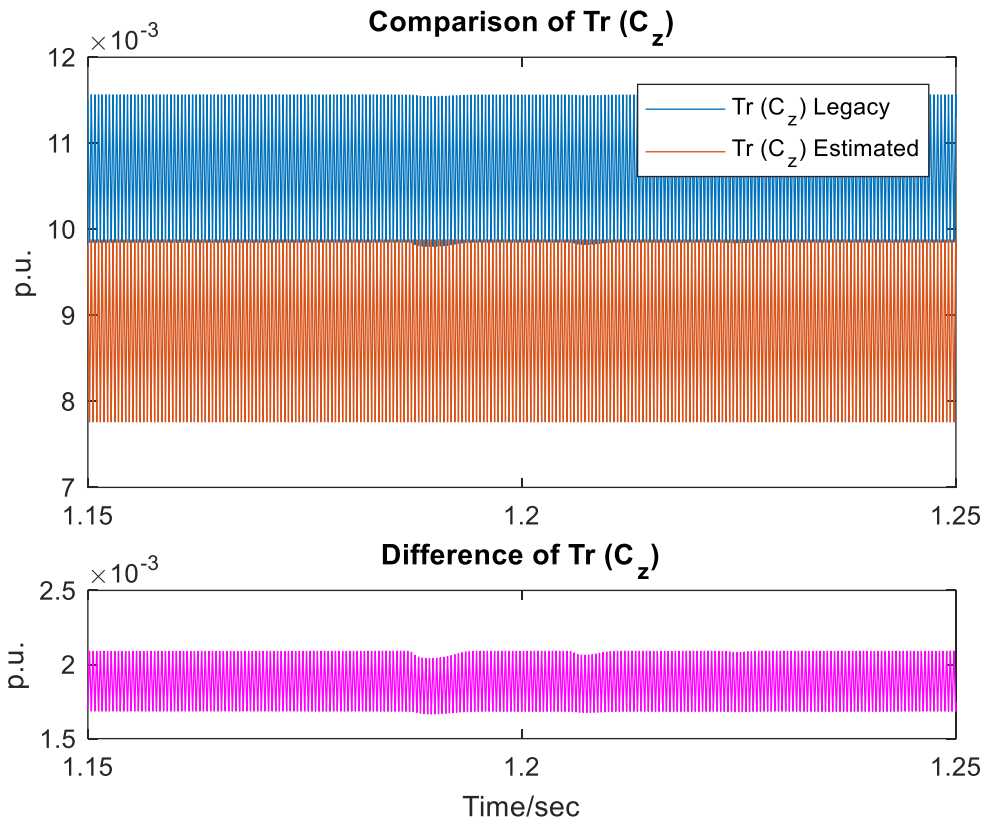

Figure 6-15 Comparison results of $Tr\{\boldsymbol{C}_{\hat{\boldsymbol{z}}}\}$

6.4 Summary

This Chapter has presented a validation procedure of the estimated primary samples. The methodology for the validation is achieved through performing substation level DSE using two different measurement options, respectively. The example substation system with instrumentation channels has been presented in detail. The simulation event has presented the example measurement samples of the two different measurement options. After performing the DSE on the substation system, the chi-square value, $Tr\{\boldsymbol{C}_x\}$ and $Tr\{\boldsymbol{C}_{\hat{z}}\}$ are compared. The comparison demonstrated that the estimated samples are able to achieve smaller residuals, more accurate state estimates and more accurate measurement estimates.

CHAPTER 7. EFFECTS OF INSTRUMENTATION CHANNEL ERROR CORRECTION ON PROTECTIVE RELAYS

7.1 Overview

As we discussed before, when CT saturation occurs in the instrumentation channels, the distorted secondary samples will lead to inaccurate primary measurements, which may cause relay mis-operation. The instrumentation channel error correction can be implemented to improve the reliability of protective relays.

The performance of the relay depends on the level of the error. To mitigate the effects of measurement error, legacy relays take the approach of desensitizing the relay settings to enable correct operation even in the presence of the abovementioned error. As introduced in Section 2.4, the abovementioned error may cause dependability or security problems for certain relays, which are summarized again as follows:

1) Distance relay may have a dependability problem due to CT saturation [28-29]. This is because CT saturation could result in a reduction of the current magnitude and a phase shift in the current, and thus lead to an increase in the measured impedance. Therefore, when CT saturation happens, distance relay may have a dependability problem of underreach or slower operating time under internal fault. The performance of distance relay under two internal fault events are demonstrated in Section 7.2. In each event, we compare the distance relay action using legacy or estimated measurement samples.

2) Current differential relay may have a security problem due to CT saturation [30-33]. This is because CT saturation may lead to substantial operating current under external fault, and thus an unnecessary trip decision may be issued. As examples, the performance of current differential relay under two external fault events are demonstrated in Section 7.3. In each event, we compare the current differential relay action using legacy or estimated measurement samples.

3) Setting-less relay may also have a security problem due to CT saturation because the distorted inaccurate measurement may result in a poor fit to the protection zone model and a very low confidence level, and thus an unnecessary trip decision may be issued. Hence, the performance of setting-less relay under two external fault events are demonstrated in Section 7.4. In each event, we compare the setting-less relay action using legacy or estimated measurement samples.

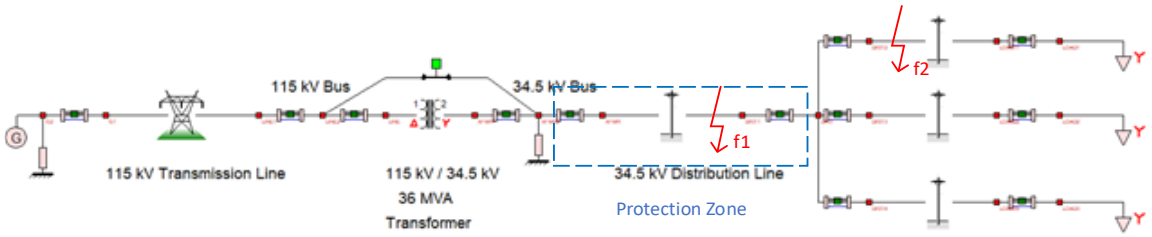

Figure 7-1 One-line diagram of simulation system with protection zone description

The simulation system has already been introduced in Chapter 6. As shown in Figure 7-1, the protection zone we are interested in is the 34.5 kV distribution line. The sequence parameters of the protection zone are listed in Table 7-1.

Table 7-1 Sequence parameters of the 34.5 kV distribution line

Parameters	Value
Positive (Negative) sequence series impedance (Z_1)	$1.4941\angle 78.67^{\circ}\Omega$
Zero sequence series impedance (Z_0)	$7.0942\angle 78.33^{\circ}\Omega$
Positive (Negative) sequence shunt susceptance (Y1)	$0.0181\angle 90^{\circ} m\Omega$
Zero sequence shunt susceptance (Y_0)	$0.0073\angle 90^{\circ} m\Omega$

As shown in Figure 6-2, instrumentation channels are measuring the three-phase voltage and current for the protection zone. For current instrumentation channel, the CT ratio is 800:5A with the error class of 10C100. The instrumentation cable is #10 copper cable with a length of 96 meters. The burden resistance is 0.1 Ω. For voltage instrumentation channel, the PT ratio is 19.919 kV:115V. The instrumentation cable is #10 copper cable with the length 96 meters. The burden resistance is 100 Ω. The secondary side measurement of each instrumentation channel is measured by Merging Unit with of 0.1%. The standard deviation for legacy current and voltage is 0.002 and 0.0071. The standard deviation for estimated current and voltage is 0.00102 and 0.0013.

7.2 Distance Protection

The settings of distance protection are listed in Table 7-2. The distance relay is installed at 34.5 kV Bus side and Zone 1 is able to cover 85% of protection zone.

Table 7-2 Distance protection settings (34.5 kV Bus side)

Functions	Settings
Zone 1	$1.27\angle 78.6^{\circ}\Omega$
Zone 2	$1.94\angle 78.6^{\circ}\Omega$, 0.15 sec delay
Zone 3	$3.88\angle 78.6^{\circ}\Omega$, 0.5 sec delay

7.2.1 Event 1 --- A Three-Phase Internal Fault

As shown in Figure 7-1, a three-phase fault occurs on 34.5 kV distribution line at 0.078 sec at f1, which is 3 km away from the 34.5 kV bus (The total length of the protection zone is 4 km). Since the fault occurs at 75% of protection zone, the correct impedance "seen" by the distance relay should enter zone 1 when the fault occurs. Next, we compare the performance of distance relay using estimated measurement samples and legacy measurement samples, respectively.

1) Performance of distance relay using estimated measurement samples

The three-phase estimated measurement samples at 34.5 kV bus side are shown in Figure 7-2 for the period [0.07, 0.2] sec.

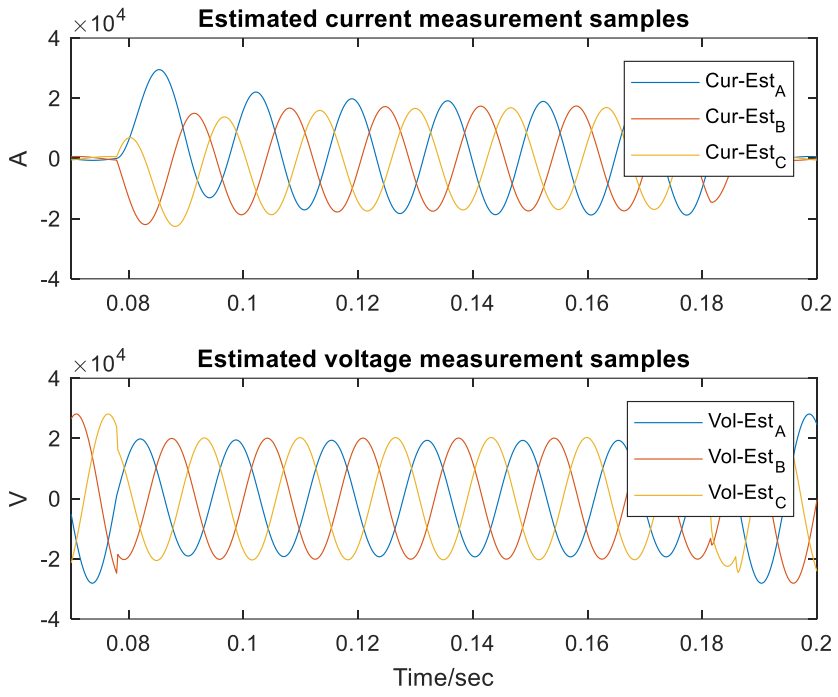

Figure 7-2 Three-phase estimated current and voltage measurement samples for a three-phase internal fault, distance protection

The trace of the impedance "seen" by the relay using the estimated measurement samples, superimpose on its characteristic, is shown in Figure 7-3. It can be seen from Figure 7-3 that the "impedance" enters zone 1 immediately when the fault occurs. Thus, the distance relay will issue a trip decision at t=0.078 sec, which is a correct identification of this internal fault.

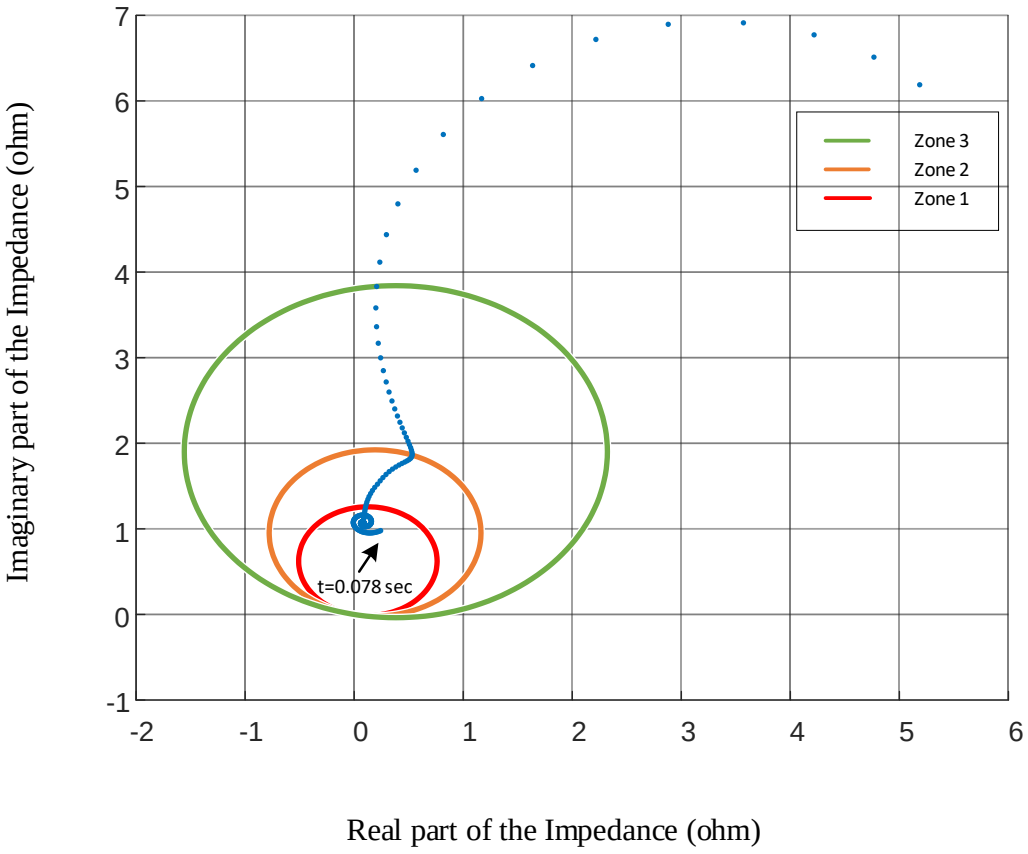

Figure 7-3 Trace of impedance during a three-phase internal fault using estimated measurement samples

2) Performance of distance relay using legacy measurement samples

The three-phase legacy measurement samples are shown in Figure 7-4 for the period [0.07, 0.2] sec. It is obvious that the legacy current samples are distorted after fault occurs, which could result in a reduction of the current magnitude and a phase shift in the

current. Therefore, the impedance “seen” by the relay could be increased due to current distortion.

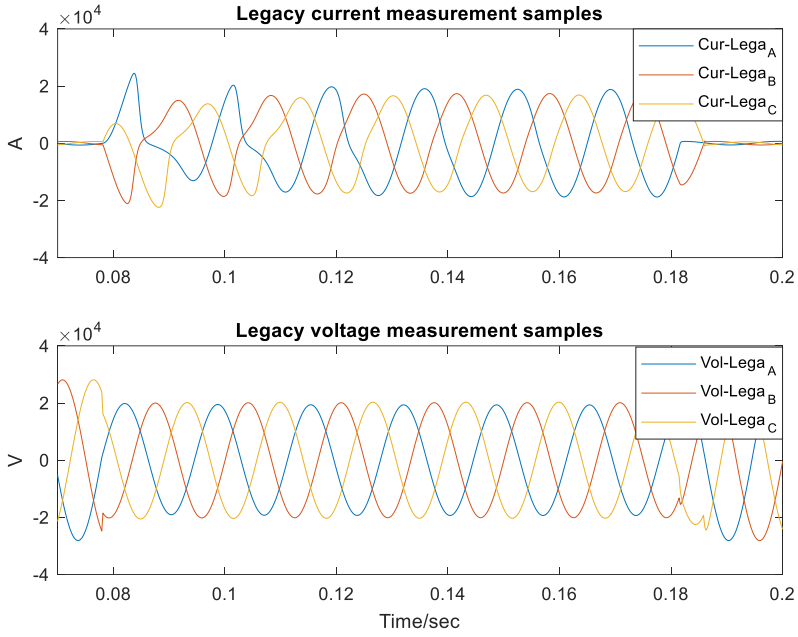

Figure 7-4 Three-phase legacy current and voltage measurement samples, distance protection

The trace of the impedance “seen” by the relay using the legacy measurement samples, superimpose on its characteristic, is shown in Figure 7-5. The impedance “seen” by the relay fails to enter zone 1when the fault occurs. Until t=0.092 sec, the impedance enters zone 1. Therefore, the distance relay will issue a trip decision at t= 0.092 sec. Compared with distance relay response using the estimated measurement samples, the legacy measurement samples will cause a delay of 0.014 sec in isolating this internal fault.

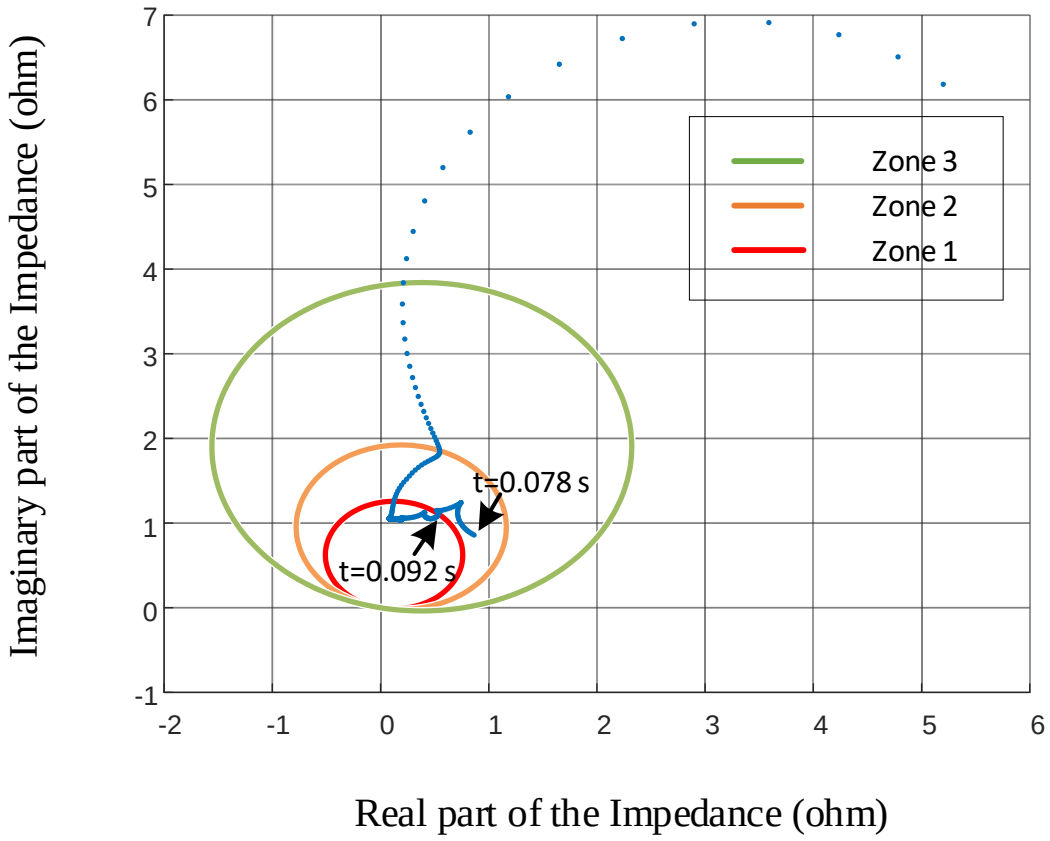

Figure 7-5 Trace of impedance during a three-phase internal fault using legacy measurement samples

7.2.2 Event 2 --- An Inter-Phase Internal Fault

As shown in Figure 7-1, an inter-phase AB fault occurs on 34.5 kV distribution line at 70% of protection zone at t=0.25 sec. Again, the correct impedance "seen" by the distance relay should enter zone 1 when the fault occurs. Next, we compare the performance of distance relay using estimated measurement samples and legacy measurement samples, respectively.

1) Performance of distance relay using estimated measurement samples

The three-phase estimated measurement samples at 34.5 kV bus side are shown in Figure 7-6 for the period [0.24, 0.37] sec.

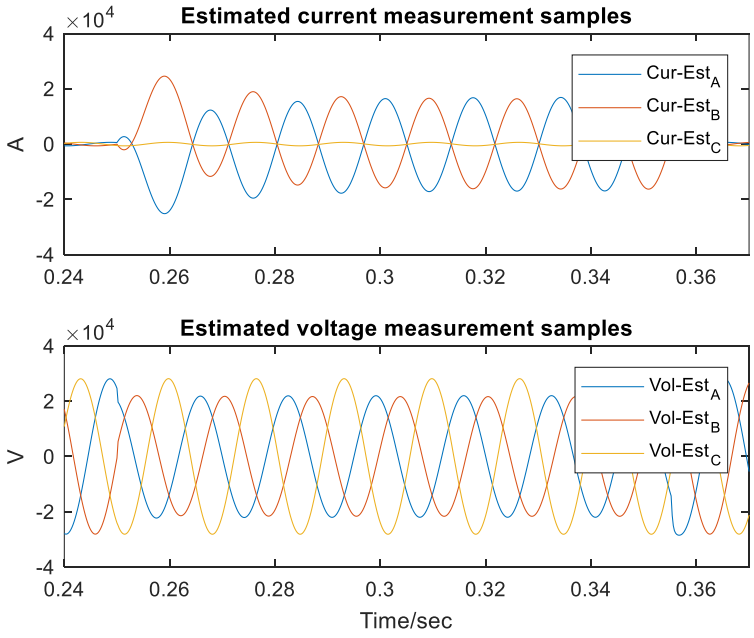

Figure 7-6 Three-phase estimated current and voltage measurement samples for an inter-phase AB internal fault, distance protection

The trace of the impedance "seen" by the relay using the estimated measurement samples, superimpose on its characteristic, is shown in Figure 7-7. Again, the "impedance" enters zone 1 immediately when the fault occurs. Thus, the distance relay will issue a correct trip decision at t=0.25 sec for this internal fault.

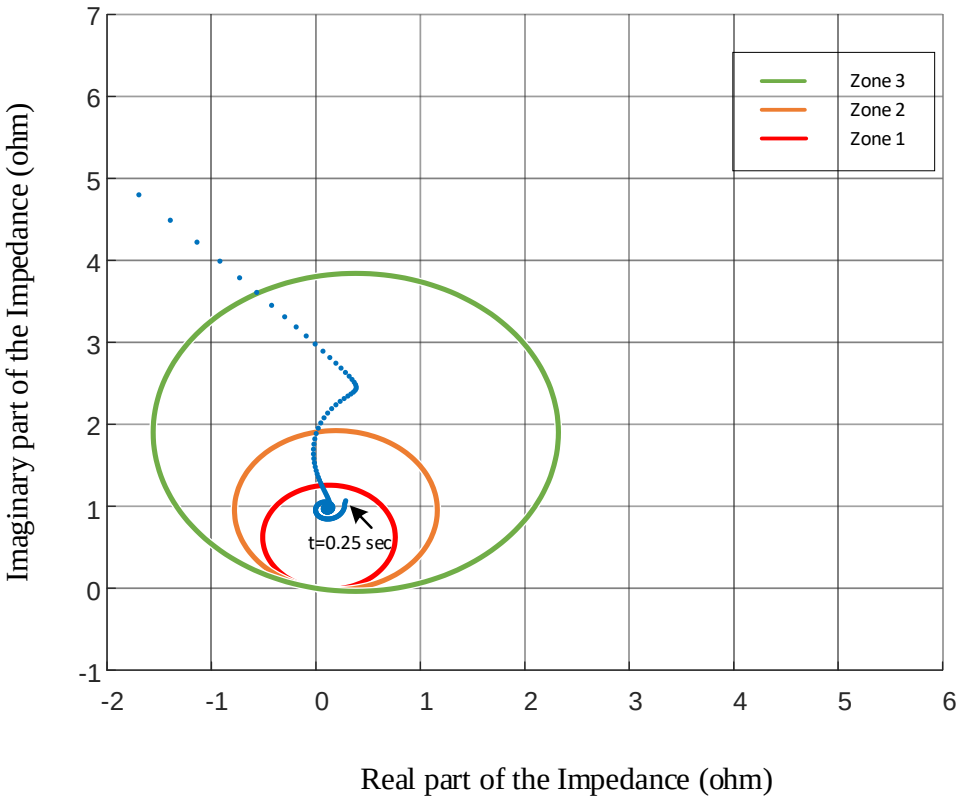

Figure 7-7 Trace of impedance during an inter-phase AB internal fault using estimated measurement samples

2) Performance of distance relay using legacy measurement samples

The three-phase legacy measurement samples are shown in Figure 7-8 for the period [0.24, 0.37] sec. Again, the impedance "seen" by the relay could be increased due to current distortion.

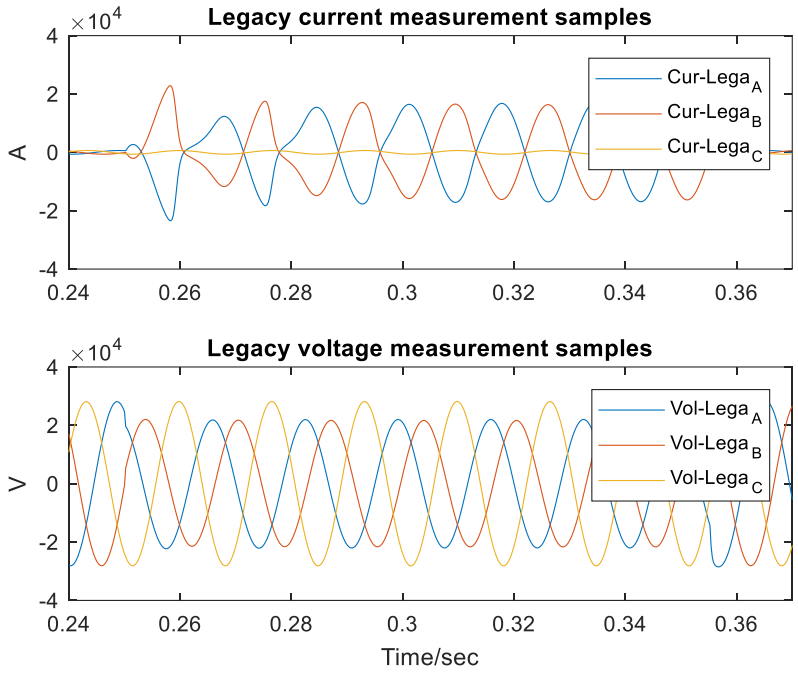

Figure 7-8 Three-phase legacy current and voltage measurement samples for an inter-phase AB internal fault, distance protection

The trace of the impedance "seen" by the relay using the legacy measurement samples, superimpose on its characteristic, is shown in Figure 7-9. The impedance "seen" by the relay fails to enter zone 1when the fault occurs until t=0.27 sec. Compared with distance relay response using the estimated measurement samples, the legacy measurement samples will cause a delay of 0.02 sec in isolating this internal fault.

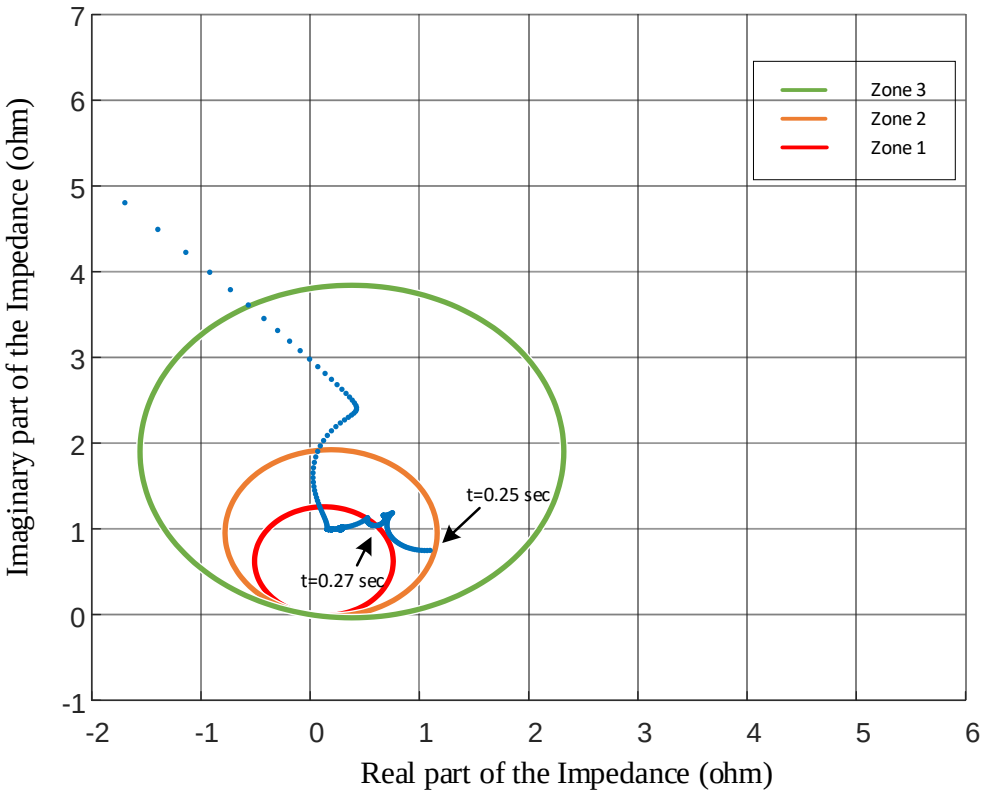

Figure 7-9 Trace of impedance during an inter-phase AB internal fault using legacy measurement samples

Summary: The above two events shows that when CT saturation introduces large errors (on average about 80% errors in these events)**,** the distorted legacy measurement samples can lead to an obvious increase in the impedance "seen" by distance relay, which can cause a delay in distance relay operation. However, when using the estimated measurement samples, the distance protection can correctly detect these internal faults and trip the device promptly.

7.3 Current Differential Protection

The current differential relay is installed at both sides of the 34.5 kV distribution line. The current differential relay will trip if both settings are exceeded: 1) The operating current referring to the primary side exceeds 10 A and 2) The operating current to restraining current ratio exceeds 20%.

7.3.1 Event 1 --- A Three-Phase to Neutral External Fault

As shown in Figure 7-1, a three-phase to neutral fault occurs on f2, one km from the protection zone at t=0.862 sec. Next, we compare the performance of current differential relay using estimated measurement samples and legacy measurement samples, respectively.

1) Performance of current differential relay using estimated measurement samples

The estimated current measurement samples at both terminal of the protection zone is shown in Figure 7-10 for the period [0.8, 0.95] sec. The results of the current differential relay during the fault is shown in Figure 7-11. When this external fault happens, the operating current referring to the primary side is about 100 A, but the operating current to restraining current ratio is less than 4%, which is far less than the 20% setting. Therefore, when using the estimated measurement samples, the current differential protection is able to correctly identify the fault as an external one and will not issue any trip signal.

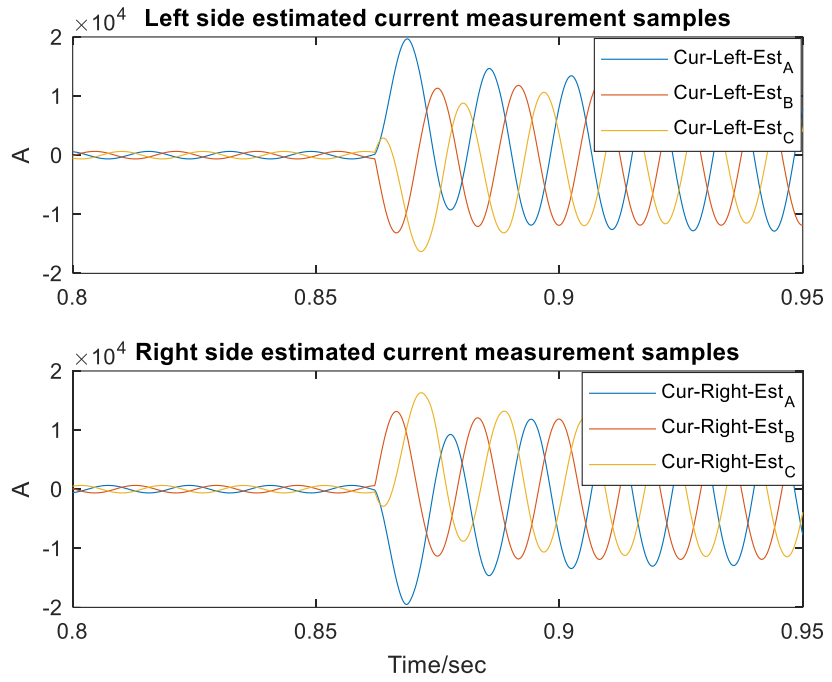

Figure 7-10 Terminal estimated current measurement samples for a three-phase to neutral external fault, current differential protection

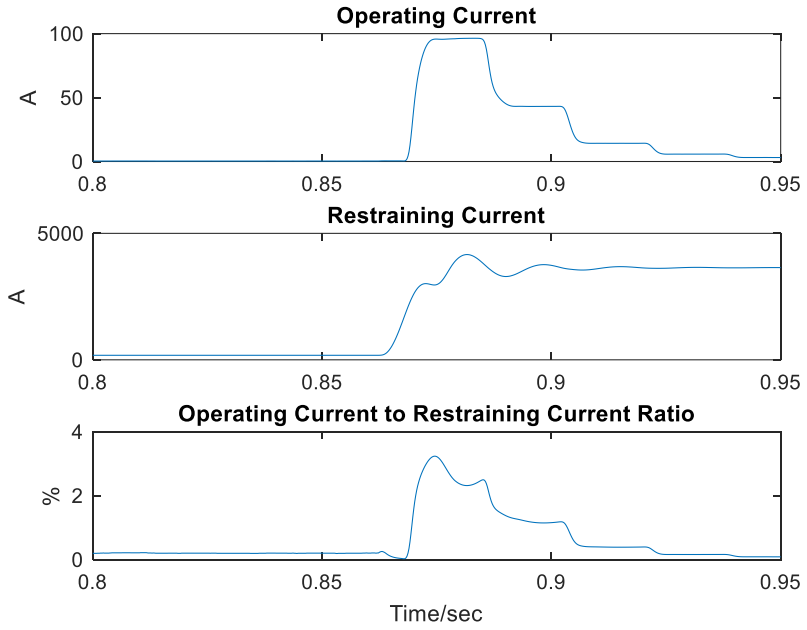

Figure 7-11 Results of current differential protection for a three-phase to neutral external fault, using estimated measurement samples

2) Performance of current differential relay using legacy measurement samples.

The legacy current measurement samples at both terminal of the protection zone is shown in Figure 7-12 for the period [0.8, 0.95] sec. It is obvious that the legacy samples are distorted after fault occurs, which can cause a much higher operating current and a much larger operating current to restraining current ratio. As shown in Figure 7-13, the operating current is about 900 A and the operating current to restraining current ratio is about 35%, which is more than the 20% setting. Therefore, when using the legacy measurement samples, the current differential relay will issue a trip decision, which is incorrect.

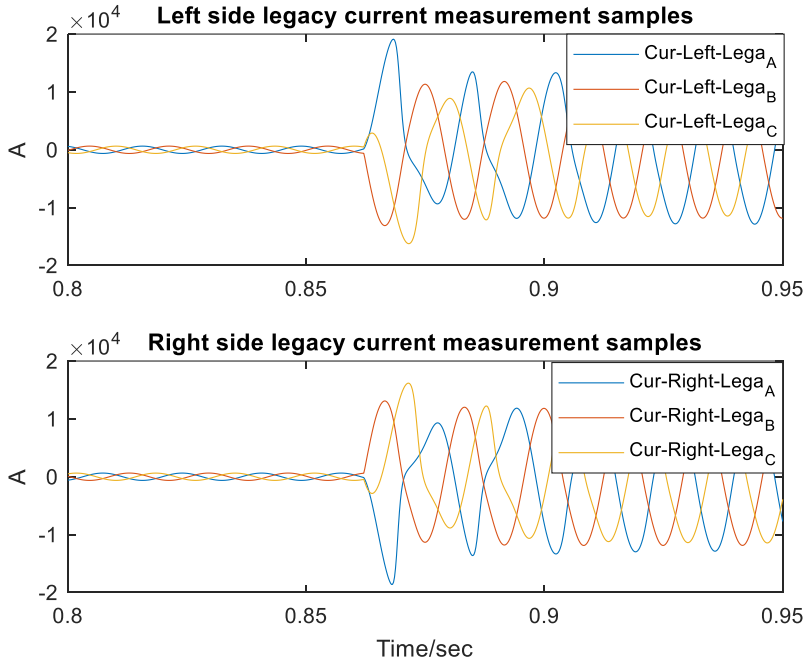

Figure 7-12 Terminal legacy current measurement samples for a three-phase to neutral external fault, current differential protection

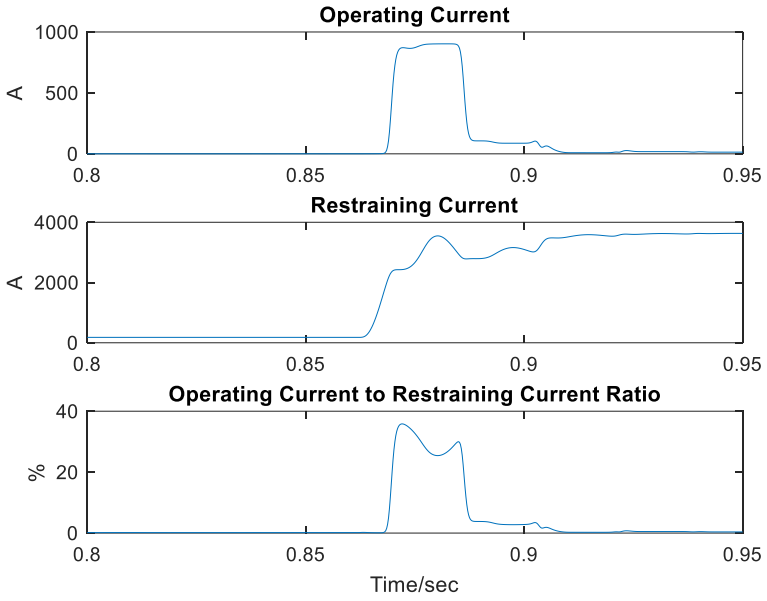

Figure 7-13 Results of current differential protection for a three-phase to neutral external fault, using legacy measurement samples

7.3.2 Event 2 --- An Inter-Phase to Neutral External Fault

As shown in Figure 7-1, an inter phase to neutral (AB-N) fault occurs on f2 (one km from the protection zone) at t=0.696 sec. Next, we compare the performance of current differential relay using estimated measurement samples and legacy measurement samples, respectively.

1) Performance of current differential relay using estimated measurement samples

The estimated current measurement samples at both terminal of the protection zone is shown in Figure 7-14 for the period [0.66, 0.78] sec. The results of the current differential relay during the fault are shown in Figure 7-15. When this external fault happens, the operating current referring to the primary side is about 50 A, but the operating current to restraining current ratio is less than 3%, which is far less than the

20% setting. Therefore, when using the estimated measurement samples, the current differential protection is able to correctly identify the fault as an external one and will not issue any trip signal.

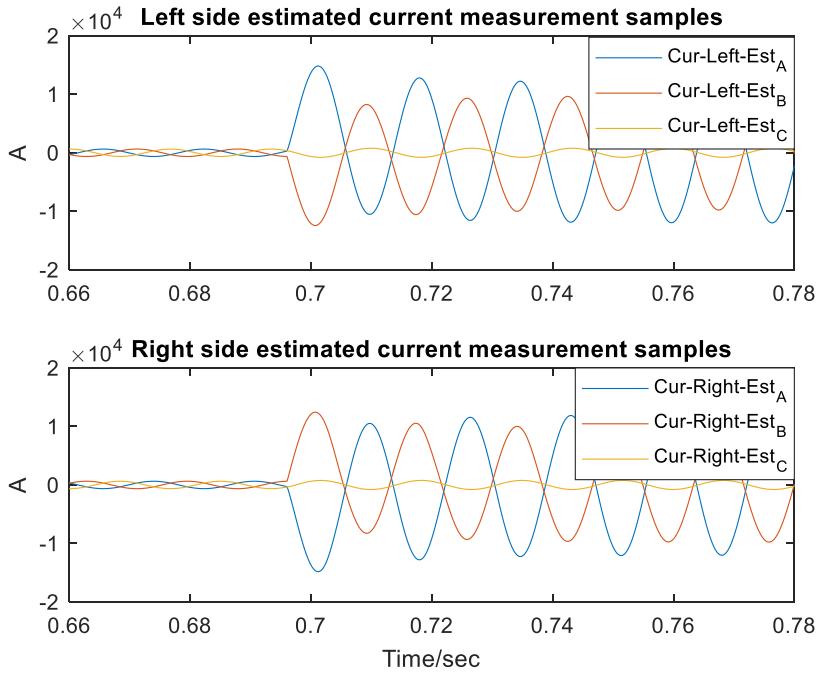

Figure 7-14 Terminal estimated current measurement samples for an inter-phase to neutral (AB-N) external fault, current differential protection

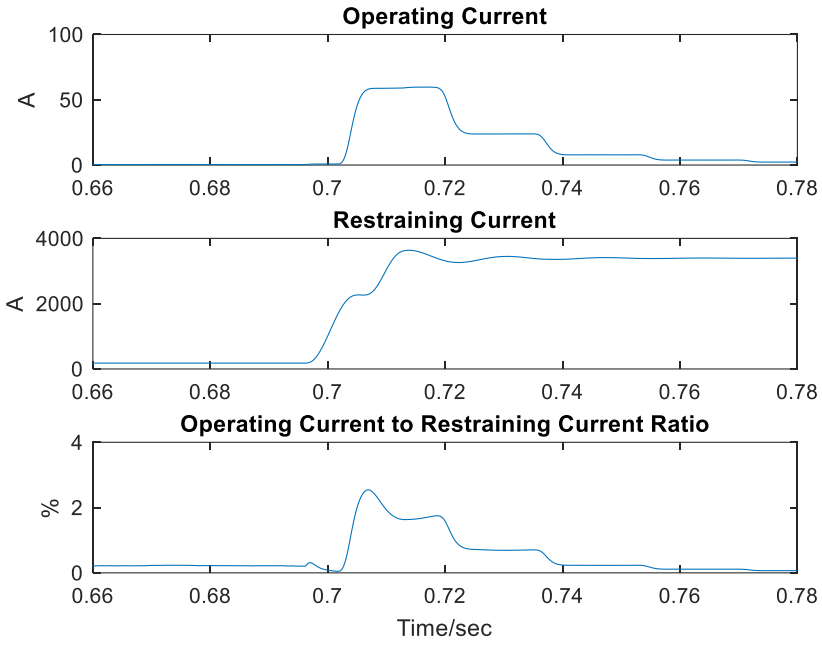

Figure 7-15 Results of current differential protection for an inter-phase to neutral (AB-N) external fault, using estimated measurement samples

2) Performance of current differential relay using legacy measurement samples

The legacy current measurement samples at both terminals of the protection zone are shown in Figure 7-16 for the period [0.66, 0.78] sec. It is obvious that the legacy samples are distorted after fault occurs, which can cause a much higher operating current and a much larger operating current to restraining current ratio. As shown in Figure 7-17, the operating current is about 700 A and the operating current to restraining current ratio is about 30%, which is more than the 20% setting. Therefore, when using the legacy measurement samples, the current differential relay will issue a false trip decision.

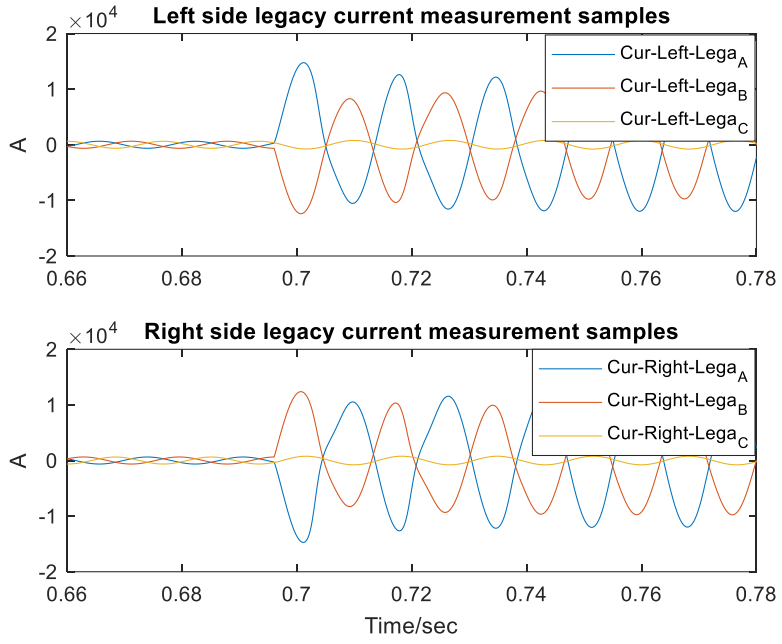

Figure 7-16 Terminal legacy current measurement samples for an inter-phase to neutral (AB-N) external fault, current differential protection

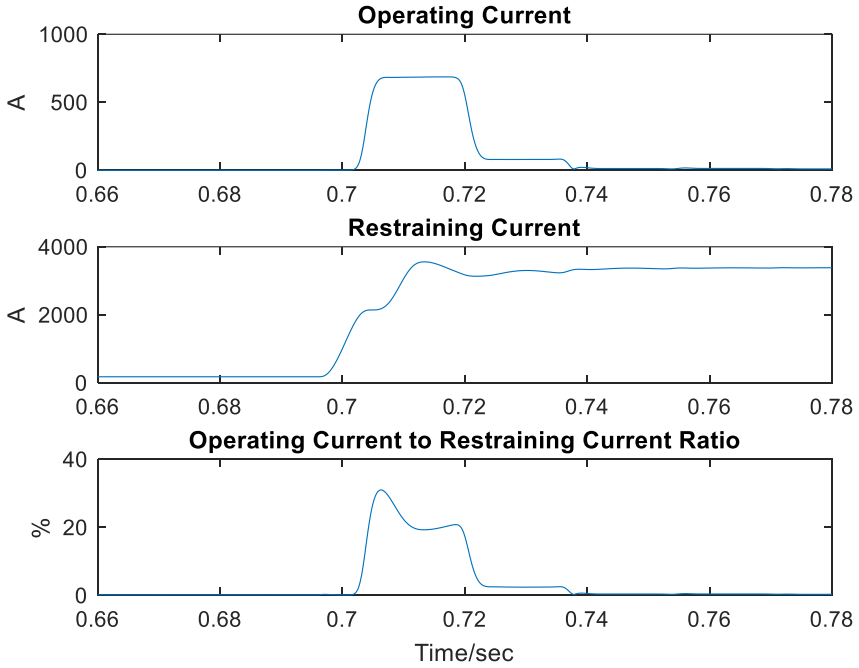

Figure 7-17 Results of current differential protection for an inter-phase to neutral (AB-N) external fault, using legacy measurement samples

Summary: In case of the external faults, when CT saturation introduces large errors, the legacy measurement samples can lead to very large operating current, thus the current differential relay will issue a false trip decision. However, when using the estimated measurement samples, the current differential protection can correctly identify the fault as an external one and will not issue the trip signal.

7.4 Setting-Less Protection

The setting-less relay is installed at both sides of the 34.5 kV distribution line. The setting-less protection delay time and reset time is set as 0.015 sec and 0.033 sec. The trip logic for setting-less relay has been described in Section 4.3.

7.4.1 Event 1 --- A Three-Phase to Neutral External Fault

As shown in Figure 7-1, a three-phase to neutral fault occurs on f2, one km from the protection zone at t=0.862 sec. Next, we compare the performance of setting-less relay using estimated measurement samples and legacy measurement samples, respectively.

1) Performance of setting-less relay using estimated measurement samples

The estimated current and voltage measurement samples at both terminals of the protection zone are shown in Figure 7-18 for the period [0.82, 0.89] sec.

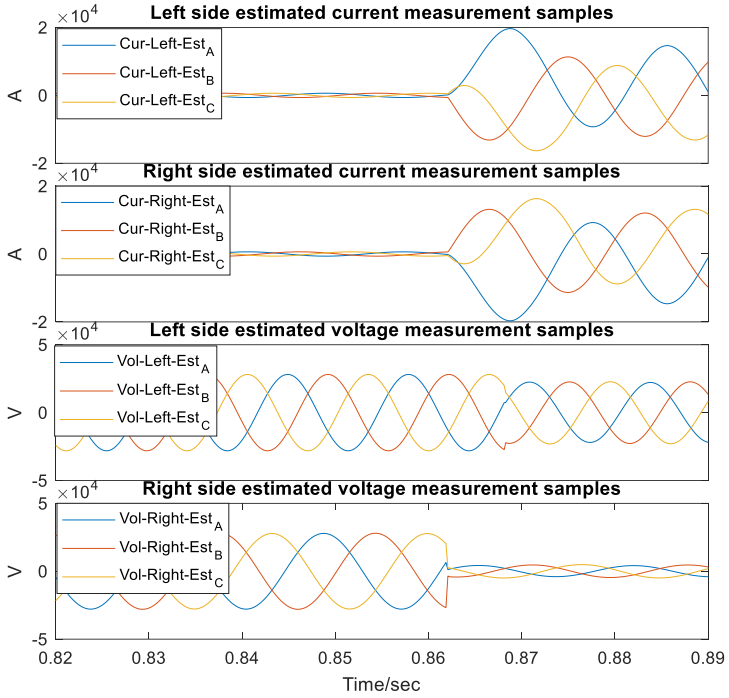

Figure 7-18 Terminal estimated measurement samples for a three-phase to neutral external fault, setting-less protection

The setting-less protection results using the estimated measurement samples are demonstrated in Figure 7-19. It shows that when fault occurs, the confidence level stays around 100% except for a very short period. This high confidence level means the protection zone is healthy so that the setting-less protection is able to correctly identify this fault as an external one when using the estimated measurement samples.

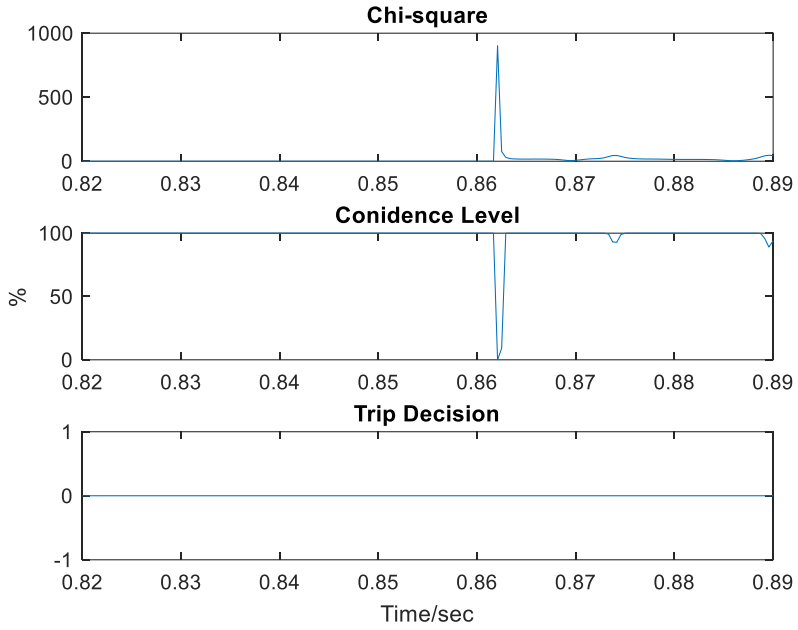

Figure 7-19 Results of setting-less protection for a three-phase to neutral external fault, using estimated measurement samples

2) Performance of setting-less relay using legacy measurement samples

The legacy current and voltage measurement samples at both terminals of the protection zone are shown in Figure 7-20 for the period [0.82, 0.89] sec. It is obvious that due to CT saturation, the confidence level drops to zero during the fault, as shown in Figure 7-21, so that the setting-less protection will falsely issue a trip decision of the protection zone when using the legacy measurement samples.

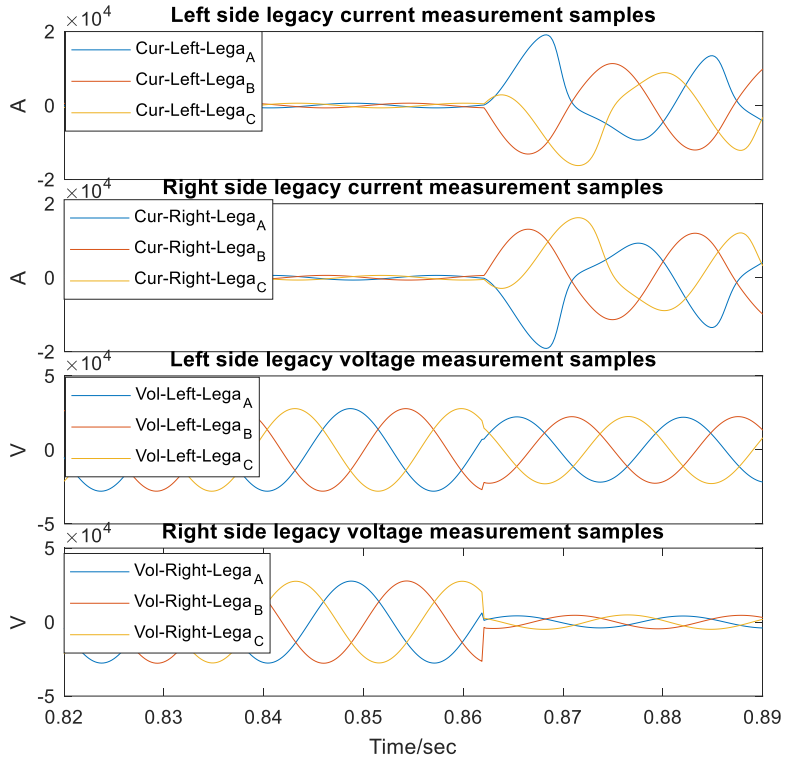

Figure 7-20 Terminal legacy measurement samples for a three-phase to neutral external fault, setting-less protection

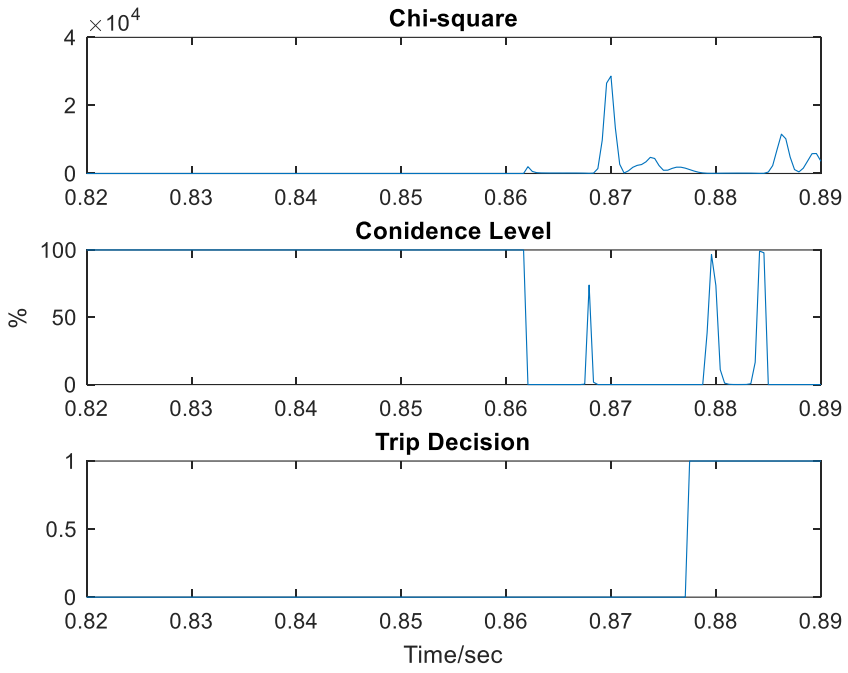

Figure 7-21 Results of setting-less protection for a three-phase to neutral external fault, using legacy measurement samples

7.4.2 Event 2 --- An Inter-Phase to Neutral External Fault

As shown in Figure 7-1, an inter phase to neutral (AB-N) fault occurs on f2 (one km from the protection zone) at t=0.696 sec. Next, we compare the performance of setting-less relay using estimated measurement samples and legacy measurement samples, respectively.

1) Performance of setting-less relay using estimated measurement samples

The estimated current and voltage measurement samples at both terminals of the protection zone are shown in Figure 7-22 for the period [0.665, 0.725] sec.

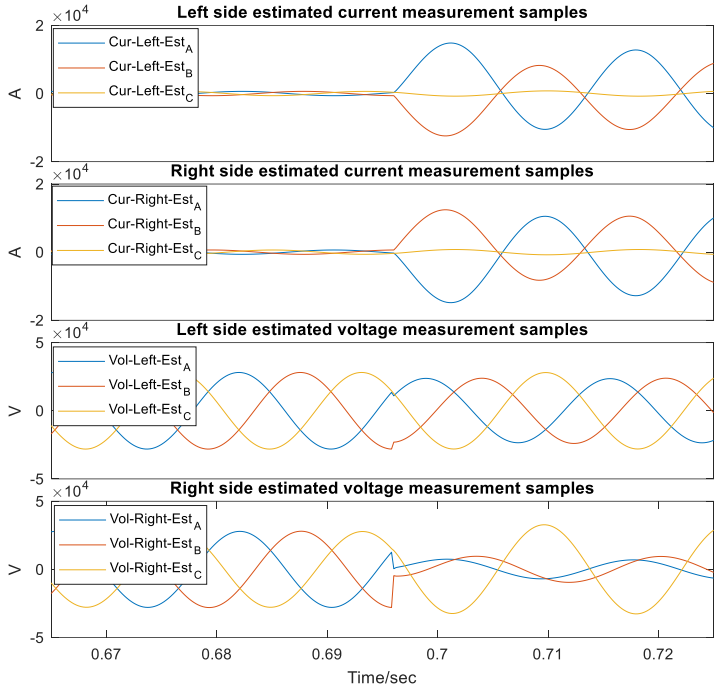

Figure 7-22 Terminal estimated measurement samples for an inter-phase to neutral (AB-N) external fault, setting-less protection

The setting-less protection results using the estimated measurement samples are demonstrated in Figure 7-23. Since the confidence level stays around 100% except a very short period, the setting-less protection is able to correctly identify this fault as an external one when using the estimated measurement samples.

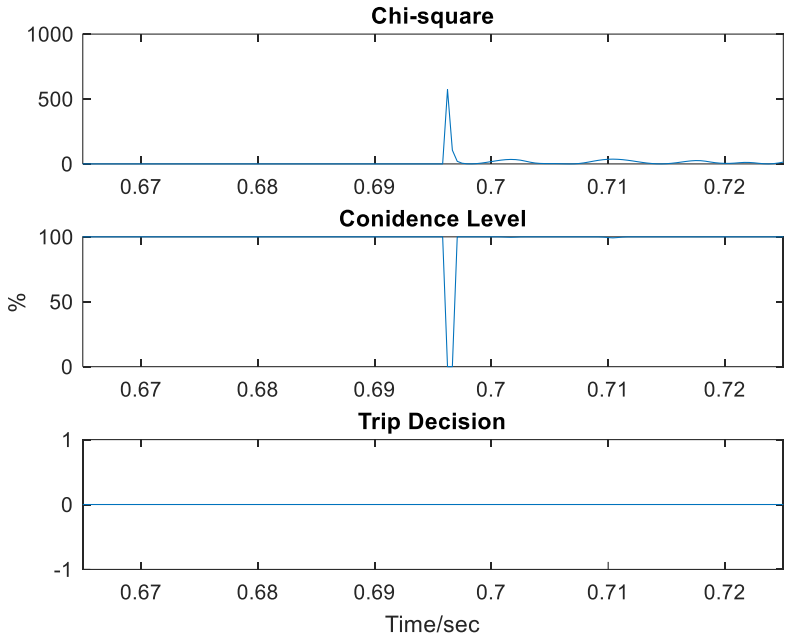

Figure 7-23 Results of setting-less protection for an inter-phase to neutral (AB-N) external fault, using estimated measurement samples

2) Performance of setting-less relay using legacy measurement samples

The legacy current and voltage measurement samples at both terminals of the protection zone are shown in Figure 7-24 for the period [0.665, 0.725] sec. Again, the distortion of legacy current samples leads to the confidence level dropping to zero, as shown in Figure 7-25, so that the setting-less protection will falsely issue a trip decision of the protection zone when using the legacy measurement samples

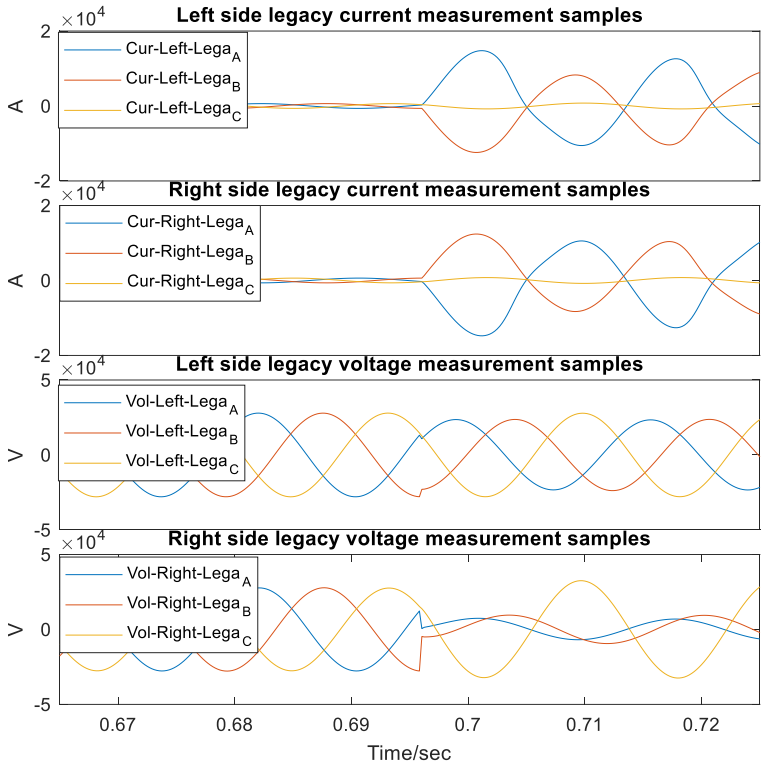

Figure 7-24 Terminal legacy measurement samples for an inter-phase to neutral (AB-N) external fault, setting-less protection

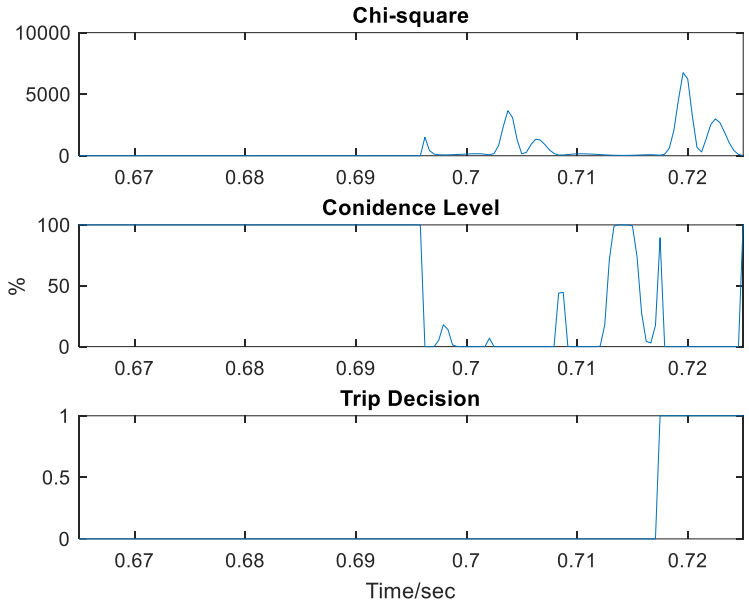

Figure 7-25 Results of setting-less protection for an inter-phase to neutral (AB-N) external fault, using legacy measurement samples

Summary: In case of the external fault, when large errors introduced by CT saturation, the inaccurate legacy measurement samples could not match the protection zone model, which leads to a very low confidence level, causing the setting-less relay to issue a false trip decision. However, the estimated measurement samples can have a much better match to the protection zone model and therefore the setting-less relay can correctly identify the fault as an external one and will not issue the trip signal.

7.5 Summary

The effects of instrumentation channel error correction on protective relays are discussed in this Chapter. The performance of three typical protection schemes is presented using estimated measurement samples and legacy measurement samples, respectively. The results show that when large instrumentation channel errors introduced by CT saturation, using the legacy measurement samples can lead to slower operation for distance relay in case of internal faults and false trip decision during external faults for current differential relay and setting-less relay. However, the relay performance (dependability and security) can be greatly improved and the mis-operations can be avoided if using the estimated measurement samples.

CHAPTER 8. CONCLUSIONS, CONTRIBUTIONS AND FUTURE WORK

8.1 Conclusions

A reliable operation of power system is crucial to nowadays increasing electricity demand. The protective relay takes responsibility to isolate the faulty components in a power system with high security and dependability. If a relay has a mis-operation or fails to interrupt a faulty power system component timely, it may cause wide disturbances and blackouts, even cascading failures of power system. The performance of the relay is determined by the quality and validity of the measurements as the relay input. However, large errors introduced by instrumentation channels will lead to inaccurate primary measurement samples, which can result in a relay mis-operation. Therefore, to make the protective relay reliable, it is essential to correct errors introduced by instrumentation channels.

8.2 Contributions

The contributions of this dissertation are:

A promising method based on WLS-DSE has been proposed to correct the errors introduced by instrumentation channels. This method can be integrated within MU to produce a point-by-point estimate of primary value, which is suitable for real-time protective relays. The error correction results have demonstrated that the proposed method is able to accurately reconstruct the CT primary samples in different

saturation scenarios and with different CT ratios. Meanwhile, the error correction method is also effective to reproduce PT primary side voltage with high accuracy.

A validation procedure of the estimated primary samples has been achieved via substation DSE. The legacy measurement samples and the estimated measurement samples are used respectively to perform substation DSE. The comparison of Chi-square value, $Tr\{\boldsymbol{C}_x\}$ and $Tr\{\boldsymbol{C}_{\hat{z}}\}$ are demonstrated to show that the estimated samples are able to achieve more accurate results.

The effects of instrumentation channel error correction on protective schemes are investigated for three typical protection schemes including distance protection, current differential protection as well as setting-less protection. The relay performance is compared when using the legacy measurement samples and the estimated measurement samples, respectively for each protection scheme. The results show that when large instrumentation channel errors introduced by CT saturation, the legacy measurement samples can result in a delay of detecting internal fault for distance relay and a false trip decision under external faults for current differential relay and setting-less relay. However, the estimated measurement samples can correctly identify internal faults and avoid mis-operation in case of external faults.

8.3 Future Research Directions

The proposed instrumentation channel error correction is based on the assumption that the instrumentation channel is healthy. If the instrumentation channel is not healthy in case of some hidden failures, such as CT short circuit, the proposed method is not able to estimate the primary quantities. More research needs to be done on how to obtain the primary quantities when instrumentation channel is not healthy.

In addition, the instrumentation channel error correction method can cope with new challenges in waveform distortion, such as instrumentation channel distorted waveform caused by geomagnetic disturbances (GMD). GMD occurs due to solar wind interacts with Earth's magnetic field. The geometrically induced current (GIC) during GMD events can drive instrument transformers to saturation and thus can lead to distorted waveforms. Research on applying the instrumentation channel error correction during GMD events is also an essential research topic.

Furthermore, the proposed instrumentation channel error correction method and its effects on protective relays are tested in simulation systems with satisfactory results. The next step is to test it in the field on a real power system to evaluate its actual performance.

PUBLICATIONS

[1] **Y. Kong**, S. Meliopoulos, and G. Cokkinides, "On-line current instrumentation channel error correction within merging units using constraint WLS dynamic state estimation," *2018 North American Power Symposium (NAPS)*, Fargo, ND, USA, 2018***. (2018 NAPS Best Paper Award First Prize)***

[2] S. Meliopoulos, G. Cokkinides, J. Xie, and **Y. Kong**, "Instrumentation Error Correction within Merging Units," 2018 Georgia Tech Fault & Disturbance Analysis Conf., Atlanta, Georgia, May 2018

[3] **Y. Kong**, S. Meliopoulos, and G. Cokkinides, "Study on effects of DSE-based instrumentation channel error correction on protective relays," (To be submitted).

[4] **Y. Kong**, S. Meliopoulos, and G. Cokkinides, "DSE-based instrumentation channel error correction and validation of the estimated samples," (To be submitted).

APPENDIX A. TRANSMISSION LINE MODEL

This appendix describes the dynamic model of transmission lines. A transmission line is modeled as a multi-section model as shown in Figure A-1 and each section is a π-equivalent circuit, as shown in Figure A-2.

In Figure A-1, $\boldsymbol{i}_{lk}(t)$ and $\boldsymbol{i}_{rk}(t)$ are three phase and neutral current vectors at each terminal of transmission line section *k*; $\boldsymbol{v}_{k}(t)$ and $\boldsymbol{v}_{k+1}(t)$ are three phase and neutral voltage vectors at each terminal of transmission line section *k*

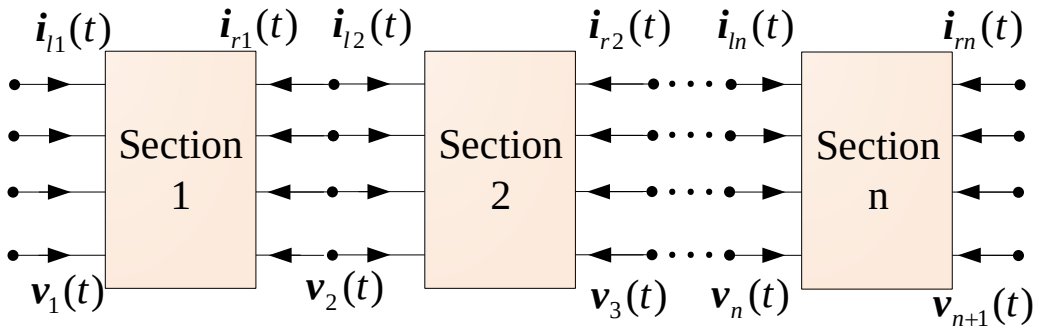

Figure A-1 Multi-section model of transmission line

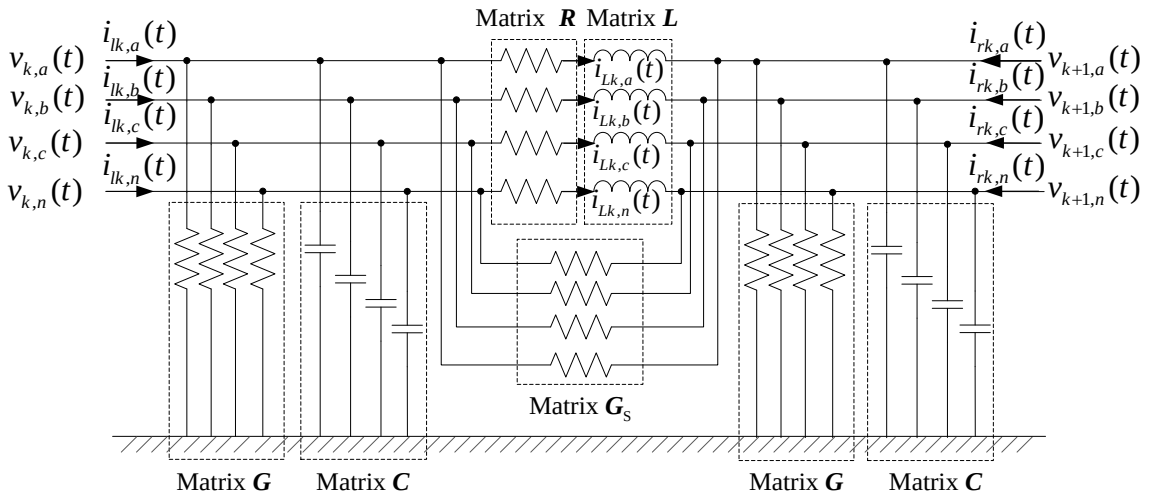

Figure A-2 π - Equivalent circuit of each section

In Figure A-2, the matrices $\boldsymbol{R}$, $\boldsymbol{L}$, $\boldsymbol{G}$, $\boldsymbol{C}$ and $\boldsymbol{G}_S$ represent series resistance, series inductance, shunt conductance, shunt capacitance and stabilizing conductance matrices of each section. Each section model can be described as:

$$\boldsymbol{i}_{lk}(t) = \left(\boldsymbol{G} + \boldsymbol{G}_S\right) \cdot \boldsymbol{v}_k(t) - \boldsymbol{G}_S \cdot \boldsymbol{v}_{k+1}(t) + \boldsymbol{C} \cdot \frac{d\boldsymbol{v}_k(t)}{dt} + \boldsymbol{i}_{Lk}(t)$$

$$\boldsymbol{i}_{rk}(t) = \left(\boldsymbol{G} + \boldsymbol{G}_S\right) \cdot \boldsymbol{v}_{k+1}(t) - \boldsymbol{G}_S \cdot \boldsymbol{v}_k(t) + \boldsymbol{C} \cdot \frac{d\boldsymbol{v}_{k+1}(t)}{dt} - \boldsymbol{i}_{Lk}(t) \qquad \text{(A-1)}$$

$$\boldsymbol{0} = -\boldsymbol{v}_k(t) + \boldsymbol{v}_{k+1}(t) + \boldsymbol{R} \cdot \boldsymbol{i}_{Lk}(t) + \boldsymbol{L} \cdot \frac{d\boldsymbol{i}_{Lk}(t)}{dt}$$

Where $\boldsymbol{v}_k(t) = \begin{bmatrix} v_{k,a}(t) \\ v_{k,b}(t) \\ v_{k,c}(t) \\ v_{k,n}(t) \end{bmatrix}$, $\boldsymbol{v}_{k+1}(t) = \begin{bmatrix} v_{k+1,a}(t) \\ v_{k+1,b}(t) \\ v_{k+1,c}(t) \\ v_{k+1,n}(t) \end{bmatrix}$, $\boldsymbol{i}_{Lk}(t) = \begin{bmatrix} i_{Lk,a}(t) \\ i_{Lk,b}(t) \\ i_{Lk,c}(t) \\ i_{Lk,n}(t) \end{bmatrix}$

$\boldsymbol{i}_{lk}(t) = \begin{bmatrix} i_{lk,a}(t) \\ i_{lk,b}(t) \\ i_{lk,c}(t) \\ i_{lk,n}(t) \end{bmatrix}$, $\boldsymbol{i}_{rk}(t) = \begin{bmatrix} i_{rk,a}(t) \\ i_{rk,b}(t) \\ i_{rk,c}(t) \\ i_{rk,n}(t) \end{bmatrix}$

The definition of state variables and through variables in Equation (A-1) are listed in Table A-1 and Table A-2, respectively.

Table A-1 States of section k, π - Equivalent circuit model

Index	Variable	Description
1	$v_{k,a}(t)$	phase A voltage, left terminal (V)
2	$v_{k,b}(t)$	phase B voltage, left terminal (V)
3	$v_{k,c}(t)$	phase C voltage, left terminal (V)
4	$v_{k,n}(t)$	phase N voltage, left terminal (V)
5	$v_{k+1,a}(t)$	phase A voltage, right terminal (V)
6	$v_{k+1,b}(t)$	phase B voltage, right terminal (V)
7	$v_{k+1,c}(t)$	phase C voltage, right terminal (V)
8	$v_{k+1,n}(t)$	phase N voltage, right terminal (V)
9	$i_{Lk,a}(t)$	phase A current through inductance (A)
10	$i_{Lk,b}(t)$	phase B current through inductance (A)

11	$i_{Lk,c}(t)$	phase C current through inductance (A)
12	$i_{Lk,n}(t)$	phase N current through inductance (A)

Table A-2 Through variables of section *k*, *π* - Equivalent circuit model

Index	Variable	Description
1	$i_{lk,a}(t)$	phase A current, left terminal (A)
2	$i_{lk,b}(t)$	phase B current, left terminal (A)
3	$i_{lk,c}(t)$	phase C current, left terminal (A)
4	$i_{lk,n}(t)$	phase N current, left terminal (A)
5	$i_{rk,a}(t)$	phase A current, left terminal (A)
6	$i_{rk,b}(t)$	phase B current, left terminal (A)
7	$i_{rk,c}(t)$	phase C current, left terminal (A)
8	$i_{rk,n}(t)$	phase N current, left terminal (A)

APPENDIX B. THREE-PHASE TRANSFORMER MODEL

This appendix describes a three-phase two-winding transformer model. The three-phase transformer model is constructed by connecting three single-phase models into one composite model. The equivalent circuit of single-phase two-winding transformer is illustrated in Figure B-1.

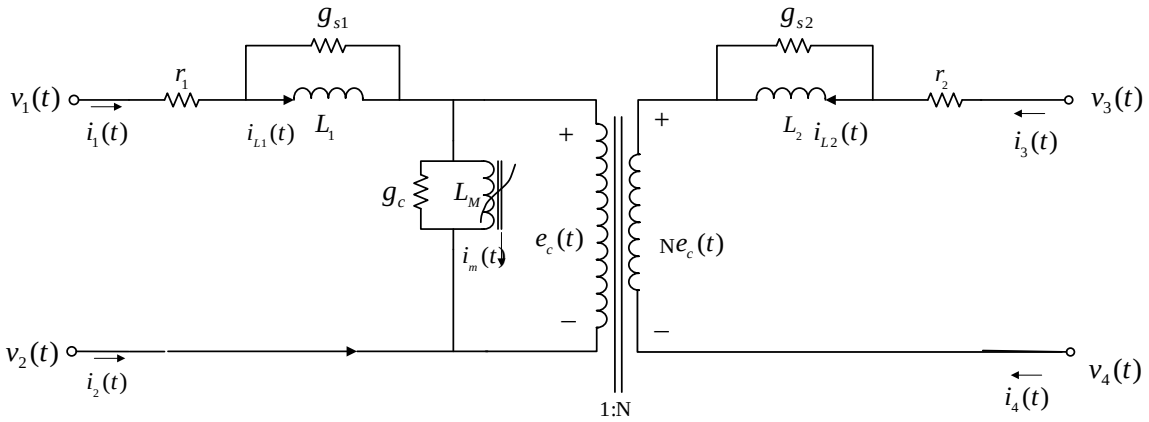

Figure B-1 Equivalent circuit of single-phase two-winding transformer

The single-phase transformer model is described as:

$$i_1(\mathrm{t}) = i_{L1}(\mathrm{t}) + g_{s1}L_1\frac{di_{L1}(\mathrm{t})}{dt}$$

$$i_2(\mathrm{t}) = -i_{L1}(\mathrm{t}) - g_{s1}L_1\frac{di_{L1}(\mathrm{t})}{dt}$$

$$i_3(\mathrm{t}) = i_{L2}(\mathrm{t}) + g_{s2}L_2\frac{di_{L2}(\mathrm{t})}{dt}$$

$$i_4(\mathrm{t}) = -i_{L2}(\mathrm{t}) - g_{s2}L_2\frac{di_{L2}(\mathrm{t})}{dt}$$

$$0 = v_2(\mathrm{t}) - v_1(\mathrm{t}) + r_1 i_{L1}(\mathrm{t}) + (r_1 g_{S1} + 1) L_1 \frac{di_{L1}(\mathrm{t})}{dt} + e_c(\mathrm{t})$$

$$0 = v_4(\mathrm{t}) - v_3(\mathrm{t}) + r_2 i_{L2}(\mathrm{t}) + (r_2 g_{S2} + 1) L_2 \frac{di_{L2}(\mathrm{t})}{dt} + N e_c(\mathrm{t})$$

$$0 = i_{L1}(\mathrm{t}) + N i_{L2}(\mathrm{t}) - i_m(\mathrm{t}) + g_{s1} L_1 \frac{di_{L1}(\mathrm{t})}{dt} + N g_{s2} L_2 \frac{di_{L2}(\mathrm{t})}{dt} - g_m e_c(\mathrm{t})$$

$$0 = e_c(\mathrm{t}) - \frac{d\lambda(\mathrm{t})}{dt}$$

$$0 = i_m(\mathrm{t}) - i_0 \left(\frac{\lambda(\mathrm{t})}{\lambda_0} \right)^n$$

The state variables and through variables are listed in Table B-1and Table B-2.

Table B-1 States of single-phase two-winding transformer

Index	Variable	Description
1	$v_1(t)$	Primary bus voltage (V)
2	$v_2(t)$	Primary bus voltage, neutral (V)
3	$v_3(t)$	Secondary bus voltage (V)
4	$v_4(t)$	Secondary bus voltage, neutral (V)
5	$i_{L1}(t)$	Current through primary inductance (A)
6	$i_{L2}(t)$	Current through secondary inductance (A)

7	$e_c(t)$	Voltage generated by the flux (V)
8	$\lambda(t)$	Flux linkage (Web)
9	$i_m(t)$	Magnetizing current (A)

Table B-2 Through variable of single-phase two-winding transformer

Index	Variable	Description
1	$i_1(t)$	Primary current (A)
2	$i_2(t)$	Primary current, neutral (A)
3	$i_3(t)$	Secondary current (A)
4	$i_4(t)$	Secondary current, neutral (A)

Next, three single-phase transformer models are connected to construct a three-phase transformer model. The number of external states in three-phase transformer is determined by the connection configurations. The internal states are defined by directly appending the internal states of each bank to the state vector. There are four types of connection configuration: 1) WYE-WYE; 2) WYE-DELTA; 3) DELTA-WYE and 4) DEALTA-DELTA. How to map the external state index of each bank to a three-phase external state index for each connection configuration is illustrated as follows.

1) WYE-WYE

The WYE-WYE connection configuration is shown in Figure B-2. The state variable consists of 8 external states and then each bank internal states appended to the state vector. The mapping of each bank external state index to the three-phase model is listed in Table B-3.

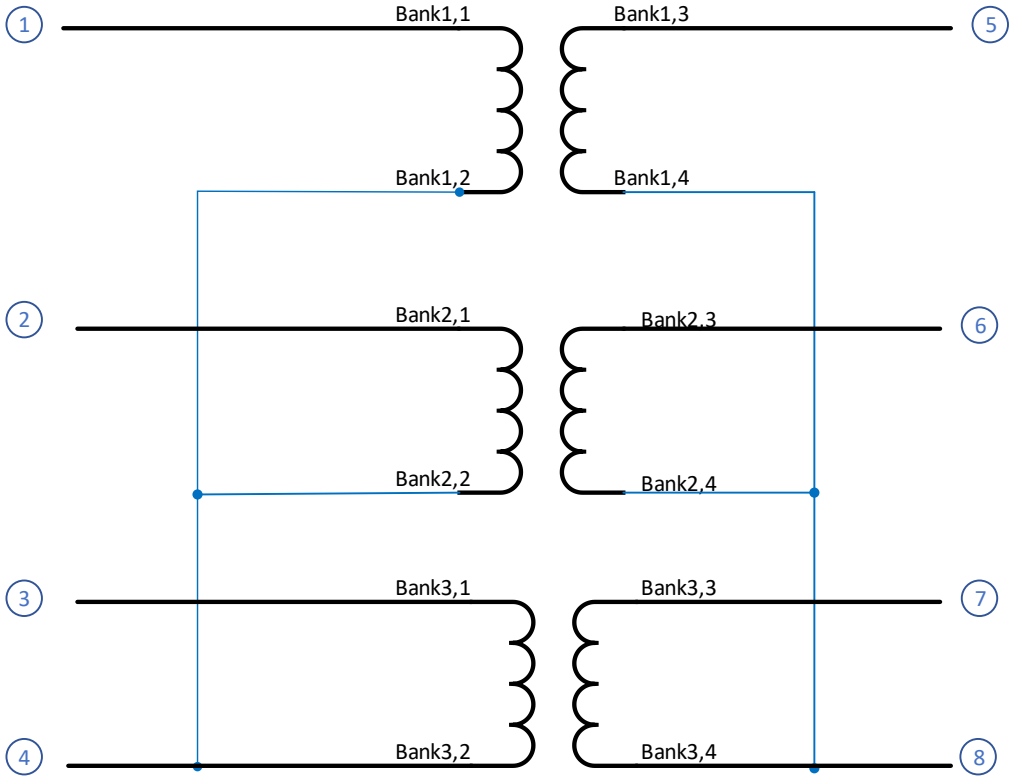

Figure B-2 WYE-WYE connection configuration

Table B-3 External state index mapping to three-phase model, WYE-WYE connection configuration

Bank	External State Index Mapping to three-phase model
1	1,4,5,8
2	2,4,6,8
3	3,4,7,8

2) WYE-DELTA

The WYE-DELTA connection configuration is shown in Figure B-3. The state variable consists of 7 external states and then each bank internal states appended to the state vector. The mapping of each bank external state index to the three-phase model is listed in Table B-4.

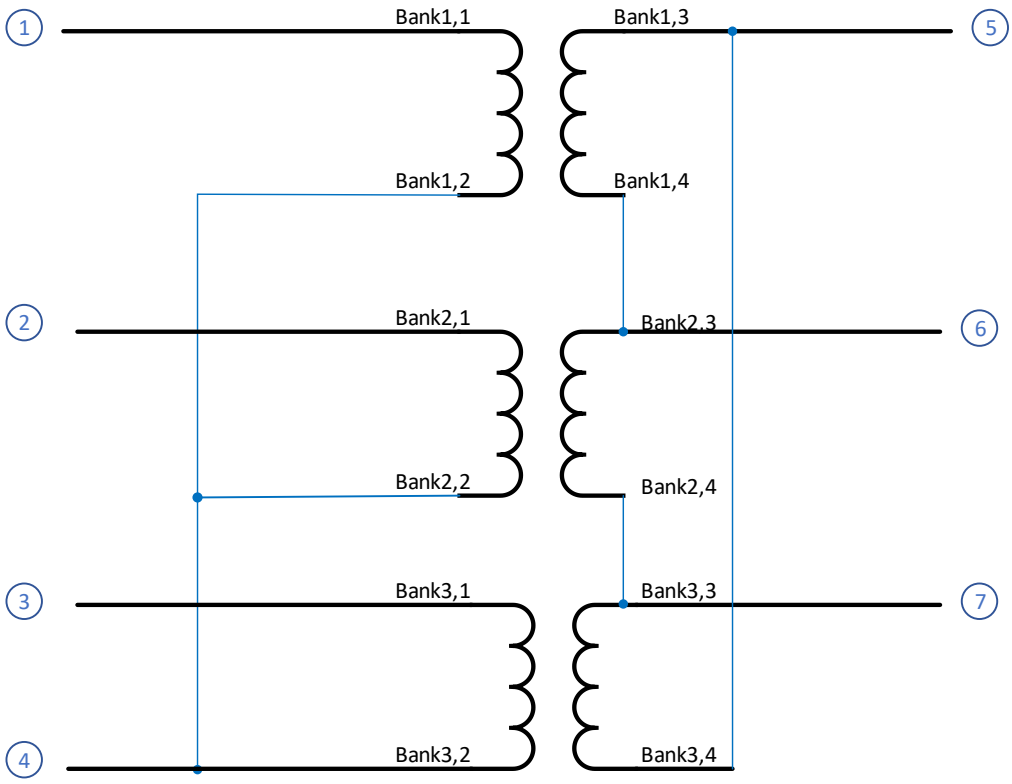

Figure B-3 WYE-DELTA connection configuration

Table B-4 External state index mapping to three-phase model, WYE-DELTA connection configuration

Bank	External State Index Mapping to three-phase model
1	1,4,5,6
2	2,4,6,7
3	3,4,7,5

3) DEALTA-WYE

The DELTA-WYE connection configuration is shown in Figure B-4. The state variable consists of 7 external states and then each bank internal states appended to the state vector. The mapping of each bank external state index to the three-phase model is listed in Table B-5.

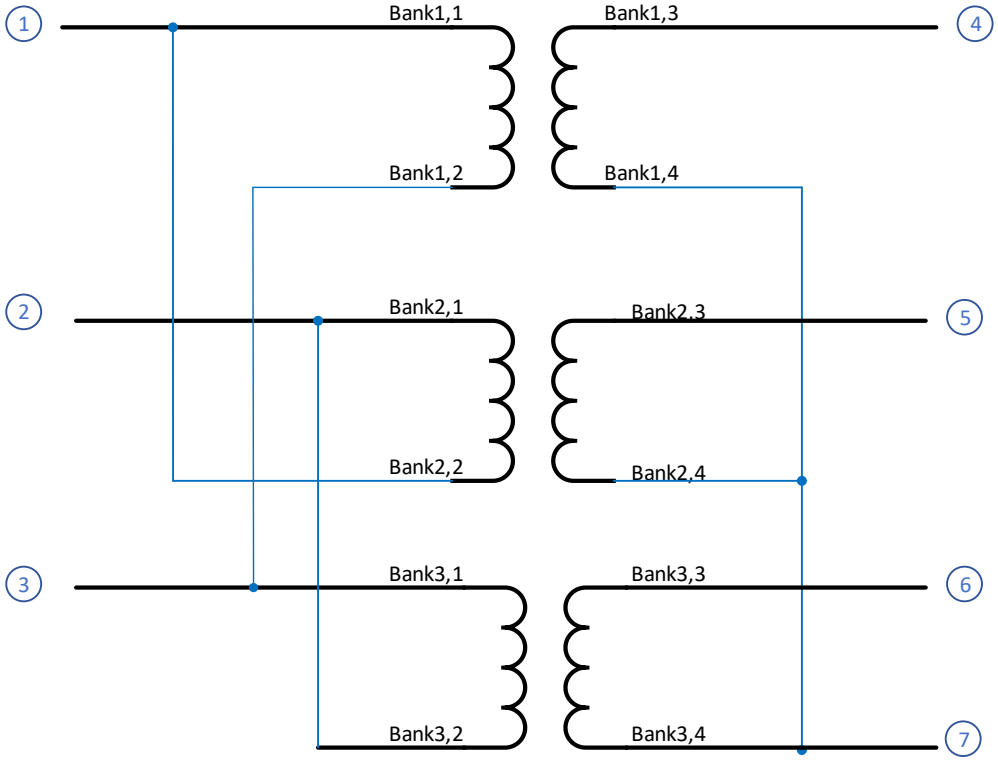

Figure B-4 DELTA-WYE connection configuration

Table B-5 External state index mapping to three-phase model, DELTA-WYE connection configuration

Bank	External State Index Mapping to three-phase model
1	1,3,4,7
2	2,1,5,7
3	3,2,6,7

4) DEALTA-DELTA

The DELTA-DELTA connection configuration is shown in Figure B-5. The state variable consists of 6 external states and then each bank internal states appended to the state vector. The mapping of each bank external state index to the three-phase model is listed in Table B-6.

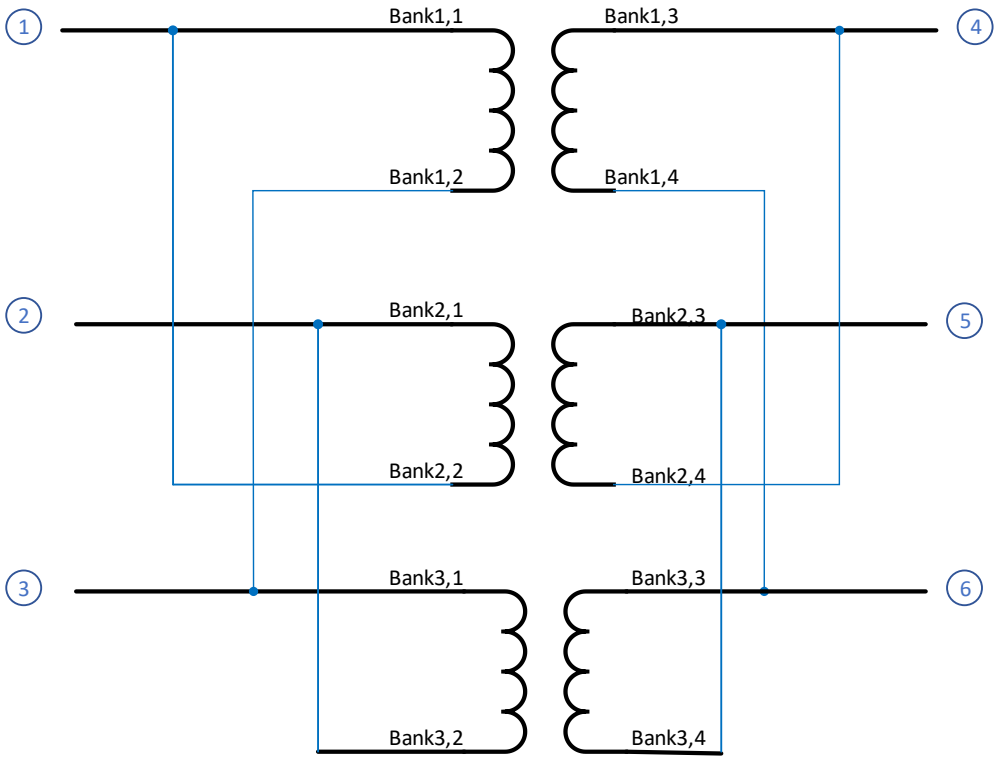

Figure B-5 DELTA-DELTA connection configuration

Table B-6 External state index mapping to three-phase model, DELTA-DELTA connection configuration

Bank	External State Index Mapping to three-phase model
1	1,3,4,6
2	2,1,5,4
3	3,2,6,5

The transformer model used in this dissertation is the three-phase model, DELTA-WYE configuration.

REFERENCES

[1] Enerdata, “Global Energy Statistical Yearbook 2018”, https://yearbook.enerdata.net/electricity/electricity-domestic-consumption-data.html.

[2] A. P. Meliopoulos, " Power System Relaying, An Introduction”.

[3] Protection System Misoperation Task Force, “Misoperations report,” NERC Planning Committee, 2014

[4] NERC System Protection and Control Subcommittee, “Reliability Fundamentals of System Protection,” NERC 2010.

[5] NERC Reliability Risk Management, “FERC/NERC Staff Report on the September 8, 2011 Southwest Blackout Event”, NERC 2011.

[6] L. J. Powell, "Current Transformer Burden and Saturation," *IEEE Trans. Ind. Appl.*, vol. IA-15, no. 3, pp. 294-303, May 1979.

[7] F. Haghjoo and M. H. Pak, "Compensation of CT Distorted Secondary Current Waveform in Online Conditions," *IEEE Trans. Power Del.*, vol. 31, no. 2, pp. 711-720, April 2016.

[8] J. R. Linders, et al., "Relay performance considerations with low-ratio CTs and high-fault currents," *IEEE Trans. Ind. Appl.*, vol. 31, no. 2, pp. 392-404, March-April 1995.

[9] L. A. Kojovic, "Impact of current transformer saturation on overcurrent protection operation," *IEEE Power & Energy Society General Meeting*, Chicago, IL, USA, 2002, pp. 1078-1083 vol.3.

[10] P. K. Gangadharan, T. S. Sidhu and A. Klimek, "Influence of current transformer saturation online current differential protection algorithms," *IET Gener., Transm., Distrib.*, vol. 1, no. 2, pp. 270-277, Mar. 2007.

[11] K. W. Chen and S. T. Glad, "Estimation of the primary current in a saturated transformer," *Proc. of the 30th IEEE Conference on Decision and Control*, Brighton, UK, 1991, pp. 2363-2365 vol.3.

[12] Y. C. Kang, et al., "Development and hardware implementation of a compensating algorithm for the secondary current of current transformers," *Proc. Inst. Elect. Eng., Electr. Power Appl.*, vol. 143, no. 1, pp. 41-49, Jan. 1996.

[13] Y. C. Kang, J. K. Park, S. H. Kang, A. T. Johns and R. K. Aggarwal, "An algorithm for compensating secondary currents of current transformers," *IEEE Trans. Power Del.*, vol. 12, no. 1, pp. 116-124, Jan. 1997.

[14] Z. Lu, J. S. Smith and Q. H. Wu, "Morphological Lifting Scheme for Current Transformer Saturation Detection and Compensation," *IEEE Trans. Circuits Syst. I*, vol. 55, no. 10, pp. 3349-3357, Nov. 2008.

[15] F. Li, Y. Li and R. K. Aggarwal, "Combined wavelet transform and regression technique for secondary current compensation of current transformers," *IEE Proc - Gener., Transm., Distrib.*, vol. 149, no. 4, pp. 497-503, July 2002.

[16] Jiuping Pan, Khoi Vu and Yi Hu, "An efficient compensation algorithm for current transformer saturation effects," *IEEE Trans. Power Del.*, vol. 19, no. 4, pp. 1623-1628, Oct. 2004.

[17] C. S. Yu, "Detection and Correction of Saturated Current Transformer Measurements Using Decaying DC Components," *IEEE Trans. Power Del.*, vol. 25, no. 3, pp. 1340-1347, July 2010.

[18] J. Pihler, B. Grcar and D. Dolinar, "Improved operation of power transformer protection using artificial neural network," *IEEE Trans. Power Del.*, vol. 12, no. 3, pp. 1128-1136, July 1997.

[19] D. C. Yu, J. C. Cummins, Z. Wang, H. J. Yoon, L. A. Kojovic and D. Stone, "Neural network for current transformer saturation correction", *Proc. IEEE Transm. Distrib. Conf.*, pp. 441-446, 1999.

[20] D. C. Yu and J. C. Cummins, "Correction of current transformer distorted secondary currents due to saturation using artificial neural networks", *IEEE Trans. Power Del.*, vol. 16, no. 2, pp. 189-194, Apr. 2001.

[21] H. Khorashadi-Zadeh and M. Sanaye-Pasand, "Correction of saturated current transformers secondary current using ANNs", *IEEE Trans. Power Del.*, vol. 21, no. 1, pp. 73-79, Jan. 2006.

[22] B. Ge, A. T. Almeida and F. J. T. E. Ferreira, "Estimation of primary current in saturated current transformer using flexible Neural network", *Trans. Instrum. Meas. Control*, vol. 28, no. 1, pp. 81-91, 2006.

[23] W. Rebizant, "Current-transformer saturation detection with genetically optimized neural networks", *IEEE Trans. Power Del.*, vol. 22, no. 2, pp. 820-827, Apr. 2007.

[24] Y. Hong and P. Chang-Chian, "Detection and correction of distorted current transformer current using wavelet transform and artificial intelligence," *IET Gener., Transm., Distrib*, vol. 2, no. 4, pp. 566-575, July 2008.

[25] K. Erenturk, "ANFIS-Based Compensation Algorithm for Current-Transformer Saturation Effects," *IEEE Trans. Power Del.*, vol. 24, no. 1, pp. 195-201, Jan. 2009.

[26] D. Gallo, C. Landi and M. Luiso, "Real-time digital compensation of current transformers over a wide frequency range", *IEEE Trans. Instrum. Meas.*, vol. 59, no. 5, pp. 1119-1126, May 2010.

[27] Takoi K. Hamrita, Bonnie S. Heck and A.P. Sakis Meliopoulos, "On-line correction of errors introduced by instrument transformers in transmission-level steady-state waveform measurements," *IEEE Trans. Power Del.*, vol. 15, no. 4, pp. 1116-1120, Oct. 2000.

[28] J. Mooney, " Distance Element Performance Under Conditions of CT Saturation," *2008 61st Annual Conference for Protective Relay Engineers.*, College Station, TX, 2008, pp. 491-497.

[29] K. Wannous and P. Toman, " The impact of current transformer saturation on the distance protection," *2016 17th International Scientific Conference on Electric Power Engineering (EPE)*, Prague, 2016, pp. 1-5.

[30] F. Mahfoud, G. C. Lazaroiu, T. Kherbek and T. Hayder, " Improvement of differential protection performance by external faults associated with a current transformer saturation," *2017 International Conference on ENERGY and ENVIRONMENT (CIEM)*, Bucharest, 2017, pp. 83-86.

[31] N. Villamagna and P. A. Crossley, " A CT saturation detection algorithm using symmetrical components for current differential protection," *IEEE Trans. Power Del.*, vol. 21, no. 1, pp. 38-45, Jan. 2006.

[32] C. Wu and Q. Yu, " Analysis and Countermeasure of Delay of Line Differential Protection Caused by CT Transient Saturation in Faults in Wind Farms," *2018 Chinese Automation Congress (CAC)*, Xi'an, China, 2018, pp. 3209-3212.

[33] N. Chothani and B. Bhalja, " A new differential protection scheme for busbar considering CT saturation effect," *2011 24th Canadian Conference on Electrical and Computer Engineering (CCECE)*, Niagara Falls, ON, 2011, pp. 000007-000010.

[34] A. P. S. Meliopoulos et al., " Dynamic State Estimation-Based Protection: Status and Promise," *IEEE Trans. Power Del.*, vol. 32, no. 1, pp. 320-330, Feb. 2017.

[35] A. P. S. Meliopoulos, G. J. Cokkinides, Z. Tan, S. Choi, Y. Lee and P. Myrda, " Setting-Less Protection: Feasibility Study," *2013 46th Hawaii International Conference on System Sciences*, Wailea, Maui, HI, 2013, pp. 2345-2353.

[36] Y. Liu, A. P. S. Meliopoulos, R. Fan, L. Sun and Z. Tan, " Dynamic State Estimation Based Protection on Series Compensated Transmission Lines," *IEEE Trans. Power Del.*, vol. 32, no. 5, pp. 2199-2209, Oct. 2017.

[37] G. K. Stefopoulos, G. J. Cokkinides and A. P. Meliopoulos, "Quadratic integration method for transient simulation and harmonic analysis," *2008 13th International Conference on Harmonics and Quality of Power*, Wollongong, NSW, 2008, pp. 1-6.

[38] A. P. Meliopoulos, "Chapter 7 in Power System Modeling, Analysis and Control".

[39] Yuan Kong, A.P. Meliopoulos, and Georgia Cokkinides, "On-line current instrumentation channel error correction within merging units using constraint WLS dynamic state estimation", *2018 North American Power Symposium (NAPS)*, Fargo, ND, USA, 2018.

[40] A. P. S. Meliopoulos et al., "Transmission level instrument transformers and transient event recorders characterization for harmonic measurements," *IEEE Trans. Power Del.*, vol. 8, no. 3, pp. 1507-1517, Jul. 1993